MICROWAVE ASSISTED SYNTHESIS, CHARACTERIZATION AND BIOLOGICAL STUDIES OF ISONICOTINOYL-HYDRAZONES AND THEIR MANGANESE (II) COMPLEXES

Mitthu Lal Gurjar[a], Chetna Ameta[a], Rakshit Ameta[b], Kiran Meghwal[a] and Pinki Bala Punjabi[a]*

Keywords: Mn (II) complexes; Schiff base; Antimicrobial activity; microwave.

The Schiff base ligands 1-(2-furanyl) ethanone isonicotinoylhydrazone (L^5H), 1-(2-thienyl)ethanone isonicotinoylhydrazone (L^6H), 1-(2-pyridyl)ethanone isonicotinoylhydrazone (L^7H), 1-(2-naphthyl)ethanone isonicotinoylhydrazone (L^8H), were prepared by the condensation reaction of isonicotinic acid hydrazide with corresponding ethanons in 1:1 molar ratio, respectively, in ethanol under microwave exposure. The Mn (II) complexes have been prepared by mixing $MnCl_2.4H_2O$ in 1:1 and 1:2 molar ratios with monofunctional bidentate ligands. The structure of the ligands and their transition metal complexes were confirmed by the elemental analysis, molecular weight determinations, IR, electronic and EPR spectral studies. On the basis of these studies it is clear that the ligands coordinated to the metal atom in a monobasic bidentate mode, by O∩N donor system. Thus a tetrahedral environment around the Mn(II) ion has been proposed. The antimicrobial activity of Schiff base ligands and their respective Mn(II) complexes were tested against some of pathogenic bacterial and fungal strains. The results indicated that the complexes showed higher activity than the parent ligands.

*Corresponding Authors
E-Mail: gmlgurjar@gmail.com, pb_punjabi@yahoo.com
[a] Department of Chemistry, Mohanlal Sukhadia University, Udaipur 313002, Rajasthan, India
[b] Department of Chemistry, J.R.N Rajasthan Vidyapeeth (Deemed to be University), Udaipur 313001, Rajasthan, India

Introduction

Coordination compounds are the backbone of modern inorganic and bio-inorganic chemistry and chemical industry. These compounds provide critical insights into the functioning and structures of vital components of biological systems. Coordination compounds also find extensive applications in metallurgical process, analytical and medicinal chemistry.[1] Amongst the coordination compounds, Schiff base complexes are of considerable importance and have been known since the mid nineteenth century.[2,3] Metal-complexes of Schiff bases have occupied a central place in the development of coordination chemistry after the work of Jorgensen and Werner.[4]

Chelating ligands containing N and O donor atoms show broad biological activity and are of special interest because of the variety of ways in which they are bonded to metal ions. It is known that the existence of metal ions bonded to biologically active compounds may enhance their activities.[5-6] There has been considerable interest in coordination chemistry of manganese(II) compounds because of their potential utilities as model compounds of manganese containing proteins which would show significant involvement of manganese in various biological systems. Manganese(II) complexes with Schiff base ligands are becoming increasingly important as biochemical, analytical and antimicrobial reagents, in the design of molecular ferromagnets, in materials chemistry and so on.[8-10] The biological importance of Schiff base complexes of Mn(II) has been referred by number of studies.[11-13]

Green chemistry is the effort of reducing or eliminating the use or generation of hazardous substances during chemical procedures[14,15] to keep environment pollution free. Microwave chemistry as a green method of synthesis has an edge over conventional heating methods for conducting chemical reactions for lead development by pharmaceutical and biotechnology companies.[16] Nowadays the microwave technology is being used for the synthesis of organic and inorganic compounds, as well as for thermal treatment of many materials at laboratorial and industrial scales.[17]

Due to the growing interest of pharmacological properties of nitrogen and oxygen containing Schiff base ligands and their metal complexes, a systematic study of the stereochemical and biological aspects of the Mn(II) complexes of substituted isonicotinylhydrazone have been undertaken. In the present investigation and as synthesized ligands and their complexes have also been tested *in vitro* for antifungal and antibacterial activity.

Experimental

All the chemicals and reagents used were of AR grade and dried and distilled before use. The $MnCl_2.4H_2O$ was purchased from Alfa Caesar. 1-(2-furanyl)ethanone, 1-(2-thienyl)ethanone, 1-(2-pyridyl)ethanone and 1-(2-naphthyl)ethanone and isonicotinic acid hydrazide were purchased from Sigma Aldrich. Apparatus fitted with Quickfit interchangeable joints was used to carry out the reactions under completely anhydrous conditions.

Preparation of the ligands

All ligands L^5H, L^6H, L^7H and L^8H were prepared by the condensation reaction of isonicotinic acid hydrazide with 1-(2-furanyl)ethanone, 1-(2-thienyl)ethanone, 1-(2-pyridyl)-

ethanone and 1-(2-naphthyl)ethanone in 1:1 molar ratio respectively using ethanol as solvent (Scheme 1). The reaction mixture was subjected under microwave radiations for 5-10 minutes. Reaction progress monitored by TLC and after completion of reactions, the solution was concentrated under reduced pressure, which on cooling gave dark yellow crystalline precipitates (Approx 90 % yield). These were washed and recrystallized in alcohol.

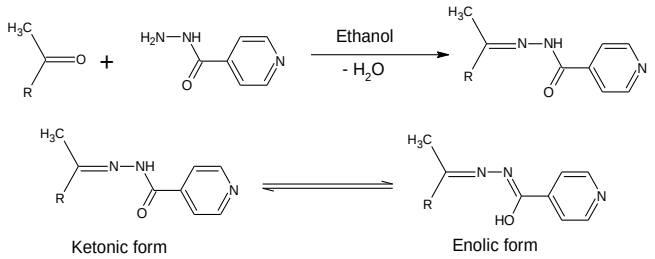

where R= 2-furanyl, 2-thienyl, 2-pyridyl and 2-naphthyl

Preparation of the complexes

Microwave method was employed for the synthesis of the metal complexes of the as- synthesized ligands. A fixed amount of hydrated manganese dichloride ($MnCl_2.4H_2O$) in dry methanol was mixed with a methanolic solution of the synthesized ligands in 1:1 and 1:2 molar ratios. The reaction mixture was subjected under microwave radiations for 7-9 minutes. The resulting mixture was then concentrated under reduced pressure. The resulting compounds were washed with methanol followed by drying in *vacuum* for about one hour to get the final product. The low value of molar conductivity (7.0-11.5 ohm^{-1} cm^2 mol^{-1}) of $1x10^{-3}$ M solutions of the resulting manganese(II) complexes in anhydrous dimethylformamide adequately supports their non-electrolytic nature.

Physical measurements and analytical methods

The molecular weights were determined by the Rast Camphor method.[18] The metal contents were analysed gravimetrically. Sulfur and nitrogen were determined by Messenger's[19] and Kjeldahl's methods,[20] respectively. Carbon and hydrogen analyses were performed at the CDRI, Lucknow. Infrared spectra were recorded on a Nicolet Magna FTIR-550 spectrophotometer using KBr pellets. The electronic spectra were recorded on a Varian–Cary/5E spectrophotometer at Central University Gujarat. EPR spectra of the complexes were monitored on Varian E-4X band spectrometer at Central University Gujarat.

Antimicrobial studies

Bioefficiacies of the synthesized compounds were checked *in vitro*. The *in vitro* antifungal activities of the ligands and their complexes have been evaluated against two pathogenic fungi, *Candida albicans* and *Aspergillus niger* using by the agar plate technique.[21] The potato dextrose agar (PDA) medium was prepared in the laboratory to maintain the fungal growth. For PDA preparation, 20 g potato was extracted with distilled water (100 mL) at 100 ºC for 1 h and it was filtered off by cotton filter. The potato juice was then mixed with 2 g dextrose and 1.5g agar and finally the pH of the prepared PDA media was adjusted at 7. Solutions of the test compounds in methanol at 50, 100 and 200 ppm concentrations were prepared and then were mixed with the medium. The medium was then poured into petri plates and the spores of fungi were placed on the medium with the help of inoculum's needle. These petri plates were wrapped in the polythene bags containing a few drops of alcohol and were placed in an incubator at 25±2 °C. The activity was determined after 96 h of incubation at room temperature (25 ºC). The controls were also run and three replicates were used in each case The linear growth of the fungus was obtained by measuring the diameter of the fungal colony after four days and the percentage inhibition was calculated as 100x(*C*-*T*)/*C*, where *C*=diameter of the fungus colony in the control plate after 96 h and *T*=diameter of the fungal colony in the test plates after the same period. The antifungal screening data of compounds were compared with the standard (Fluconazole).

In vitro antibacterial screening is generally performed by disc diffusion method[22] for primary selection of the compounds as therapeutic agents. The antibacterial activity of the ligands and their manganese complexes were evaluated against of two bacteria including Gram-positive (*Bacillus subtilis)* and Gram-negative (*Escherichia coli)*. The nutrient agar medium having the composition peptone 5 g, beef extract 5 g, NaCl 5 g, agar-agar 20 g and distilled water 1000 mL was pipetted into the Petri dish. When it solidified, 5.0 mL of warm seeded agar was applied. The seeded agar was prepared by cooling the molten agar to 40 °C and then added the 10 mL of bacterial suspension. The compounds were dissolved in methanol in 500 and 1000 ppm concentrations. Paper discs of Whatman No.1 filter paper measuring diameter of 5mm were soaked in these solutions. The discs were dried and placed on the medium previously seeded with organisms in Petri plates at suitable distance. The Petri plates were stored in an incubator at 28±2 °C for 24 h. The diameters of the zone of inhibition produced by the compounds were compared with the standard antibiotic (Streptomycin). The zone of inhibition thus formed around each disc containing the test compounds was measured accurately in mm.

Determination of minimum inhibitory concentration (MIC)

Minimum Inhibitory Concentration, MIC, is the lowest concentration of test agent that inhibited visible growth of bacteria after 18 h incubation at 37 °C. The determination of the MIC involves a semiquantitative test procedure, which gives an approximation to the least concentration of an antimicrobial needed to prevent microbial growth. The minimum inhibitory concentration was determined by liquid dilution method.[23] Stock solutions of Mn(II) complexes with 10-50 mg mL^{-1} concentrations were prepared with aqueous methanol solvent. Inoculum of the overnight culture was prepared. In a series of tubes, 1 mL each of Mn(II) complex solutions with different concentrations were taken and 0.4 mL of the inoculum was added to each tubes. Further 3.5 mL of the sterile water was added to each of the test tubes. These test tubes were incubated for 24 h and observed for the presence of turbidity. The absorbance of the suspension of the inoculum was observed with

spectrophotometer at 555 nm. The end result of the test was the minimum concentration of antimicrobial (test materials) which gave a clear solution, i.e., no visual growth.[24]

Results and Discussion

The elemental analysis and spectral data are consistent with the formulation of compounds as $[MnCl(L)(H_2O)]$ and $[Mn(L)_2]$. Molecular weight determinations indicate their monomeric nature. The reactions of $MnCl_2.4H_2O$ with the synthesized ligands were carried out in unimolar and bimolar ratios in methanol solution proceed with the formation of M←N and M-O bonds yielding the substitution products. The reactions proceed as shown in Scheme 2.

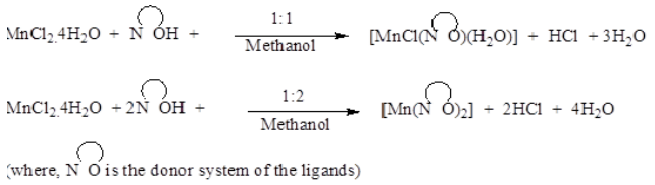

Scheme 2. Preparation route of the complexes

The reason for synthesizing metal complexes by microwave method is due to its ecofriendly nature. The microwave mediated reactions occur more safely, reduce the amount of waste products and increases the yield of pure required products. The physical properties and analytical data of the synthesized ligands and their metal complexes are enlisted in Table 1. The bonding pattern and the geometry of these complexes have been deduced on the basis of IR, UV and ESR spectral studies.

Infrared spectral data

A comparison of the characteristic IR absorption bands of the ligand and corresponding metal complexes reveal important features for establishing the facts that the ligands (L^5H, L^6H, L^7H and L^8H) behave as monofunctional bidentate N∩O donor for bonding to the metal atom. The broad band due to ν_{NH} vibrations disappears in the spectra of manganese(II) complexes, indicating the deprotonation of this group on coordination with the metal atom. In the IR spectra of the complexes appropriate shifts of ligand bands was noted due to complex formation. The $\nu_{C=O}$ and $\nu_{C=N}$ stretching bands that appeared in the free ligands at 1715-1705 cm^{-1} and 1600-1590 cm^{-1}, respectively, are shifted to lower frequency in the complexes and observed in the ranges 1700–1690 cm^{-1} and 1580–1570 cm^{-1} for $\nu_{C=O}$ and $\nu_{C=N}$, respectively.

Table 1. Analytical data and physical properties of the ligands and their complexes

Synthesized compounds	Colour	Melting Point (^{0}C)	Found (Calculated) (%)			Mol. Wt. Found (calculated)
			N	S	Mn	
L^5H	Yellow	160-165	18.2 (18.32)	-	-	228.35 (229.23)
L^6H	Light yellow	199-205	18.74 (17.12)	13.93 (13.07)	-	244.5 (245.29)
L^7H	Light yellow	130-134	22.74 (23.31)	-	-	239.3 (240.24)
L^8H	Light yellow	220(d)	15.4 (14.52)	-	-	289.5 (290.33)
$[MnCl(L^5)(H_2O)]$	Pink	165	12.10 (12.48)	-	15.84 (16.31)	334.81 (336.63)
$[Mn(L^5)_2]$	Light pink	173(d)	16.77 (16.43)	-	10.39 (10.74)	509.64 (511.39)
$[MnCl(L^6)(H_2O)]$	Light pink	225(d)	11.54 (11.91)	10.01 (9.09)	15.24 (15.57)	350.27 (352.69)
$[Mn(L^6)_2]$	Light pink	248(d)	16.07 (15.46)	9.94 (10.10)	11.27 (11.79)	542.51 (543.52)
$[MnCl(L^7)(H_2O)]$	Light pink	199(d)	16.72 (16.11)	-	15.17 (15.80)	345.56 (347.62)
$[Mn(L^7)_2]$	Light pink	187(d)	20.81 (21.00)	-	10.89 (10.29)	530.80 (533.44)
$[MnCl(L^8)(H_2O)]$	Light pink	235(d)	10.23 (10.60)	-	14.24 (13.86)	398.50 (397.73)
$[Mn(L^8)_2]$	Light pink	212(d)	13.60 (13.30)	-	8.08 (8.69)	632.54 (633.59)

d = decomposition

These bands are assigned to a $\nu_{C=O}$ and $\nu_{C=N}$ stretches of reduced bond order. This can be attributed to delocalisation of metal electron density (t_{2g}) to the π-system of the ligand,[25] indicating coordination of oxygen of C=O and nitrogen of the C=N moieties to the metal atoms.[26] The IR spectra of the ligands display two sharp bands around 3230-3200 cm^{-1} and 3455-3380 cm^{-1} assignable to ν_{sym} and ν_{asym} vibrations of the NH_2 group, respectively. These bands remain unchanged in the manganese(II) complexes of the ligands, indicating non-involvement of the NH_2 group in coordination. In the spectra of (1:1) manganese(II) complexes, a band observed at 830-860 cm^{-1} was assigned to the rocking mode of the coordinated water molecule. The band due to the ν_{Mn-Cl} appears in the region 335-322 cm^{-1}. These bands are absent in the spectra of manganese(II) complexes synthesized in (1:2) molar ratio. Some bands of low intensity appearing in the spectra of manganese(II) complexes in the region 439-420 cm^{-1} and 600-585 cm^{-1} can be assigned to ν(Mn←N) and ν(Mn-O)[27] vibrations, respectively, which do not appear in the spectra of ligands confirming that the chelation takes place through the bidentate (N∩O) donor system.

Table 2. IR spectral data of the ligands and their Mn(II) complexes

Synthesized compounds	IR spectral data (cm^{-1})				
	***ν*(C=O)**	**ν(C=N)**	**ν(M-O)**	**ν(M←N)**	**ν(M-Cl)**
L^4H	1715	1600	-	-	-
L^5H	1710	1593	-	-	-
L^9H	1709	1596	-	-	-
$L^{10}H$	1705	1600	-	-	-
$[MnCl(L^5)(H_2O)]$	1690	1570	585	439	322
$[Mn(L^5)_2]$	1700	1575	597	438	330
$[MnCl(L^6)(H_2O)]$	1697	1580	600	420	325
$[Mn(L^6)_2]$	1695	1573	592	437	333
$[MnCl(L^7)(H_2O)]$	1699	1975	589	438	330
$[Mn(L^7)_2]$	1700	1578	595	422	328
$[MnCl(L^8)(H_2O)]$	1700	1576	590	426	332
$[Mn(L^8)_2]$	1698	1579	600	438	335

Table 3. Electronic spectral data of the Mn(II) complexes.

Synthesized compounds	Transitions	Spectral bands(cm^{-1})	μ_{eff} (BM)
$[MnCl(L^5)(H_2O)]$	$^6A_1 \rightarrow {}^4T_2$ (ν_1)	16540	5.73
	$^6A_1 \rightarrow {}^4E$ (ν_2)	22800	
$[Mn(L^5)_2]$	$^6A_1 \rightarrow {}^4T_2$ (ν_1)	16880	5.88
	$^6A_1 \rightarrow {}^4E$ (ν_2)	22400	
$[MnCl(L^6)(H_2O)]$	$^6A_1 \rightarrow {}^4T_2$ (ν_1)	16900	5.91
	$^6A_1 \rightarrow {}^4E$ (ν_2)	20000	
$[Mn(L^6)_2]$	$^6A_1 \rightarrow {}^4T_2$ (ν_1)	16740	5.99
	$^6A_1 \rightarrow {}^4E$ (ν_2)	22700	
$[MnCl(L^7)(H_2O)]$	$^6A_1 \rightarrow {}^4T_2$ (ν_1)	16900	5.69
	$^6A_1 \rightarrow {}^4E$ (ν_2)	22650	
$[Mn(L^7)_2]$	$^6A_1 \rightarrow {}^4T_2$ (ν_1)	16830	6.10
	$^6A_1 \rightarrow {}^4E$ (ν_2)	22630	
$[MnCl(L^8)(H_2O)]$	$^6A_1 \rightarrow {}^4T_2$ (ν_1)	16760	6.05
	$^6A_1 \rightarrow {}^4E$ (ν_2)	22300	
$[Mn(L^8)_2]$	$^6A_1 \rightarrow {}^4T_2$ (ν_1)	17100	6.05
	$^6A_1 \rightarrow {}^4E$ (ν_2)	23600	

Table 4. ESR spectral data of the Mn(II) complexes

Synthesized compounds	H_0	g^{II} value	Temp. (^{0}C)	Frequency (ν)
$[MnCl(L^5)(H_2O)]$	3285.02	1.9900	25	9.38
$[Mn(L^5)_2]$	3350.72	2.0000	25	9.38
$[MnCl(L^6)(H_2O)]$	3294.66	2.0200	25	9.38
$[Mn(L^6)_2]$	3364.57	1.9920	25	9.38
$[MnCl(L^7)(H_2O)]$	3350.25	2.0000	25	9.38
$[Mn(L^7)_2]$	3255.65	1.9994	25	9.38
$[MnCl(L^8)(H_2O)]$	3217.21	2.0130	25	9.38
$[Mn(L^8)_2]$	3175.59	2.0103	25	9.38

Table 5. MIC (μg mL^{-1}) values of the ligands and their complexes

Synthesized compounds	*Bacillus subtilis*	*Escherichia coli*	*Candida albicans*	*Aspergillus niger*
L^5H	34.0±0.3	30.0±0.2	29.0±0.1	38.0±0.2
L^6H	30.0±0.1	31.0±0.2	33.0±0.2	28.0±0.1
L^7H	39.0±0.3	34.0±0.2	33.0±0.4	30.0±0.3
L^8H	32.0±0.1	38.0±0.2	39.0±0.1	32.0±0.2
$[MnCl(L^5)(H_2O)]$	20.0±0.2	20.0±0.3	22.0±0.3	24.0±0.3
$[Mn(L^5)_2]$	20.0±0.2	24.0±0.2	21.0±0.2	20.0±0.1
$[MnCl(L^6)(H_2O)]$	20.0±0.1	22.0±0.2	18.0±0.1	23.0±0.1
$[Mn(L^6)_2]$	19.0±0.1	19.0±0.1	19.0±0.1	22.0±0.1
$[MnCl(L^7)(H_2O)]$	19.0±0.1	21.0±0.3	20.0±0.2	22.0±0.2
$[Mn(L^7)_2]$	20.0±0.4	23.0±0.3	22.0±0.3	22.0±0.2
$[MnCl(L^8)(H_2O)]$	19.0±0.2	20.0±0.3	22.0±0.3	23.0±0.3
$[Mn(L^8)_2]$	20.0±0.2	19.0±0.2	21.0±0.2	18.0±0.1

The significant IR bands of the ligands and their metal complexes along with their tentative assignments are reported in Table 2.

Electronic spectral analysis

Electronic spectral and magnetic susceptibility results have supported to establish the geometry of the metal complexes. The expected tetrahedral geometry of the manganese(II) complexes was supported by the bands at 16540-17100 cm^{-1} and 20000-23600 cm^{-1} due to the $^6A_1 \rightarrow {}^4T_2(\nu_1)$ and $^6A_1 \rightarrow {}^4E(\nu_2)$ transitions, which are characteristics of tetrahedral geometry.[29] The observed magnetic moment value of 5.69-6.10 BM indicates that manganese(II) complexes are paramagnetic in nature consisting five unpaired electrons.

These data along with the tentative assignments are presented in Table 3.

ESR spectral analysis and magnetic moment

The ESR spectrum of manganese(II) complexes was recorded at room temperature. The spectrum consists of a single broad peak from which the Lande splitting factor ('*g*' value) has been calculated (Table 4). The '*g*' value lie in the range 1.9900–2.0200, which is characteristic of tetrahedral geometry. Lande splitting factor ('*g*' values) has been calculated by the following formulae:

$$g = \frac{h\nu}{\beta H}$$

where

h= Planck's constant (6.625×10^{-34} J s)

ν = frequency ($\nu = 9.38 \times 10^9$ Hz)

β = Bohr magneton (9.27×10^{-24} J $Tesla^{-1}$)

On the basis of above studies, a tetrahedral environment around the metal atom has been proposed.

Antimicrobial assay

Determination of minimum inhibitory concentration (MIC) of the synthesized ligands and their corresponding metal complexes were carried out on selected fungi, *Candida albicans* and *Aspergillus niger* and two bacteria, Gram-positive (*Bacillus subtilis)*, and Gram-negative (*Escherichia coli)* and the MIC values calculated for the ligands and their manganese(II) complexes as shown in (Table 5).

The results indicated that the ligands and their metal complexes were the most active in inhibiting the growth of the tested organisms between 18-39 μg mL^{-1} MIC values for selected bacteria and fungi. The results showed that all the free ligands were appreciably less active compared to their manganese(II) complexes. This indicated that the complexation to metal enhances the activity of the ligand. This may be explained by Tweedy's chelation theory[28], according to which chelation reduces the polarity of the central metal atom because of partial sharing of its positive charge with the ligand, due to which the lipophilic character of the metal chelate increases and favours its permeation through the lipid layer of cell membrane.

It has also been proposed that the ultimate action of the compounds is the denaturation of one or more proteins of the cell as a result of which normal cellular processes are impaired[29] and deactivation of various cellular enzymes that play a vital role in different metabolic pathways of these microorganisms.

Conclusions

Microwave (MW) irradiation is an efficient and environmentally-benign method to accomplish various inorganic and organic syntheses to afford products in higher yields in shorter reaction periods. Manganese(II) complexes synthesized in 1:1 and 1:2 molar ratios were found to possess tetra-coordinated tetrahedral structure. Biological data of the complexes and the ligands showed that the complexes are more active than the parent ligands.

Table 6. Antifungal and antibacterial screening data for the ligands and their complexes

Synthesized compounds	Antifungal activity, % (conc. in ppm)						Antibacterial activity, % (conc. in ppm)			
	Inhibition after 96 h						Diameter (mm) of inhibition zone after 24 h			
	Candida albicans			*Aspergillus niger*			*Bacillus subtilis*		*Eschirichia coli*	
	50	**100**	**200**	**50**	**100**	**200**	**500**	**1000**	**500**	**1000**
L^5H	23	41	46	22	29	48	10	11	8	9
L^6H	24	44	40	25	31	52	17	13	15	12
L^7H	27	47	42	26	30	53	14	13	10	12
L^8H	25	45	49	23	33	51	13	12	16	14
$[MnCl(L^5)(H_2O)]$	29	49	45	28	35	56	15	13	14	13
$[Mn(L^5)_2]$	32	50	49	29	38	59	12	15	12	14
$[MnCl(L^6)(H_2O)]$	30	52	46	30	40	57	14	16	15	13
$[Mn(L^6)_2]$	32	55	42	31	42	61	16	17	13	15
$[MnCl(L^7)(H_2O)]$	39	57	49	34	49	64	15	18	14	16
$[Mn(L^7)_2]$	42	50	43	37	52	66	17	20	15	18
$[MnCl(L^8)(H_2O)]$	40	52	47	40	50	62	20	18	16	20
$[Mn(L^8)_2]$	39	49	44	42	52	65	15	17	15	19
Flucanazole	60	70	73	55	68	85	-	-	-	-
Streptomycin	-	-	-	-	-	-	19	22	18	21

References

[1]http://www.ncert.nic.in/book_publishing/NEW%20BOOK%202020 07/class12/chemistry%20I/9.pdf

[2]Ettling, C., Untersuchungen über das ätherische Oel der Spiraea Ulmaria und die salicylige Säure, *Ann. Chem. Pharm.*, **1840**, *35*, 241. https://doi.org/10.1002/jlac.18400350302

[3]Schiff, H., Eine neue Reihe organischer Basen, *Ann. Chem.* **1864**, *131*, 118, https://doi.org/10.1002/jlac.18641310113

[4]Basolo, F., Johnson, R. C., "*Coordination Chemistry; The Chemistry of Metal Complexes". W.A. Benjamin, Inc*., *New York*, **1964,** 8.

[5]Canpolat, E., Kaya, M., Studies on mononuclear chelates derived from substituted Schiff-base ligands (part 2): Synthesis and characterization of a new 5-bromosalicyliden- *p* -aminoacetophenoneoxime and its complexes with Co(II), Ni(II), Cu(II) and Zn(II), *J. Coord. Chem.*, **2004**, *57*, 1217. https://doi.org/10.1080/00958970412331285913

[6]Yildiz, M., Dulger, B., Koyuncu, S. Y., Yapici, B. M., Synthesis and antimicrobial activity of bis (imido) Schiff bases derived from thiosemicarbazide with some 2-hydroxyaldehydes and metal complexes, *J. Indian Chem. Soc.*, **2004**, *81*, 7.

[7]Majumder, A. Rosair, G. M. Mallick, A. Chattopadhyay N. and Mitra, S. Synthesis, structures and fluorescence of nickel, zinc and cadmium complexes with the N,N,O-tridentate Schiff base *N*-2-pyridylmethylidene-2-hydroxy-phenylamine, *Polyhedron.*, **2006**, *25*, 1753. https://doi.org/10.1016/j.poly.2005.11.029

[8]Matsushita, T., Asada, H., Nakamura, Negoro, T. S., Yaguchi, Y., Sugino, S., Fujiwara, M., Preparation and characterization of novel manganese(III) complexes with Schiff base ligands and their reactivities toward hydrogen peroxide, *J. Inorg. Biochem.*, **2001,** *86*, 321.

[9]Yu, Y. Y., Zhao, G. L., Wen, Y. H., syntheses, Characterizations, crystal structures and antibacterial activities of two zinc (II) complexes with a Schiff base derived from o-vanillin and p-toluidine, *Chinese J. Struct. Chem.*, **2007**, *26*, 1395.

[10]Guo, H. M., Zhao, G. L., Yu, Y. Y., Synthesis, characterization, crystal structures and antibacterial activities of transition metal (Ⅱ) complexes with a Schiff base derived from o-vanillin and p-toluidine, *Chinese J. Inorg. Chem.* **2008**, 24, 1393.

[11]O'Donnell, M. The enantioselective synthesis of α-amino acids by phase-transfer catalysis with achiral Schiff base esters, J., *Acc. Chem. Res.*, **2004**, *37*, 506. https://doi.org/10.1021/ar0300625

[12]Raman, N., Kulandaisamy, A., Shunmugasundaram, A., Jeyasubramanian, K., Redox and antimicrobial studies of transition metal(II) tetradentate Schiff base complexes, *Trans. Met. Chem.*, **2001**, *26*, 131.

[13]Wang, J. L., Ding, F., Miao, F. M., Bis{4-[α-(4-acetylphenyl-imino)benzyl]-3-methyl-1-phenylpyrazol-5-onato}aqua-copper(II), *Acta Cryst.***, 2003**, *59*, 128**.**

[14]Anastas, P. T., Warner, J. C., *Green Chemistry-Theory and Practice*, Oxford University Press, **1998.**

[15]Anastas, P. T., Heine, C. G. M., Williamson, T. C., Eds, *ACS Symposium*, *Series 767*, *Green Chemical Synthesis and Processes*, American Chemical Society, Washington DC **2000**.

[16]Katritzky, A. R., Cai, C., Suzuki, K., Singh, S. K., Facile Syntheses of Oxazolines and Thiazolines with *N*-Acylbenzotriazoles under Microwave Irradiation, *J. Org. Chem*., **2004**, *69*, 811. https://doi.org/10.1021/jo0355092

[17]Chakravorty, R., Sirohi R., Kishore, D., A green chemistry approach to the synthesis of isatoic anhydrides from anthranilic acid derivatives, *J. Indian Chem. Soc.*, **2006**, *83*, 519.

[18]Vogel, A. I., *A Textbook of Organic Quantitative Analysis*, *Fifth edition*, Pearson Education Ltd., London, UK, **2004**, 243.

[19]Vogel, A.I., A Textbook of Quantitative Chemical Analysis, sixth edition, Pearson Education Ltd., London, UK, **2006**, 498.

[20]Vogel, A.I., A Textbook of Quantitative Chemical Analysis, sixth edition, Pearson Education Ltd., London, UK, **2006**, 387.

[21]Madigan, M., Martinko, J., *Brock Biology of Microorganisms* (11th ed.), **2005** Prentice Hall. ISBN 0-13-144329-1.

[22]Zaidan, M. R. S., Noor Rain, A., Badrul, A. R., Adlin, A., Norazah, A., In vitro screening of five local medicinal plants for antibacterial activity using disc diffusion method, *Tropical Biomed.*, **2005,** *22*, 165.

[23]Wiegand, I., Hilpert, K., Hancock, R. E., Agar and broth dilution methods to determine the minimal inhibitory concentration (MIC) of antimicrobial substances, *Nat. Protoc.*, **2008**, *3(2)*, 163. https://doi.org/10.1038/nprot.2007.521

[24]Lambert, R. J. W., Pearson, J., Susceptibility testing: accurate and reproducible minimum inhibitory concentration (MIC) and non-inhibitory concentration (NIC) values, *J. Appl. Microbiol.*, **2000**, *88*, 784. https://doi.org/10.1046/j.1365-2672.2000.01017.x

[25]Al-Jeboori, M. J., Al-Dujaili, A. H., Al-Janabi, A. E., Coordination of carbonyl oxygen in the complexes of polymeric *N*-crotonyl-2-hydroxyphenylazomethine, *Trans. Met. Chem.*, **2009**, *34*, 109. https://doi.org/10.1007/s11243-008-9165-9

[26]El-Sonbati, A. Z., El-Bindary, A. A., Al-Sarawy, A. A., Stereochemistry of new nitrogen containing heterocyclic aldehyde. IX. Spectroscopic studies on novel mixed-ligand complexes of Rh(III),*Spectrochim. Acta A Mol. Biomol. Spectrosc.*, **2002**, *58*, 2771. https://doi.org/10.1016/S1386-1425(02)00021-5

[27]Riyadh M. Ahmed, Enaam I. Yousif, and Mohamad J. Al-Jeboori, Co(II) and Cd(II) Complexes Derived from Heterocyclic Schiff-Bases: Synthesis, Structural Characterisation, and Biological Activity, *Sci. World J.*, **2013,** Article ID 754868.

[28]Tweedy, B. G., *Phytopathology*, **1964**, *55*, 910.

[29]Lehninger, A. L., Biochemistry, Second edition, Worth Publishers, New York, **1975**, 519.

Received: 10.01.2018.
Accepted: 22.03.2018.

ELECTROREDUCTION OF MANGANESE(II) CHLORIDE IN KCl-NaCl AND KCl-KF MELTS

Nodari Gasviani,[a] Gulnara Kipiani,[a] Shalva Andguladze[b] Marine Khutsishvili[a] and Nino Skhiladze[a]

Keywords: electroreduction; manganese chloride; molten salts; voltammetry.

The electroreduction of manganese(II) chloride from chloride (NaCl-KCl) and fluoride-chloride (KCl-KF) melts has been studied in air atmosphere by polarography. In both melts, metallic manganese was obtained and the mechanism of the reduction of manganese(II)–ions was elucidated. Optimal parameters of the process could also be established.

* Corresponding Authors
Tel: +995 (032) 2 30 14 30
E-Mail: nodargasviani@mail.ru
[a] R. Agladze Institute of Inorganic Chemistry and Electrochemistry of Ivane Javakhishvili Tbilisi State University, Georgia, Tbilisi, Mindeli str. 11, 0186
[b] Georgian Technical University, Georgia, Tbilisi, Kostava str. 77, 0175

INTRODUCTION

Electrolytic preparation of metallic manganese and manganese alloys from melts and solutions has high industrial importance. Electrochemical preparation of metallic manganese from melts economically can only be competitive with the known electrochemical method based on aqueous or ionic liquid electrolyte solutions if the target compounds are special material like high-melting metal composites or alloys.[1,2]

EXPERIMENTAL

For the preparation of metallic manganese anhydrous $MnCl_2$ was used as a depolarizer. The experiments were carried out in the melts K, Na/Cl and K/Cl, F between 973 and 1023 K temperatures.

Voltammetric characteristics were taken using the potentiostat PI-50-1. Three electrode cell was used. A platinum wire was used as the cathode, glass-graphite crucible - as the anode and as the melt container. Platinum plate presented the reference electrode. The use of lead reference electrode was proved to be consistently unappropriated.

RESULTS AND DISCUSSION

The purity of KCl-NaCl was checked using voltammetry (Fig. 1). After addition of $MnCl_2$ to the melt KCl-NaCl (briefly over 1-2 minutes) only one wave occurs on the voltammogram (Fig. 1, curve 2), but after a period two additional waves appear (Fig. 1, curves 3, 4). The height of all three waves was nearly equal, the potentials were found to be -0.6÷ - 0.7, -0.78÷-1.0 and -1.1÷-1.3 V, respectively.

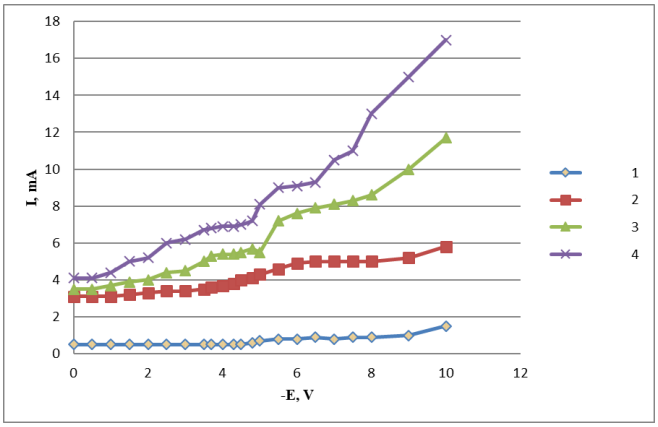

Figure 1. Voltammograms of electroreduction of manganese chloride in K,Na/Cl melt: 1-background, 2-background+$MnCl_2$ (0.2 wt.%), 3-background+$MnCl_2$ (0.6 wt. %), 4-background+$MnCl_2$(0.1 wt. %). Platinum as cathode and reference electrode, *T*=973 K

It is well known[3] that Mn(II) transforms into Mn(VI) ion melts due to oxidation with the oxygen content of the air

$$Mn^{II} \rightarrow Mn^{IV}+2e-$$

$$Mn^{IV} \rightarrow Mn^{VI}+2e-$$

The three waves observed on the voltammograms shows the three-step reduction of Mn(VI) to metallic manganese according to the following scheme:

$$Mn^{VI}+2e^- \rightarrow Mn^{IV} \quad \text{wave I}$$

$$Mn^{IV}+2e^- \rightarrow Mn^{II} \quad \text{wave II}$$

$$Mn^{II}+2e^- \rightarrow Mn \quad \text{wave III}$$

The electrolysis at the potentials corresponds to limiting currents of waves I and II did not produce any precipitate because the electrolysis products formed at the cathode (intermediate compounds) could re-dissolve in the electrolyte.

Table 1. Experimental and calculated data of the first stage of Mn(VI) electroreduction in the KCl-NaCl-$MnCl_2$ melt [$MnCl_2$]=2•10^{-5}mol cm^{-3}, *T*=973K.

V s^{-1}	E_p, V	$E_{p/2}$, V	$E_{p/2}$-E_p, V	E_p^a, V	E_p^c-E_p^a, V	$E_{1/2}$, V	$E_{1/2}$-E_p	Number of electrons calculated		
0.1	0.750	0.654	0.096	0.645	0.105	0.702	0.048	1.93	1.78	1.94
0.2	0.758	0.657	0.101	0.657	0.101	0.712	0.046	1.84	1.94	2.02
0.5	0.758	0.652	0.106	0.673	0.058	0.713	0.045	1.75	2.2	2.06
1	0.752	0.663	0.089	0.650	0.102	0.707	0.045	2.08	1.81	2.06
2	0.751	0.668	0.083	0.670	0.081	0.708	0.043	2.2	2.27	2.16

According to X-ray phase analysis, metallic manganese was obtained at the potential corresponding to the limiting current of wave III. All three stages were proved to be two-electron reduction processes. The analysis of the waves was carried out in semi-logarithmic coordinates **E**-lg(i_{lim}-*i*) and *E*-lg(i_{lim}/i_d-*i*).

The analysis of the wave I showed that the *E* - log(i_{lim}-*i*) relationship was linear. The process was reversible and may be described by the Kolthoff – Lingane[4] equation:

$$E = E_{1/2} + \frac{RT}{nF}\lg(i_d - i)$$

Comparison of the experimental and calculated data related to the process at wave I can be seen in Table 1. The number of the electrons was calculated by the following formulas[5]:

$$E_{p/2} - E_p = 2.2\frac{RT}{nF}$$

$$E_p^c - E_p^a = 2.2\frac{RT}{nF}$$

$$E_p - E_{1/2} = 1.1\frac{RT}{nF}$$

where

$E_{p/2}$, E_p, E_p^c and E_p^a are the potentials of half-peak, peak, cathode peak and anode peak potentials, respectively;

$E_{1/2}$ – potential of the half–wave (taken from stationary voltammetric characteristics,

n – the number of electrons.

As it can be seen from Table 1, the first stage is a two-electron reduction process.

The analysis of the wave II showed linear *E* – log (*i*/(i_{lim}-*i*) relationship, thus the wave can be described by the Heyrovsky-Ilkovich equation[5]

$$E = E_{1/2} - \frac{RT}{nF}\lg\frac{i}{i_{lim} - i}$$

The theoretical value of angle coefficient 2.303*RT*/*nF* at 973 K was found to be 0.036 at *n*=2, which is very close value to the experimentally found K_{ex} = 0.041 which confirms the presence of a two-electron reduction process.

The analysis of wave III unambiguously shows linear E - logi/i_{lim}-i relationship. The electrolysis at the potential corresponding to limiting current of this wave resulted in a solid product – metallic manganese. This process is irreversible.

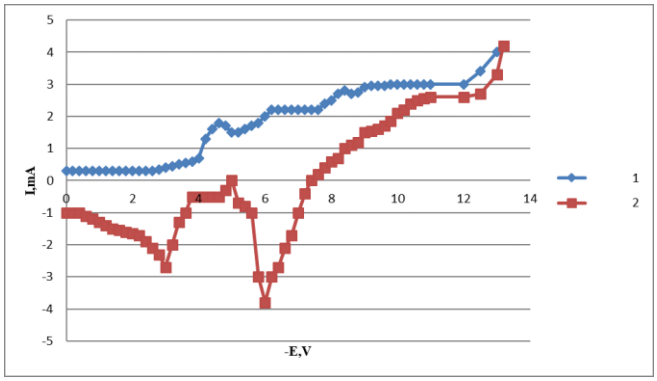

Figure 2. Cyclic voltammograms of Mn(VI) electroreduction. $MnCl_2$ (transforms into Mn(VI)) was added to the K,Na/Cl (I) melt in 0.6 wt. % amount, 1-cathodic curve, 2-anodic curve. Polarization rate was 0.1 V s^{-1}, *T*=973 K, platinum is a cathode

The cyclic voltammetric curves (Figure 2) showed the appearance of the process which is described by the Frumkin – Bagotski equation.[7]

$$\frac{\Delta E}{\Delta \lg\frac{i}{i_{lim} - i}} = 2.3\frac{RT}{\alpha n_\alpha}$$

To establish the effect of the background composition (in particular, of fluoride ions) on the electroreduction of manganese chloride some experiments were repeated in K//Cl,F melt. Replacement of chloride by chloride-fluoride mixture induced a change on the electroreduction curve of Mn(VI) (Figure 3).

In the K/Cl,F melt, at >0.4 wt.% manganese chloride content, two cathodic waves and one anodic peak could be fixed -0.95÷- 1.1, -1.4÷-1.5, and -1.08 V respectively (Fig. 4, curve 1 and 2).

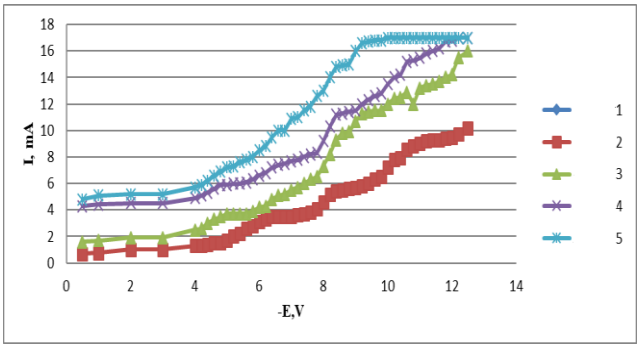

Figure 3. Voltammograms of Mn(VI) electroreduction. C_{MnCl2}=1.0 wt. %. Curves 1.4 were taken in KCl –NaCl melts at T = 973 K, curves 3.4 were taken in KCl –KF melt at T=1023 K. Polarization rate (V s^{-1}) was 0.1-2.3 and 0.5-4.5, respectively. Platinum was the cathode and platinum – oxygen was the reference electrode.

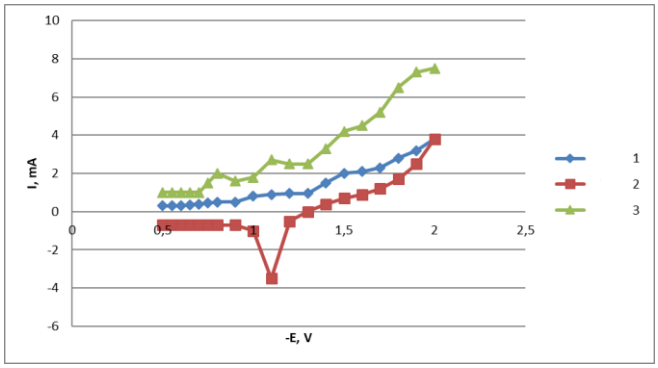

Figure 4. Voltammograms of Mn(VI) elecctroreduction. Background melt: KCl-KF. $MnCl_2$ (oxidized to Mn(VI)) was added in wt. %: 0.2 curves 1.2, 0.4 curve 3. Polarization rate was 0.2 V s^{-1}, platinum as anode, T=1023 K.

The peak heights were increased with increasing the polarization rate. At higher $MnCl_2$ concentration (C_{MnCl2}>0.4 wt. %) four waves of cathode reduction were observed at -0.65÷-0.75, -0.95÷-1.05 V, -1.3÷-1.5V and -1.55÷-1.65 V (Fig. 4, curve 3), respectively. Together with these, two pronounced peaks of anodic oxidation at E_a^{I}=-0.6 V and E_a^{II}=-1.05 V (Fig. 5), respectively, were occurred.

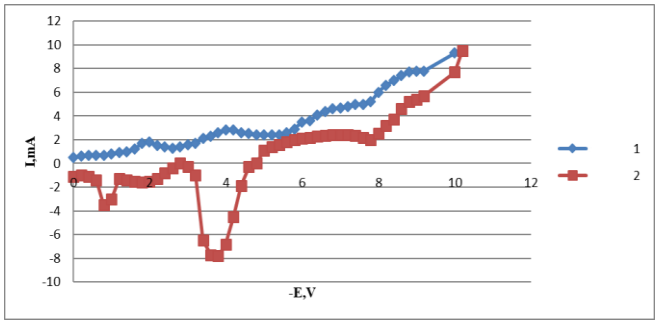

Figure 5. Cyclic voltammograms of Mn(VI) electroreduction in the K/Cl,F melt. C_{MnCl2}=1,0 wt. % 1. cathodic curve, 2-anodic curve. Polarization rate was 0.1 V s^{-1}, T=1023 K.

The first three waves correspond to Mn(VI) reductions observed in the pure chloride melt (shifted to the electronegative side) which might be explained with the formation of analogous mixed chloride – fluoride complexes of chlorides formed in pure chloride melt. The fourth wave in the range of -1.55÷-1.65 V belongs to a pure fluoride complex formed in the melt.

The large difference between anodic and cathodic peaks: E_c-E_a=0.7 V for the last stage shows the irreversible nature of the process (Fig 5). By potentiostatic electrolysis at the potential, corresponds to limiting current (1.7 V), metallic manganese was obtained. The analysis of the last stage of manganese chloride electroreduction in K/Cl,F melt showed that the wave could be described by Frumkin-Bagotski equation. The values of, αn_α calculated by experimental dependence were found to be 1.94÷2.1.

CONCLUSION

The composition of the background melt has considerable influence on the electroreduction of manganese chloride.[8] In the chloride melt in the presence of air the Mn–ions transform into Mn^{VI}. The electroreduction of Mn^{VI} occurs in three stages. First and second reversible stages are two-electron reduction processes without deposit formation at the cathode. The third stage results in metallic Mn formation, the process is irreversible.

The addition of KF into the chloride melt causes changes in the electroreduction process of $MnCl_2$ due to the formation of chloride-fluoride mixed and fluoride complexes. The discharge potentials are shifted to the negative side, and a new wave could be observed belong to the pure fluoride complex reduction. The preparation of metallic manganese can be performed from both melts (K, Na/Cl-$MnCl_2$ and K/Cl, F-$MnCl_2$).

REFERENCES

[1]Zhu, J., Dai, L., Yu, Y., Cao, J., Wang, L., A direct electrochemical route from oxides to TiMn2 hydrogen storage alloy, Chin. J. Chem. Eng., 2015, 23(11), 1865-1870; DOI: 10.1016/j.cjche,2015,08,033; Qiu, Z-Y., Li, Q-F., Effects of MnCl2 on improving the electro-deposition layer of Al-Mn alloy in the NaCl-AlCl3 molten salts, Xiyou Junshu Cailiao yu Gongcheng (Rare Metal Mater. Eng.,) 1994, 23(6), 32-35; Tan, J. H., Chen, H. Y., Zhang, S. T., Xiang, Q., The comparison of electrolysis manganese craft on stainless steel and titanium, Adv. Mater. Res., 2011, 194-196, 275-282, DOI: 10.428/www.scientific.net/AMR.194-196.275; Chung, P. P., Cantwell, P. A., Wilcox, G. D., Critchlow, G. W., Electrodeposition of zinc-manganese alloy coatings from ionic liquid electrolytes, Trans. Inst. Metal Finishing, 2008, 86(4), 211-219. DOI: 10.1179/174591908X327572; Chen, P. Y., Hussey, C. L., The electrodeposition of Mn and Zn-Mn alloys from the room-temperature tri-1-butylethylammonium bis(trifluoromethane)sulfonyl)imide ionic liquid, Electrochim: Acta, 2007, 52(5), 1857-1864; DOI:10.1016/j.electacta.2006.07.049; Sylla, D., Savall, C., GAdouleau, M., Rebere, C., Creus, J., Refait, Ph., Electrodeposition of Zn-Mn alloys on steel using an alkaline pyrophosphate-based electrolytic bath, Surf. Coat. Technol., 2005, 200(7), 2137-2145. DOI 10.1016/j.surfcoat.2004.11.020.

[2]Kuzmovich, V. V., Delimarski, Yu. K., In *"Fizicheskaia Chimia rasplavlennich solei I shlakov". M. Metalurgizdat,* 1962, p.p. 327-336;

[3]Agladze R.I. *Gidrometalurgicheskoe poluchenie margantsa. DPhil, Institut Metalurgii AN SSSR,* M. 1943.

[4]Kolthoff, I. M., Lingane, Y. J., Polyarografia. M.: Mir – 1940.

[5]Matsuda, H., Ayabe, Y., *"The theory of the cathode-ray polarography of Randles-Sevcik"* //Z. Elektrochem//. 1955, 59, 494-503

[6]Heyrovsky, Ya. Osnovi polyarografii. M. 1969.

[7]Frumkin, A. N., Bagotski, V. S., Iofa E. A., Kabanov B. N. *"Kinetika elektrodnich processov", Izd.MGU*, 1952

[8]Gasviani, N. A., D. Phil, *Foundation of electrochemical preparation of intermetallides, silicides and borides of the metals – V, Nb, Ta, Mo, Mn, Y, Al from oxyhalide melts* Tbilisi, 2006.

Received: 19.11.2017.

Accepted: 08.04.2018.

PHYSICO-CHEMICAL CHARACTERISTICS AND PHYSIOLOGICAL CHANGES IN *OREOCHROMIS NILOTICUS* FROM ROSETTA BRANCH OF THE RIVER NILE

S. M. Salaah[a]*, M. T. Khalil[b], N. S. Gad[a] and N. A. M. Ahmed[a]

Keywords: River Nile, Rosetta branch, fish, biochemical parameters, physico-chemical parameters.

The River Nile is the essence of life in Egypt, but during the last decades its water quality has been changed by several factors, as a result of anthropogenic activities. The western branch of the River Nile is Rosetta Branch receives different types of pollution. The main origins of most pollutants are El-Rahawy drain and industrial activities in Kafr El-Zayat city. Water samples were analysed for physico-chemical parameters and blood samples for biochemical parameters of the Nile Tilapia; *Oreochromis niloticus*, to investigate the responses of fish towards these different types of pollution. Samples were collected from three sites from Rosetta branch of the River Nile during summer 2014 and winter 2015. S2 and S3 recorded an increase in water electrical conductivity (EC), total dissolved solids (TDS), biological oxygen demand (BOD) and chemical oxygen demand (COD), while dissolved oxygen (DO) and pH have been depleted. Nitrite, nitrates and ammonia levels also showed an elevation, especially in winter. Moreover, fundamental biochemical parameters such as; glucose, total protein, total lipid, albumin, cholesterol, triglycerides, kidney functions and liver functions in blood serum of *O. niloticus* recorded remarkable alterations, indicating stressful conditions, caused by the profound pollutants and poor water quality of water at these sites.

* Corresponding Authors
Tel: + 2 010 94 84 42 24;
Fax: + 2 2792 1341
E-Mail: sallyissun@outlook.com.
[a] National Institute of Oceanography and Fisheries (NIOF), Cairo, Egypt
[b] Department of Zoology, Faculty of Science, Ain Shams University, Cairo, Egypt

INTRODUCTION

Water quality in Egypt is a major issue since water resources are limited to the River Nile, groundwater in the Delta, western desert and Sinai and the rainfall. The severity of water quality problems in Egypt varies among the different water bodies depending on water flow, population density, the extent of industrialization, social and economic conditions. The human population continuously loads the aquatic environment with foreign chemicals (pollutants) released by urban communities and industries. Pollution load in the Nile ecosystem (main River Nile, canals, and drains) has increased in the past few decades despite all the programs for pollution control. Consequently, quality of the Nile water worsened dramatically in the past few years.[1, 2] It is anticipated that the dilution capacity of the River Nile system will diminish as the program to expand irrigated agriculture moves forward and the growth in industrial capacity increases the quantity of pollutants discharged into the River Nile.[3] After passing Cairo, the River Nile pursues a north westerly direction, and divides at El-Qanater Barrage into two branches, each of which runs separately to Mediterranean Sea, forming the Delta region between both branches. The western branch is Rosetta Branch and the Eastern branch is Damietta branch. Rosetta Branch of River Nile begins from El-Qanater Barrage at south and ends at Rosetta estuary in the Mediterranean Sea. It exhibits the worst water quality along the River Nile.[4,5] Rosetta Branch receives about 12 billion m^3 $year^{-1}$ of seeping water from agriculture fields, 75 % of it is in the Nile delta region.[6] This drainage water contains dissolved salts washed from agricultural lands as well as residues of pesticides and fertilizers, pathogens, toxic organic and inorganic pollutants.[7] Industrial wastewater is the second main source of pollution because of the toxic chemicals and organic loading. Moreover, The Branch suffers from discharges of untreated sanitary and industrial wastewaters from municipalities, heavy navigation of cruises and commercial transportations.[8-10] In Egypt, fish is considered as a cheap protein food if compared with others of animal sources. Fish are very intimate contact with their environment; only a thin epithelial membrane separates the blood of the fish from the water. Fish are very susceptible to physical and chemical changes which reflected in their blood components.[12-14] Changes in the biochemical characteristics of blood and tissues are important diagnostic tool, indicate the changes in metabolism and the physiological processes of fish caused by environmental pollutants, detection and diagnosis of metabolic disturbance, disease and health during stress conditions.[15-19] Analysis of biochemical parameters could help to identify the target organs of toxicity as well as the general health status of animals and it may also provide an early warning signal in stressed organisms.[20-23]

Our objective in this study was to assess the impact of some physico-chemical characteristics on *O. niloticus* physiology.

EXPERIMENTAL

Rosetta Branch of River Nile is about 220 Km long and about 180 m wide with an average depth of 2.0 to 2.3 m. It starts from EL-Qanater EL-Khayria and ends at Rosetta Estuary. It passes through six governorates viz., EL-Qalubia, EL-Menofiya, EL-Giza, EL-Gharbiya, Kafr El-Shiekh and EL-Boheira. There are three main sources of pollution discharged into Rosetta Branch which, potentially affects and deteriorates the water quality of the branch (1) various small agricultural drains and sewage from several cities and

its neighboring villages, which discharge their wastes directly into the branch without treatment, (2) El-Rahawy drain and (3) Kafr El-Zayat industrial area.

Area of investigation

Three stations from Rosetta branch were selected according to pollution type. S1 - El-Qanater El-Khyria before bifurcation (relatively unpolluted site), S2 - in front of Al-Qata (affected by El-Rahawy drain) and S3 - in front of the Kafr El-Zayat industrial area (loaded with industrial effluents from factories) Table 1 and Figure 1.

Table 1. The latitude and longitude of sampling stations at Rosetta Branch (GPS).

Sites	Latitude	Longitude
S1	30° 10′ 22.4″	31° 8′ 34.0″
S2	30° 13′ 18.7″	30° 58′ 30.3″
S3	30° 49′ 33.7″	30° 48′ 23.6″

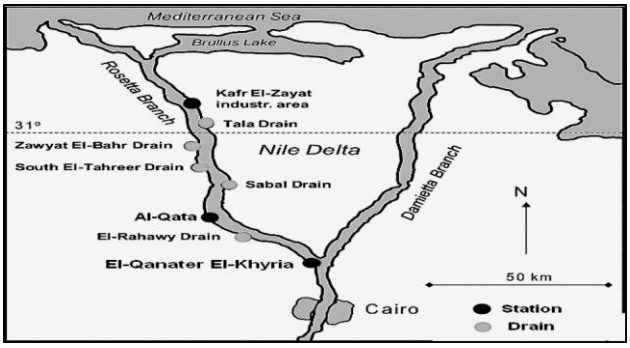

Figure 1. Map of northern Egypt showing the area of study and sampling stations in the Rosetta Branch.

Collection of samples

Water and fish samples were collected from S1, S2 and S3 in summer 2014 and winter 2015. Some physico-chemical parameters of water were done in field such as: water temperature, hydrogen ion concentration (pH), Electrical conductivity (EC), total dissolved solids (TDS), using Orion Research Ion Analyzer 399A. Water samples were stored at 4˚C and transported to the laboratory for analysis of other parameters. Water samples were analyzed according to standard method for examination of water and wastewater.[24] Determination of dissolved oxygen (DO) was carried out by using Winkler Azide titration method[25] (the modified method). Chemical oxygen demand (COD) and biological oxygen demand (BOD) and nutrient salts (nitrite, nitrate, and ammonia) were measured using Standard Methods.[24]

Blood samples (proximally 3 mL) were collected immediately from alive *O. niloticus*; blood was withdrawn from the caudal vein using a syringe. Blood was left to clot then centrifuged at 3000 r.p.m for 10 min. Supernatant serum was obtained using micropipette and stored at 4 ˚C till determination of biochemical parameters [glucose, liver functions (alanine amino transferase (ALT), aspartate amino transferase (AST), total protein and albumin, kidney functions (urea, creatinine and uric acid) and lipid profile (cholesterol and triglycerides)] in blood serum were assayed by spectrophotometer (model Jenway 6800UV/Vis double beam), and using commercially available kits in Egypt (spectrum). The experimental data were subjected to statistical analysis by one-way analysis of variance (ANOVA), the significant of difference was analyzed by the Dunnett test (compare data of all vs. control) was done by using a software program (GraphPad InStat Software, Inc.). The difference checked by one-way (ANOVA) was significance when ($P \leq 0.05$), each reading represents (Mean ± S.E) of 8 fish. Correlation Matrix was assigned using "corrplot" (Version 0.84).[26]

RESULTS AND DISCUSSION

Physical characteristics

Water temperature is known as a key factor, controlling the physiology, distribution, and behavior of fishes. In temperate and subtropical regions, which are characterized by seasonal fluctuations in water temperature, the effect of temperature is manifested at every level of biological organization. Changes in temperature affect the fluidity of lipid membranes, the conformational mobilities and activities of proteins, and the stability of DNA duplexes.[27] Water temperature in the present study followed the Egyptian climate with low values during winter season, and increased in summer (Figure 2). Temperature ranged from a lowest value of 19.1 ºC during winter at S1 to highest value 33.7 ºC during summer at S3 (Figure 2). Changes in water temperature could be due to some variables such as season, day time, depth, wind, current and water inflow. Temperature was positively correlated with pH (r = 0.86) and negatively with DO (r = 0.75) (Figure 8). Temperature was a water quality indicator that exhibited little variance between the sites and declared seasonal variations.

Electrical conductivity (EC) measures the ability of aqueous solution to carry the electrical current, solution of most inorganic compounds and more abundant ions have higher conductivity. In the present study, water samples collected from Rosetta Branch showed a highly significant increase in EC ($P \leq 0.01$) compared to S1. The reported increase in EC in the present study at S2 varied between 677.3 µmhos cm^{-1} in summer and 853.2 µmhos cm^{-1}in winter. At S3, EC recorded a highly significant increase 1520.5 µmhos cm^{-1} in summer and 1657.6 µmhos cm^{-1} in winter (Figure 2). The increase in EC at S2 and S3 mainly attributed to the sewage, domestic, agricultural and industrial effluents discharged from El-Rahawy and Kafr El-Zayat industries drains, respectively in this area, increasing the ability to convey electrical current. These results coincident with that finding by many authors.[28-30]

Total dissolved Solids (TDS) refer to suspended and dissolved matter in water. In the present work TDS showed a highly significant increase ($P \leq 0.01$) in water samples collected from S2 and S3. TDS was 3533.9 mg L^{-1} and 904.3 mg L^{-1} in winter at S1 and S2, respectively (Figure 2). This revealed high level of organic and inorganic matters produced by living organisms in this area, as well as the increase in cations and anions concentration of water as a result of winter closure.[31] TDS showed a strong positive correlations with EC (r = 0.94), that means both EC and TDS depend on each other (Figure 8). TDS in S2 and S3 exceeded the permissible limits (500 mg L^{-1}) according to Egyptian Governmental Law.[32]

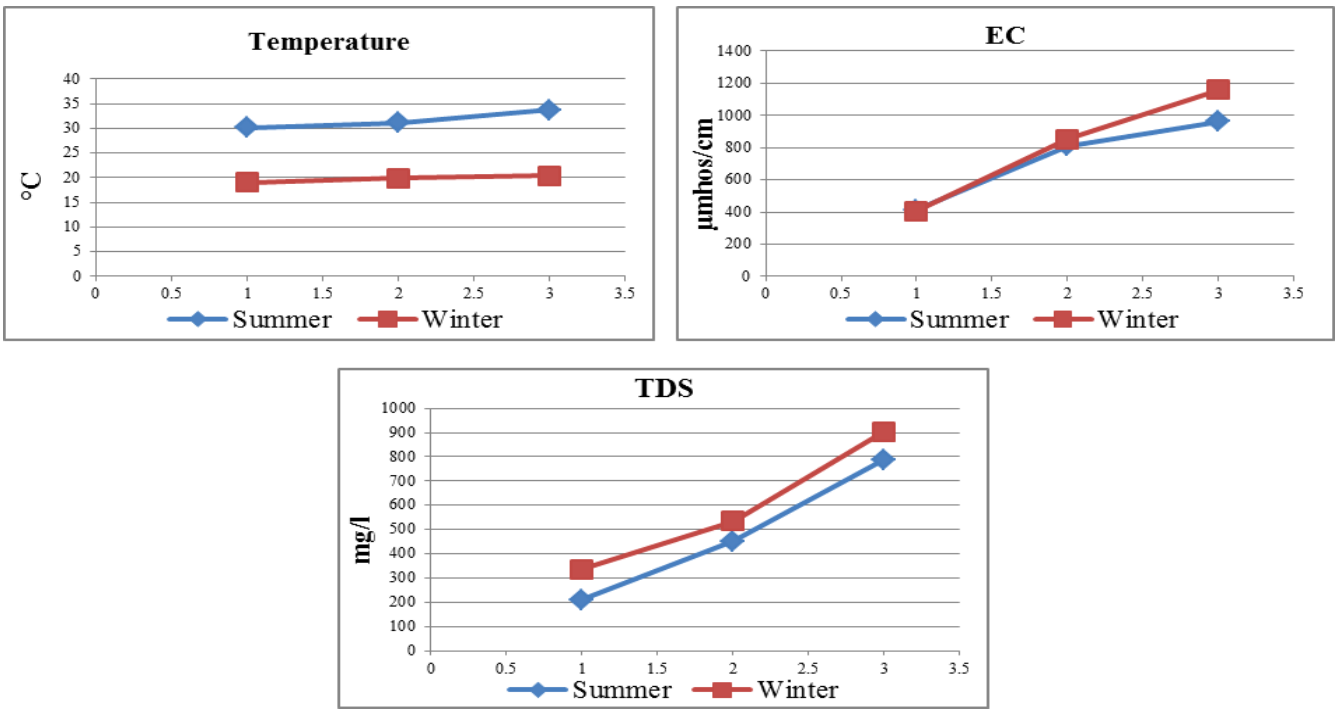

Figure 2. Seasonal variations of physical parameters: temperature, EC and TDS in Rosetta branch water during summer 2014 and winter 2015.

Chemical characteristics

Hydrogen ion concentration (pH) of natural water affects biological and chemical reaction, control the solubility of metal ions, affects fish and natural aquatic life.[33] The regional and seasonal pH values showed a tendency towards alkaline side, varied between (7.1 to 7.88) during the investigation period (Figure 3). There was a remarkable decrease in pH value (7.3 and 7.4), recorded at S2 and S3 respectively, during winter. The decrease in pH values is due to the formation of organic acids through methane and hydrogen sulphide release, by bacteria and fungi in El-Rahawy drain discharges, as well as the industrial effluents from Kafr El-Zayat Companies.[28] The pH values were within the permissible range (6.5 to 8.5) according to Egyptian Governmental Law.[32]

Dissolved oxygen (DO) is essential for a healthy aquatic ecosystem and for fish and most of aquatic animals to survive. Oxygen tends to be less soluble as temperature increases. Low levels of (DO) causes hypoxia, mortality and a massive reshaping of fish communities.[34] In the present study DO showed a negative correlation with temperature and pH (r=-0.75 and -0.74) (Figure 8).

DO in S2 and S3 showed a significant decrease ($P \leq 0.01$), comparing to S1. DO range was between 5.8 mg L^{-1} at S2 in summer and 9.3 mg L^{-1} at S1 in winter (Figure 3). Low DO in S2 is due to the extended impact of El-Rahawy drain, which directly discharges organic and inorganic pollutants into the branch water. These pollutants consume the dissolved oxygen during oxidation of nitrogenous compounds and lead to increase in ammonia processes especially during hot seasons and decrease of phytoplankton and hydrophytes. DO in the present study were within the acceptable limit (≥ 5 mg L^{-1}) recommended by Egyptian Governmental Law.[32]

Biological oxygen demand (BOD) is an important parameter for indicating organic pollution level, it determines the dissolved oxygen consumed by microorganisms to stabilize any biodegradation of organic materials.[35] A higher value of BOD indicates a decline in DO and increase the amount of organic matter**,** and a large number of microorganisms, which in turn shows a high level of pollution.[36,37]

Chemical oxygen demand (COD) is a measure of the total quantity of oxygen required to oxidize all organic material into carbon dioxide and water. It's an important parameter for stream and industrial wastes study, also serves as an index for organic matter production.[38] In the present study BOD is correlated positively with COD (r =0.79) (Figure 8). The BOD varied between 6.5 and 11.7 mg L^{-1} and COD ranged between 6.5 and 17.2 mg L^{-1} (Figure 3). Both BOD and COD showed a significant increase ($P \leq 0.01$) at S2 and S3 as compared to that at S1 reflecting the effect of the high load of organic matter, sewage, domestic, agricultural and industrial wastes discharged into Rosetta branch via El-Rahawy and Kafr El-Zayat industrial drains. BOD and COD in polluted sites exceeded the permissible limits recommended by Egyptian Governmental Law.[32]

Nitrite (NO_2^-) is an intermediate oxidation state between ammonia and nitrate. Nitrite is an invisible killer of fish because it oxidizes haemoglobin to methemoglobin in the blood, turning the blood and gills into brown and hindering respiration, also damage the nervous system, liver, spleen and kidneys of the fish.[39] Nitrate (NO_3^-) is the final oxidation product of nitrogen compounds in the aquatic environment, at the same time nitrate is considered as the only thermodynamically stable form of nitrogen in the absence of oxygen and also, in the major nitrogenous compound in the aquatic environment.[40] In the present study nitrite and nitrate peaks were 0.188 and 0.669 mg L^{-1},

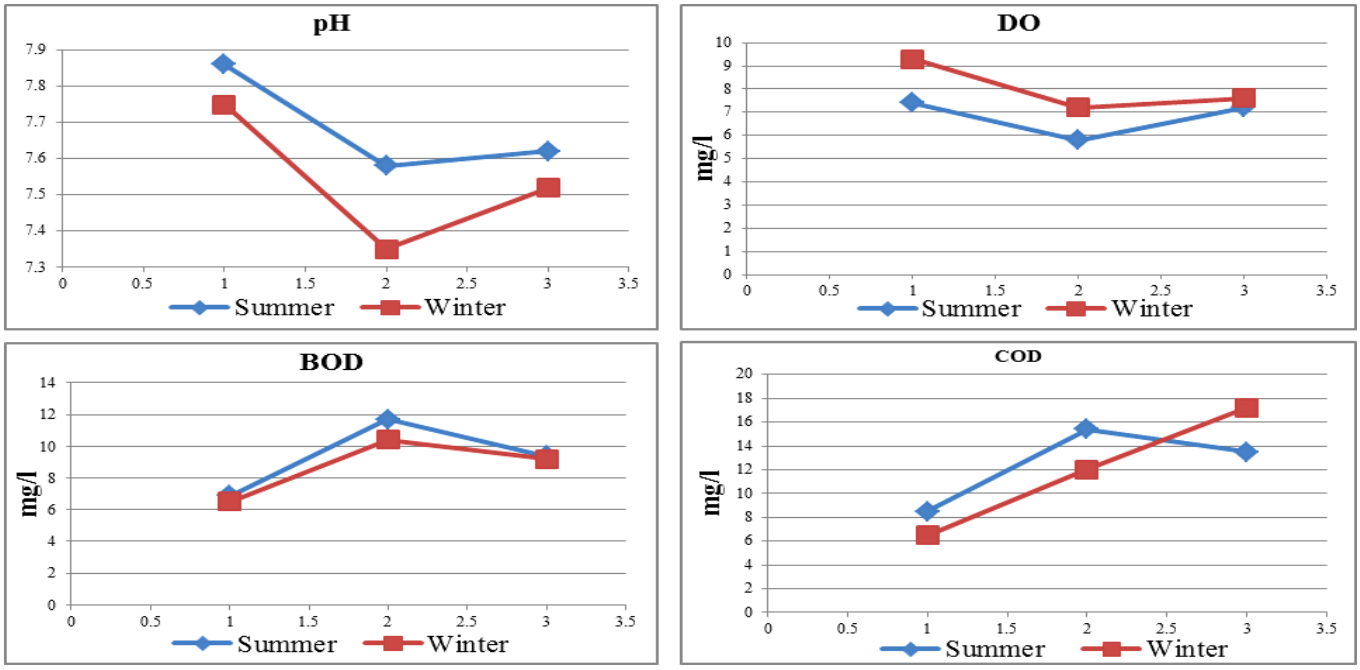

Figure 3. Seasonal variations of pH, DO, BOD and COD in Rosetta branch water during summer 2014 and winter 2015.

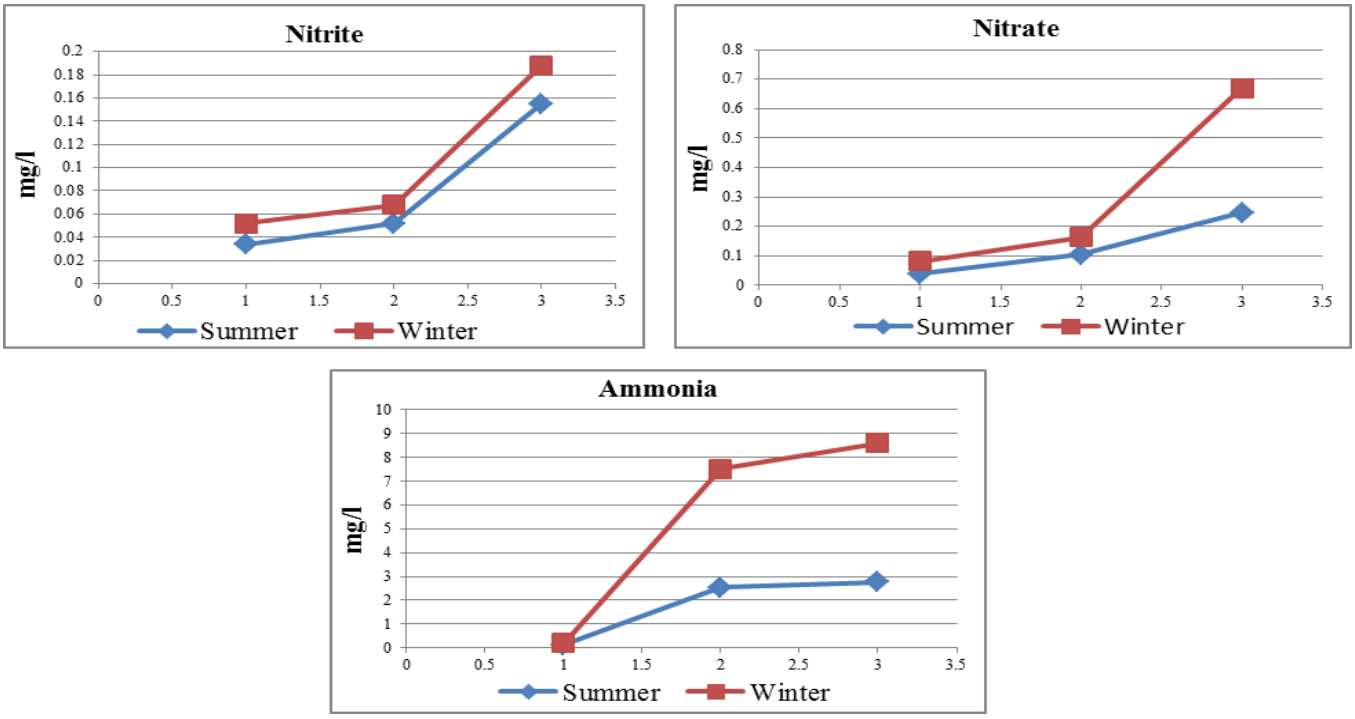

Figure 4. Seasonal variations of chemical parameters: nitrite, nitrate and ammonia in Rosetta branch water during summer 2014 and winter 2015.

recorded at S3 during winter (Figure 4). Nitrate concentrations were found to be higher than nitrite at all stations due to the fact that NO_3^- is the final stable form of nitrogen. Nitrite and nitrate were correlated positively (r = 0.91) (Figure 8). NO_2^- and NO_3^- inhibited a significant increase ($P \leq 0.01$) at S2 and S3, comparing to S1, due to the oxidation of ammonia by nitrifying bacteria and biological nitrification at S2 from El-Rahawy drain discharges. Moreover, the nitrogenous effluents at S3 from industrial area Kafr El-Zayat city producing metals, dyes and celluloid.[41]

Ammonia is the third form of nitrogen compounds which occurs naturally in water bodies, arising from the breakdown of nitrogenous organic and inorganic matter in sediment and water, excretion by biota. The most important source of

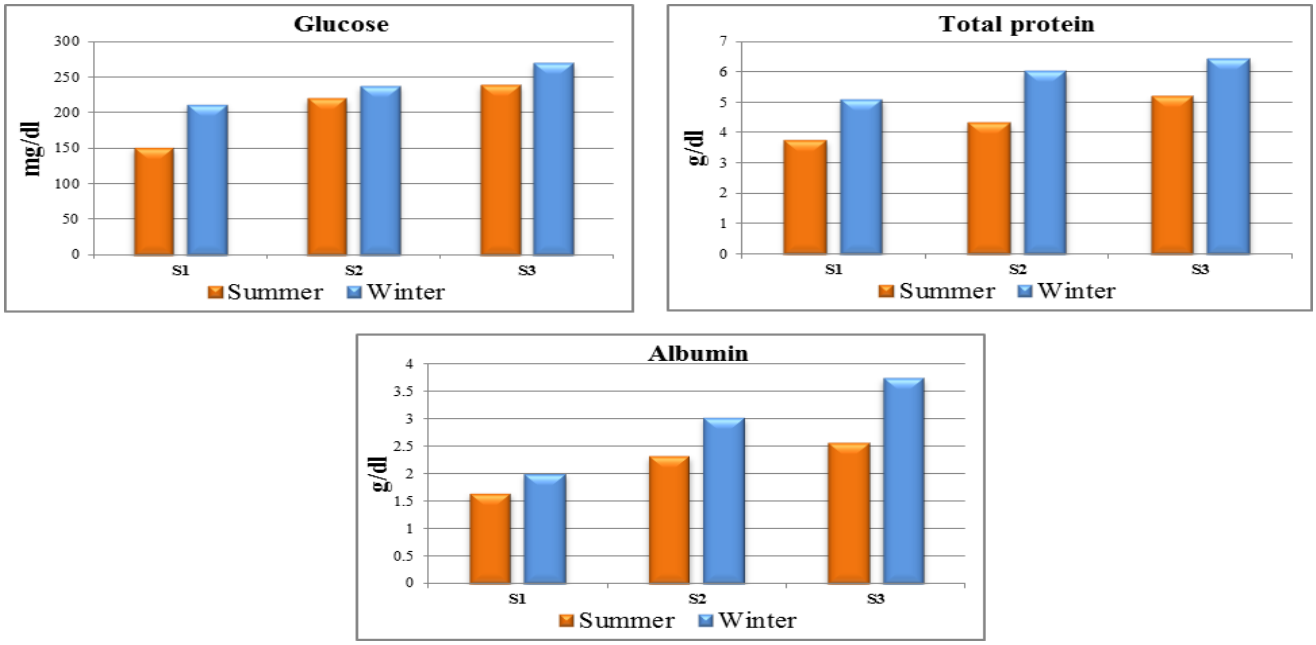

Figure 5. Seasonal variations of biochemical parameters: glucose, total protein and albumin (Mean ± S.E) in blood serum of *O.niloticus* from Rosetta branch water during summer 2014 and winter 2015.

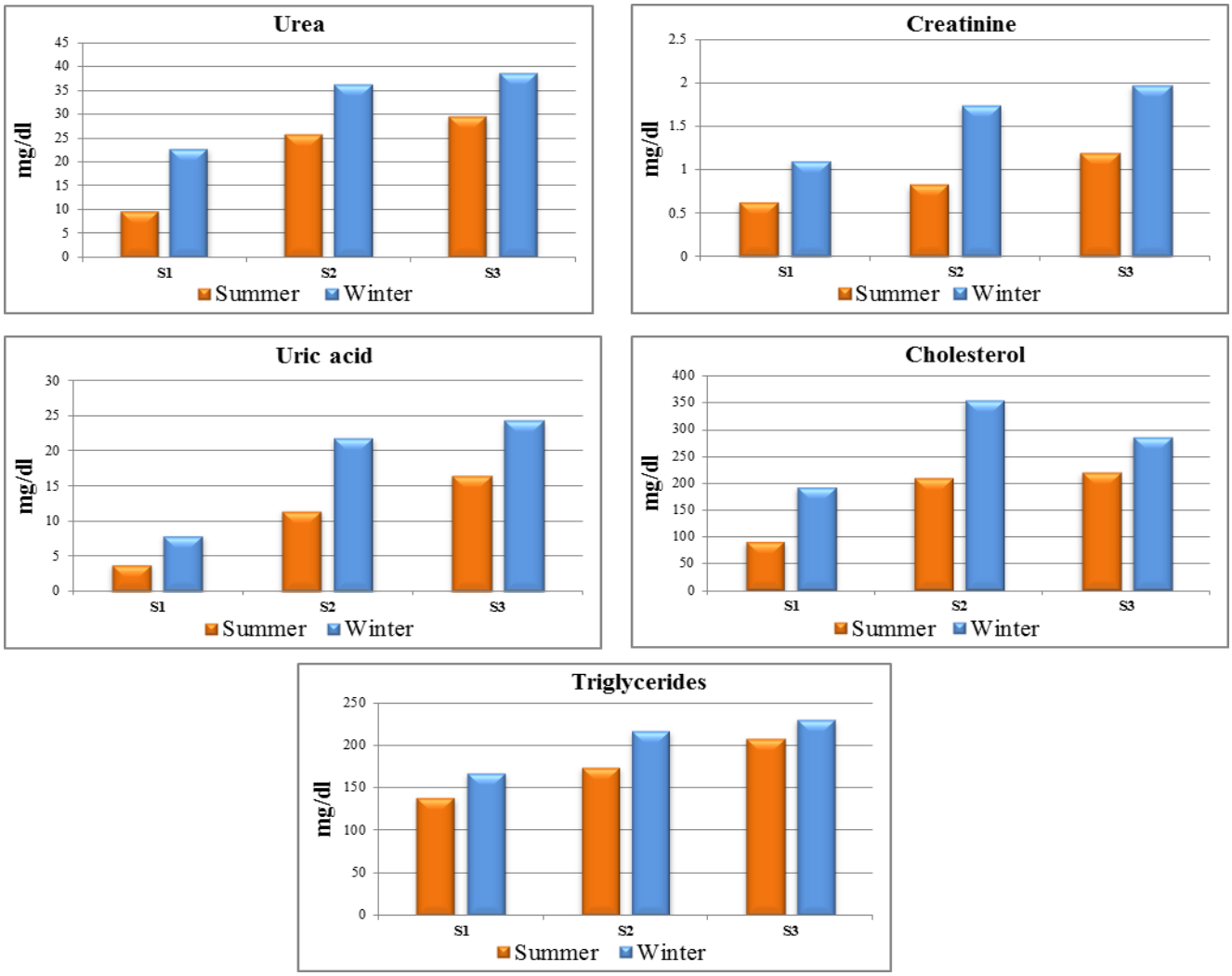

Figure 6. Seasonal variations in biochemical parameters: uric acid, cholesterol and triglycerides (Mean ± S.E) in blood serum of *O.niloticus* from Rosetta branch water during summer 2014 and winter 2015.

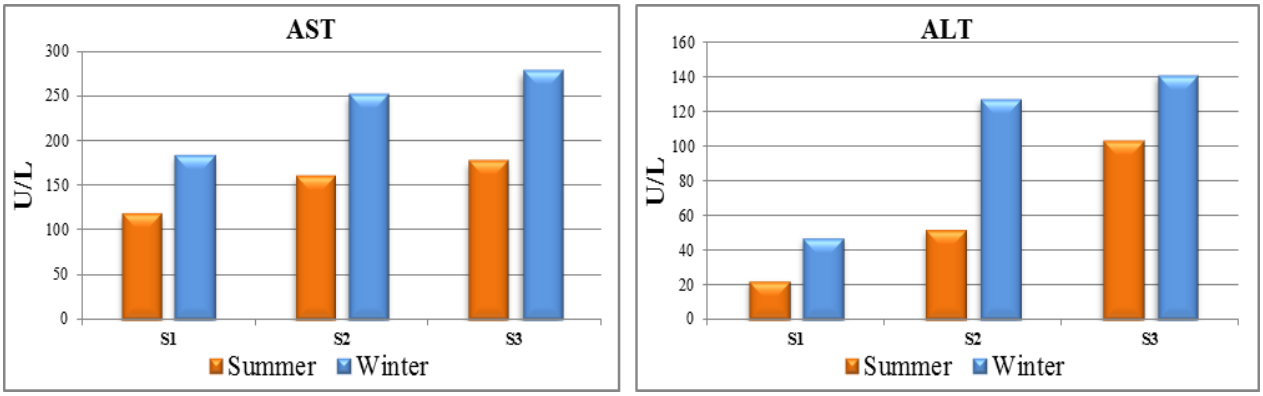

Figure 7. Seasonal variations in biochemical parameters: Aspartate aminotransferase (AST) and Alanine aminotransferase (ALT) (Mean ± S.E) in blood serum of *O.niloticus* from Rosetta branch water during summer 2014 and winter 2015

ammonia is the ammonification of organic matter, so, occurrence of ammonia in the waters used as an indicator for organic pollution.[40] In the present study ammonia range at S2 and S3 were 7.5 and 8.6 mg L^{-1} during winter (Figure 4), exhibited a highly significant increase ($P \leq 0.01$), at both sites, compared to that in S1. This may be related to the large impact of the domestic discharge from El-Rahawy

drain, which is highly loaded with organic matter and bacteria, leading to decomposition of the organic matter, exhausting dissolved oxygen and produce high level of ammonia,[37] and the industrial effluents of Kafr El-Zayat factories discharged into the branch water. The concentration of ammonia in water samples exceeded the permissible limits (0.5 mg L^{-1}) of Egyptian Governmental Law .[32] EC, TDS, nitrite, nitrate and ammonia in the present study recorded the highest values in winter, this may be due to winter closure which lowers water levels in the River Nile, leading to an increase in pollutants load which reduces the dilution effects.[30] This is in agreement with Ashry *et al*.[42]

Fish are very susceptible to physical and chemical changes which reflected in their blood components,[13] that are considered pathophysiological indicators of the whole body. The present study recorded a pronounced increase in the studied biochemical parameter in blood serum of *O. niloticus*, for example: serum glucose level at polluted sites S2 and S3 were (221.1 and 240.1 mg dL^{-1} in summer) and (238.6 and 270.4 mg dL^{-1} in winter), respectively. Both sites showed a significant increase ($P \leq 0.01$), as compared to S1 (Figure 5). Blood glucose is a sensitive and reliable indicator of environmental stress in fish.[43]

The hyperglycemic response illustrated in the present study indicated that, fish generated more glucose to produce the energy used in combating the stress induced by the environmental pollution, that possibly due to the induction of hepatic gluconeogenic enzymes and increasing substrate supply by cortisol hormones,[44] elevate the breakdown of liver glycogen or the synthesis of glucose from adipose tissue and others extrahepatic tissues, provide liver with lactate and amino acids, which serve as gluconeogenic substrates for hepatocytes to synthesize more glucose.[41] Moreover the pancreatic cell injury caused by pollutants in water enhanced glycogen breakdown in liver, and reduced insulin activity.[45]

Total serum protein is a useful indicator in diagnosis of fish disease. The majority of plasma proteins which are synthesized in the liver are used as indicators of liver impairment.[43] Also, serum albumin in fish is involved in metabolism and plays an important role in transport functions of exogenous chemicals and endogenous metabolites. Thus, serum albumin is considered as a diagnostic tool which reflects the liver function, metabolic

status and stress conditions in fishes.[44,45] In the present study, highest level of serum total protein and serum albumin of *O. niloticus* fish collected from Rosetta Branch of River Nile were 6.04 g dL^{-1} and 3.57 g dL^{-1} at S3 in winter, showed a highly significant increase ($P \leq 0.01$) as compared to S1 (Figure 5). The observed hyperproteinaemia and hyperalbuminemia in the present study may be due to activation of metabolic systems as a response to pollutants exposure, or the induction of protein synthesis and degradation of the cellular material in the liver caused by liver damage, due to the stressful condition of water pollution.[46, 47]

Urea, creatinine and uric acid are non-protein nitrogenous compounds and products of metabolism. Creatinine is a waste product largely from the muscles breakdown. Urea is the primary metabolite derived from dietary protein and tissue protein turnover.[48] Uric acid is formed by fish from exogenous and endogenous purines. It is converted in the liver to urea for excretion by the gills.[49] Urea, creatinine and uric acid are useful in diagnosis of renal function impairment, renal insufficiency, renal tubular necrosis, muscle tissue damage as well as impaired nitrogen metabolism.[50]

Concerning, the effect of water pollutants on kidney functions of *O. niloticus* collected from Rosetta Branch at S3, the obtained results revealed that, serum urea, creatinine and uric acid were 29.54, 1.19 and 16.5 mg dL^{-1} in summer and 38.78, 1.98 and 24.4 mg dL^{-1} in winter, respectively. S3 inhibited a significantly increased ($P \leq 0.01$) comparing to S1 during both the seasons (Figure 6). This response may be attribute to an impairment of renal functions and acute renal

failure, due to necrosis of renal tubules which was associated with decrease in urea, creatinine and uric acid excretion, leading to their increase in plasma.[51] Moreover, kidney damage caused by pollutants may reduce the renal blood flow and glomerular filtration rates, resulting in azotemia, which is characterized by increase in blood urea nitrogen uric acid and creatinine.[52] The reported renal failure in *O. niloticus* collected from Rosetta branch of the River Nile are in accordance with previous findings in serum of *O. niloticus* collected from different lakes (Maryut, Manzala, El-Burullus, Edku and Qarun) and the River Nile,[53] and in *O. niloticus* exposed to aquatic pollution.[54]

The main lipids classes in plasma or serum are cholesterol and triglycerides. Cholesterol is an essential structural component of cell membranes and is precursor of all steroid hormones. The outer layer of plasma is lipoproteins.[55] The level of triglycerides and cholesterol in plasma and tissues of fish are sensitive to environmental pollutants, depending on many factors such as the types of contaminants, the concentration, mode of its action, duration of exposure and fish species.[56] Both serum cholesterol and triglycerides levels in blood serum of *O. niloticus* in the present study, showed a highly significant increase ($P \leq 0.01$) at S2 and S3, during both sampling seasons, comparing to S1 (Figure 6). This increase may be due to the liver failure and renal dysfunction. The damaged liver cells release cholesterol and other lipids constituents into the circulation, also renal dysfunction may increase the total cholesterol and triglycerides in serum.[57] In addition, the increased triglyceride and cholesterol concentration in blood serum of *O. niloticus* may suggest that, a general increase in lipid mobilization must have taken place simply to fulfill the increasing demand for energy to cope with the stress of wastewater toxicity, this is in accordance with the hyperglycemic response recorded in blood serum of glucose is converted to pyruvate in the glycolytic pathway, that metabolized to acetyl-CoA in aerobic tissues and used as a precursor in the synthesis of cholesterol and fatty acids in the citric acid cycle.[58]

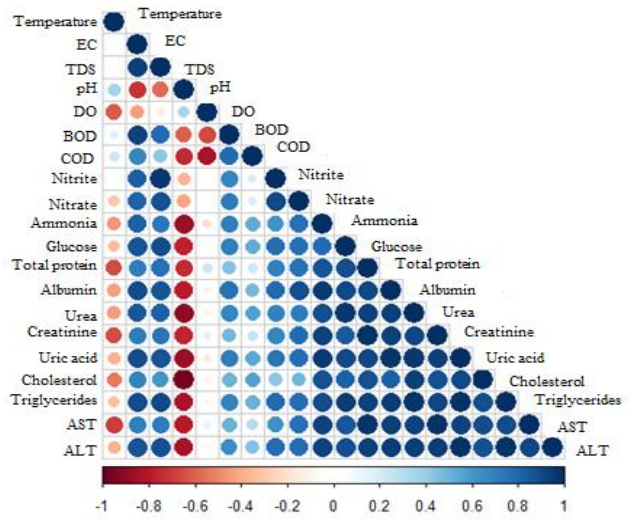

Figure 8. Correlation matrix between the physio-chemical parameters of water and the biochemical parameters in blood serum of *O.niloticus* from Rosetta branch water, during summer 2014 and winter 2015. Positive correlations are displayed in blue and negative correlations in red colour. Colour intensity and the size of the circle are proportional to the correlation coefficients.

All chemical reactions in the cell are catalyzed by enzymes and introduction of foreign chemicals in the cell generally disturbed enzyme functions. The transaminases (AST and ALT) are key enzymes known to play a key role in mobilizing of L-amino acids for gluconeogenesis and function as links between carbohydrate and protein metabolism under altered physiological, pathological conditions.[59] Serum enzymes such as AST and ALT could be used in the diagnosis of damage caused by pollutants in various tissues such as liver, muscles and gills.[60, 61] AST and ALT used as biomarkers in ecotoxicology, because they provided an early warning of potentially hazardous alterations in contaminated aquatic organisms.[62] Serum AST increased by 1.3 and 1.4 folds at S2, and 1.4 and 1.6 folds at S3 in summer and winter, respectively. On the other hand, serum ALT increased 2.2 and 2.6 folds at S2, and 4.4 and 3 folds at S3 in summer and winter, respectively. AST and ALT activities in blood serum of *O. niloticus* in the present study showed a significant increase ($P \leq 0.01$) during the study at S2 and S3 comparing to S1 (Figure 7).

The activities of serum AST and ALT in *O. niloticus* collected from downstream Rosetta Branch of the River Nile as compared to S1 are another diagnostic indicator of the liver damage in fish collected from the polluted sites (S2 and S3). Moreover, muscle damage, intestinal and hepatopancreatic injury and myocardial impairment, leads to extensive liberation of these enzymes into the blood circulation.[63,64] Our findings are in agreement with these tilapia sp. collected from wadi El-Rayan and Lake Qarun.[65, 66] The studied biochemical parameters in blood serum of *O. niloticus* collected from Rosetta branch showed a positive correlation with EC, DO, BOD, COD, TDS, nitrite, nitrate and ammonia in water, that means these characteristics affect and relate to each other (Figure 8).

CONCLUSION

Water downstream in Rosetta branch is continuously loaded with pollutants. Particularly, at Al-Qata (S2), which receives water rich in domestic wastewaters discharged from El-Rahawy drain and agricultural wastewater coming from many small agriculture drains, in addition to industrial effluents from the industrial area of Kafr El-Zayat (S3). Increased nutrients are expected to affect biological community, fish health and water quality of Rosetta branch. This hypothesis is strengthened by finding that *O. niloticus* collected from polluted sites S2 and S3 suffers from organ dysfunction (liver and kidney), that threatens the fish health in Rosetta branch of River Nile.

REFERENCES

[1]Abdel-Satar, A. M., Water quality assessment of River Nile from Idfo to Cairo, *Egypt J. Aqua Res.*, **2005**, *31(2)*, 200–223.

[2]Abdel-Dayem, S., Abdel-Gawad, S., Fahmy, H., Drainage in Egypt: A story of determination, continuity, and success, *Irrigation and Drainage*, **2007**, *56*, S101–S111.

[3]MWRI, Survey of Nile system pollution sources, APRP-Water Policy Activity, Ministry of Water Resources and Irrigation (MWRI), EPIQ, **2002,** Report No., 64.

[4]NBI, Nile Basin water quality monitoring baseline report. Transboundary Environmental Action Project, Nile Basin Initiative, **2005**.

[5]EPADP (Egyptian public Authority for Drainage Projects), Water Quality and AvailabilityManagement NAWQAM, component 3000 finaltechnical report, National Water Research Center and the Prairie Farm Rehabilitation Administration, **2008**.

[6]World Bank, Country environmental analysis 1992-2002. The World Bank, Washington D. C, **2005**.

[7]APRP (Agricultural Policy Reform Program), Water Policy Activity Contract PCE-I-00-96-00002-00 Task order 22. *Rep*., **2002**, 64: 84.

[8]MSEA, The annual report on the quality of water of the Nile River, Ministry of State for Environmental Affairs, Egypt, **2005**.

[9]Abdel-Shafy, H. I., Aly, R. O., *Wastewater Management in Egypt*, in: Mohammed K. Zaidi (Ed), *Wastewater Reuse-Risk Assessment, Decision-Making and Environmental Security*, Springer Verlag, Netherland, **2007**, 375-382.

[10]El Bourie, M. M., El Barbary, A. A., Yehia, M. M., Motawea, E. A., Heavy metal concentrations in surface river water and bed sediments at Nile Delta in Egypt, *Suo*, **2010**, *61(1)*, 1-12.

[11]Ikem, A., Egiebor, N. O., Assessment of trace elements in canned fishes (mackerel, tuna, salmon, sardines and herrings) marketed in Georgia and Alabama (United States of America), *J. Food Compos. Anal.*, **2005**, *18(8)*, 771-787. https://doi.org/10.1016/j.jfca.2004.11.002

[12]Franchini, A., Alessandrini, F., Bolognani Fantin, A. M., Gillmorphology and ATPase activity in the goldfish *Carassius carassiusvar auratus* exposed to experimental lead intoxication, *Ital. J. Zool.*, **1994**, *61*, 29–37. http://dx.doi.org/10.1080/11250009409355856

[13]Ribelles, A., Carrasco, C., Rosety, M., Morphological and histochemical changes caused by sodium dodecyl sulphate in the gills of giltheads (*Sparus aurata, L.*), *Eur. J. Histochem.*, **1995**, *39*, 141–148.

[14]Kori-Siakpere, O., Ake, J. E. G., Idoge, E., Haematological characteristics of the African snakehead, *Parachanna obscura*, *Afr. J. Biotechnol*., **2005,** *4*, 527-530.

[15]Adhikari, S., Sarkar, B., Chatterjee, A., Mahapatra, C. T., Ayyappan, S., Effects of cypermethrin and carbofuran haematological parameters and prediction of their recovery in a freshwater teleost, *Labeo rohita* (Hamilton), *Ecotox. Environ. Safe.*, **2004**, *58*, 220–226. https://doi.org/10.1016/j.ecoenv.2003.12.003

[16]Luskova, V., Svoboda, M., Kolarova, J., The effects of diazinon on blood plasma biochemistry in carp (*Cyprinus carpio* L.), *Acta Vet Brno.*, **2002**, *71*, 117–123.

[17]Younis, E. M. 1., Abdel-Warith, A. A., Al-Asgah, N. A., Hematological and enzymatic responses of Nile tilapia *Oreochromis niloticus* during short and long term sublethal exposure to zinc, *Afr. J. Biotechnol*., **2012**, *11 (19)*, 4442–4446.

[18]Suvetha, L., Ramesh, M., Saravanan M., Influence of cypermethrin toxicity on ionic regulation and gill Na+/K+-ATPase activity of a freshwater teleost fish *Cyprinus carpio*., *Environ. Toxicol. Pharmacol*., **2010**, *29 (1)*: 44–49. DOI: 10.1016/j.etap.2009.09.005

[19]Magdy, T., Nahed, S. G., Nasr, A. M., Sally, S. M., Antioxidant Defense System Alternations in Fish as a Bio-Indicator of Environmental Pollution, *Egyptian J. Aqua. Biol. Fish*., **2017**, *21(3)*, 11-28. DOI: 10.21608/EJABF.2017.3536

[20]Zaghloul, K. H., Omar, W. A., Abo-Hegab, S., Environmental hazard risk assessment on, *Oreochromis niloticus* and Tilapia zilli fish, *J. Egypt. Ger. Sco. Zool*., **2005**, *46*, A105-A139.

[21]Dube, P. N., Shwetha, A., Hosetti, B. B., Impact of copper cyanide on the key metabolic enzymes of freshwater fish *Catla catla* (Hamilton), *Biotechnol. Anim. Husband*, **2014**, *30*, 499–508. DOI: 10.2298 BAH1403499D

[22]Ahmad, S. I., Gautam, R. K., Effect of organophosphate pesticide, nuvan on serum biochemical parameters of fresh water catfish Heteropneustes fossilis (Bloch.). *Int. Res. J. Environ. Sci*., **2014**, *3(10)*, 1-6.

[23]Al-Asgah, N. A., Abdel-Warith, A. W. A., Younis, E. S. M., Allam, H. Y., Haematological and biochemical parameters and tissue accumulations of cadmium in *Oreochromis niloticus* exposed to various concentrations of cadmium chloride, *Saudi J. Biol. Sci*., **2015**, *22(5)*, 543-550. https://doi.org/10.1016/j.sjbs.2015.01.002

[24]APHA (American Public Health Association), Standard Methods for examination of water and wastewater (22nd ed.) American Water Works Association (AWWA) and Water Environment Federation (WEF), Washington, **2002,** 1193.

[25]Winkler, L. W., The determination of dissolved oxygen in water, *Eur. J. Inorg. Chem*., **1888**, *21(2)*, 2843-2854.

[26]Taiyun W., Wiliam S. R., package "corrplot": Visualization of a Correlation Matrix (Version 0.84), **2017**, Available fromhttps://github.com/taiyun/corrplot

[27]Hochachka, P. W.. Somero, G., *Biochemical Adaptation*, Princeton University Press, Princeton, New Jersey, **1984**, 304–355.

[28]Elewa, A. A., Ghallab, M. H., Water–sediment interaction in front of El-Rahawy Drain Rosetta branch, Nile, Egypt, Presented at 4th International symposium on sediment quality assessment, Otsu. Japan, **2000**, 24-27.

[29]Abdel-Satar, A. M., Elewa, A. A., Water quality and environmental assessments of the River Nile at Rosetta branch, The 2nd Int. Conf. Exhibit .Life Environ. Alexandria, Egypt., **2001**, 136- 164.

[30]Abdo, M. H., Physico-Chemeical Studies on the Pollutants Effect in the Aquatic Environment of Rosetta Branch, River Nile, *Egypt. J. Life Sci.*, **2013**, *10(4)*, 493-501.

[31]Abdo, M. H., Sabae, S. Z., Haroon, B.M., Refaat, B. M., Mohammed, A. S., Physico-chemical characteristics, microbial assessment and antibiotic susceptibility of pathogenic bacteria of Ismailia Canal water, River Nile,. *J. Am. Sci.*, **2010**, *6(5)*, 234-250.

[32]Egyptian Governmental Law No. 48/ 1982 Decision 92. The implementer regulations for Law 48/ 1982, 92/ 2013 regarding the protection of the River Nile and water ways from pollution. *Map Periodical Bull*., **2013**, 21-30.

[33]Brooks, S., Tyler, C. R., Sumpter, J. P., Egg quality in fish: what makes a good egg? *Rev. Fish Biol. Fish*, **1997**, *7*, 387-416. https://doi.org/10.1023/A:1018400130692

[34]Prepas, E. E., Charette, T., Worldwide eutrophication of water bodies: Causes, concerns, controls, in *Treatise on Geochemistry*, Holland, H. D., Terekian, K. K. (Eds.). Elsevier, Amsterdam, Science Direct online version, **2003**, *9*, 311-331.

[35]APHA (American Public Health Association) Standard Methods for examination of water and wastewater (22nd ed.) American Public Health Association, American Water Works Association (AWWA) and Water Environment Federation (WEF), Washington, **2012**.

[36]Vaishali, W., Aher H. R., Kuchekar, S. R., Determination of physico-chemical characteristics of sewage water from Loni village, *Indian J. Environ. Ecoplan.*, **2005**, *10 (2)* 419-421.

[37]Martin, E. and Hine, R. S., A Dictionary of Biology, Oxford University Press, UK Fourth edition, **2000**, 574-603.

[38]Ravindra, K., Ameena, M. S., Kamyotra, J. S., Kaushik, C. P., Variation in spatial pattern of criteria air pollutants before and during initial rain of monsoon, *Environ. Monitoring Assess.*, **2003**, *87*, 145-153.

[39]Bhatnagar, A., Devi, P., Water quality guidelines for the management of pond fish culture, *Int. J. Environ. Sci.*, **2013**, *3(6)*: *1980-1997*. doi: 10.6088/ijes.2013030600019

[40]Seike, Y., Kondo, K., Hashitani, H., Okumura, M., Fujinaga, K., Date, Y., Nitrogen metabolism in the brackish Lake Nakanoumi IV. Seasonal variation of nitrate nitrogen, *Jpn. J. Limnol.*, **1990**, *51*, 137-147. http://doi.org/10.3739/rikusui.51.137

[41]Pitter, P., *Hydrochemistry*. Institute of Chemical Technology Publishing, Prague., **1999**, 568.

[42]Ashry, M. A., Mahmoud, S. A., Abd El-Rahman, A. A. S., Histopathological studies on the hematopoietic organs of *Clarias gariepinus* in relation to water quality criteria at different localities in the River Nile, *Nat. Sci.*, **2013**, *11(8)*, 78-88.

[43]Banaee, M., *Adverse effect of insecticides on various aspects of fish's biology and physiology: Insecticides – Basic and Other Applications Book*, Edited by Soloneski, S., Larramendy, M., Published by InTech, **2012**, Chapter 6, 101- 126.

[44]Vijayan, M. M., Aluru, N., Leatherland, J. F., Stress response and the role of cortisol in *Fish diseases and disorders*, Leatherland, J.F., Woo, P. T. K. (Eds.), CAB International, Wallingford, **2010**, *2*, 182-201.

[45]Guyton, A., *Textbook of Medical physiology*, 5th Ed. Sanders Co, Philadelphia, **1976**, 668-686.

[46]Al-Attar, A. M., Changes in Hematological Parameters of the Fish, *Oreochromis niloticus* Treated with Sublethal Concentration of Cadmium. *Pak. J. Biol. Sci.*, **2005**, *8 (3)*, 421-424.

[47]Zaki, M. S., Sharaf, N. E., Rashad, H., Mostafa, S. O., Fawzi, O. M., Diminution of aflatoxicosis in *Tilapia nilotica* fish by dietary supplementation with fix in toxin and Nigella sativa oil, *Am. Eurasian J. Agric. Environ. Sci.*, **2008**, *3*, 211-215.

[48]Ajeniyi, S. A., Solomon, R. J., Urea and creatinine of *Clarias Gariepinus* in three different commercial ponds. *Nature Sci*., **2014**, *2 (10)*, 214-138.

[49]Stoskoph, M., *Fish Medicine*, W.B. Saunders Co., **1993**, *116*, 128-129.

[50]Murray, R., Mayes, P., Granner, D., Radwel, V., *Harper's Biochemistry*, 22nd Edition, Appleton & Lange, Connecticut, **1990**, 679-693.

[51]Gowda, S., Desai, P. B., Kulkarni, S. S., Hull, V. V., Math, A. A. K., Vernekar, S. N., Markers of renal function tests, *North Am. J. Med. Sci.*, **2010**, *2 (4)*, 170–173.

[52]Chang, L., Magos, L., Suzuki, T., *Toxicology of metals*, Lewis Publishers, New York, **1996**.

[53]Elghobashy, H., Khalid, A., Zaghloul, H., Mahmoud, A., Metwally A., Effect of some water pollutants on the Nile Tilapia, *Oreochromis niloticus* collected from the River Nile and some Egyptian lakes, *Egypt. J. Aqua. Biol. Fish*, **2001**, *4 (5)*, 251-219.

[54]Abdel-Khalek, A. A., Risk assessment, bioaccumulation of metals and histopathological alterations in Nile tilapia (*Oreochromis niloticus*) facing degraded aquatic conditions, *Bull. Environ. Contam. Toxicol*., **2015**, *94*, 77–83. https://doi.org/10.1007/s00128-014-1400-9

[55]Yang, J. L., Chen, H. C., Effects of gallium on common carp (*Cyprinus carpio*): acute test, serum biochemistry, and erythrocyte morphology. *Chemosphere*., **2003**, *53*, 877–882. https://doi.org/10.1016/S0045-6535(03)00657-X

[56]Heath, A.G., *Water pollution and fish physiology*, CRC Press, Florida, **1995**.

[57]Banaee, M., Nematdoust, H. B., Ibrahim A. T. A., Sub-lethal toxicity of chlorpyrifos on Common carp, *Cyprinus carpio* (Linnaeus, 1758): Biochemical response, *Int. J. Aquat. Biol*., **2013**, *1(6)*, 281-288.

[58]Hao, M., Head, W. S., Gunawardana, S. C., Hasty, A. H., Piston, D.W., Direct effect of cholesterol on insulin secretion: a novel mechanism for pancreatic beta-cell dysfunction, *Diabetes*, **2007**, *56(9)*, 2328-2338. https://doi.org/10.2337/db07-0056.

[59]Manjunatha, B., Tirado, J., Selvanayagam, M., Sub-lethal toxicity of potassium cyanide on Nile Tilapia (*Oreochromis niloticus*): Biochemical response. *Intern. J. Pharm. and Pharmaceutical Sci*., **2015**, *7 (3)*, 379-382.

[60]Coppo, J. A., Mussart, N. B., Fioranelli, S. A., Physiological variation of enzymatic activities in blood of bullfrog, *Rana catesbeiana* (Shaw, 1802), *Rev. Vet.*, **2003**: *12*: 22–27.

[61]Chen, S. J., Zeng, M. Y., Dong, S. Y., Progress in the Study of Collagen and Active Peptide of Fisheries, *Fish. Sci.*, **2004**, *23*, 44-46.

[62]Nel, A. E., Mädler, L., Velegol, D., Xia, T., Hoek, E. M., Somasundaran, P., Klaessig, F., Castranova, V., Thompson, M., Understanding biophysico-chemical interactions at the nano-bio interface, *Nat. Mater*., **2009**, *8*, 543–557.

[63]Farkas, J., Farkas, P., Hyde, D., *Liver and gastroenterology tests*, M. Lee III (Ed.), *Basic Skills in Interpreting Laboratory Data*, American Society of Health-System Pharmacists, Bethesda, **2004**, 330–336.

[64]Mekkawy, A. A., Mahmoud, U. M., Wassif, E. T., Naguib, M., Effects of cadmium on some haematological and biochemical characteristics of *Oreochromis niloticus* (Linnaeus, 1758) dietary supplemented with tomato paste and vitamin E, *Fish Physiol. Biochem*., **2011**, 37, 71-84. https://doi.org/10.1007/s10695-010-9418-3

[65]Sabae, S. Z., Mohamed, F. A. S., Monitoring of pollution in Wadi El-Rayan lakes and its impact on fish, *Int. J. Development*, **2015a**, *4 (1)*, 1-28. DOI: 10.12816/0026682

[66]Sabae, S. Z., Mohamed, F. A. S., Effect of Environmental Pollution on the Health of *Tilapia spp*. from Lake Qarun, *Global Vet*., **2015b**, *14(3)*, 304-328. DOI: 10.5829/idosi.gv.2015.14.03.9388

Received: 10.01.2018.
Accepted: 08.04.2018.

SALT MINERALS AT WADI EL NATRUN SALINE LAKES, EGYPT. NEW IMPLICATIONS FROM REMOTE SENSING DATA

Salem Mohamed Salem[a]* and El Sayed Ahmed El Gammal[a]

Key words: Remote sensing, salt lakes, Wadi El Natrun.

The salts of Wadi El Natrun saline lakes are made up of sodium chloride (NaCl, halite), sodium sulfate (Na_2SO_4, thenardite) and sodium carbonate ($Na_2CO_3.10H_2O$, natron) deposited on the bottom of the Lakes and surrounding sabkhas. The lakes of El Raizonia, Umm Risha, El Fasda, El Beida and El Gaar are the most potential lakes for economic halite salts. Furthermore, El Beida Lake contains Na_2SO_4 salts, mixed with halite, and Umm Risha and El Fasda lakes are characterized by natron salt showings. The chemical analysis of the saline water revealed dominant Cl^-, Na^+, Ca^{2+}, CO_3^{2-}, and HCO_3^- as major ions; while Mg^{2+}, SO_4^{2-} and NO_3^- are defined as minor ions. Chemical analysis of the salt deposits of these lakes shows similarity in the mineral composition with that of the saline water indicating that the water of such lakes is the main source of the realized salt minerals.

* Corresponding Author
E-mail: salem_moher@hotmail.com
[a] National Authority for Remote sensing and Space Sciences (NARSS), 23, Josef proztito St. Elnozha Elgedida - P.O. Box 1564Alf maskanCairo, Egypt.

INTRODUCTION

Wadi El Natrun is one of the prominent geomorphological features in the North-Western Desert of Egypt. It is bounded by latitudes 30° 17`to 30°19`N and longitudes 30° 10`to 30° 25`E and is generally situated at 23 m below sea level. It rises gradually to the SW up to Gebel Hadid (185 m) and to the Gebel Qantara limestones (198 m), above sea level (Figures 1 and 2). Several salt lakes and salt flats occupy the floor of the depression along with a total length of 50 km and with an average width of 10 km, follow the NW-SE trend of the depression. The Wadi El Natrun saline lakes in Egypt and the Florida saline lakes in the USA are the only two cases of Soda lakes in the world for natural salt production. The present study focuses on the utility of the hyperspectral data of remote sensing technique for mapping and exploring the saline lakes and related salt minerals at Wadi El Natrun area. The geology of such area suggests an ideal environment for salt-mineral exploration since the occurrence of many saline lakes along the depression. These considerations are the basis for the present study.

Several studies on the geology, hydrogeology, and mineralogy of the saline deposits of Wadi El Natrun were achieved.[1-4] A comparative mineralogical study of saline deposits in the study area was carried out by.[5] Mass developments of sulfide- oxidizing phototrophic bacteria in the upper sediments and in the waters of Wadi El Natrun lakes have been observed.[6] The heavy metal concentrations (e.g. Pb, Zn, Mn, Cu, Cd, Ni, Fe and A1) were measured[3] in surface sediments that largely indicate the influence of weathering on terrigenous land sources. The increased Cl^- ion content in Wadi El Natrun brines can increase metal mobility due to the formation of soluble chloro-complexes of trace elements[4] assumed that Wadi El Natrun deposits contain traces of sodium carbonate in the form of Trona ($Na_2CO_3.NaHCO_3.2H_2O$) or Natron ($Na_2CO_3.10H_2O$), but mainly made up of Burkeite ($Na_2CO_3.2Na_2SO_4$) and Halite (NaCl). The application of the hyperspectral data in the mineralogy have been documented by several researchers.[7-9] The hyperspectral measurements have been used by[10] to determine and differentiate between the iron ore types and ferruginous lithologic units in the Bahariya depression.The hyperspectral imaging was applied by Ref.[11] to map the clay minerals in Northwestern Algeria, using the Spectral Angle Mapper and the spectral signatures of illite and kaolinite.

This study aims at the mapping of the different chemical and environmental zones of the saline lakes of Wadi El Natrun and analyzes the salt minerals within each lake.

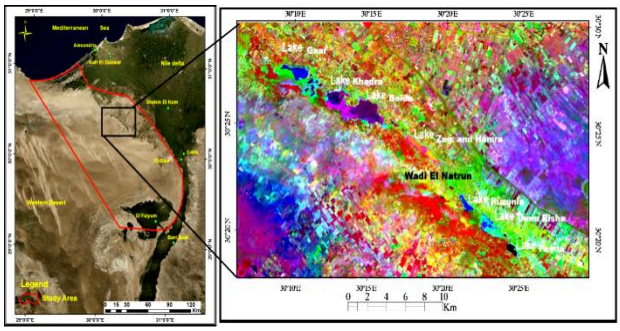

Figure 1. Location map of the Wadi ELNatrun lakes.

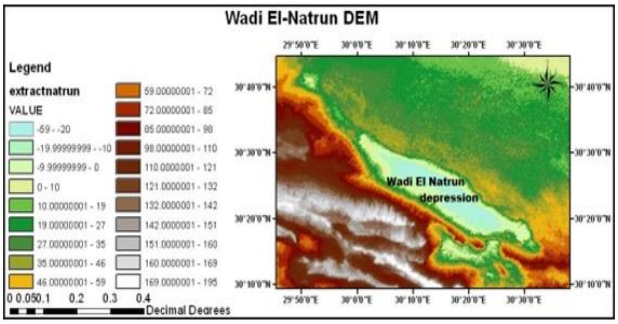

Figure 2. Digital Elevation Model (DEM) of Wadi El Natrun depression.

Geologic and morphotectonic evolution of Wadi El Natrun depression

Seven old branches of the Nile River have been illustrated by[12] using Radar Interferometry. Five of these branches have been deteriorated in the course of time, whereas two branches (Damietta and Rosetta) remain active at present. Along the westernmost part of the Delta, the ancient Canopic branch of the Nile River had silted up as a result of the re-excavation of the Bolbitic canal, which today forms the upper reaches of the Rosetta branch.[12] In this respect, the present passage of Wadi ELNatrun depression seems to be the path of the old Canopic branch. Therefore, the groundwater table is more or less closed to the recent Wadi El Natrun lakes. This is due to mixing of the old Nile bifurcation with the salt water preserved during the Miocene. Wadi El Natrun area comprises many rock units(Figure3) mapped by Ref[13].

The Mamura Formation is the basal rock unit in the sequence and it consists of interbedded fossiliferous shale, gypseous claystone, sandstone and limestone of lower Miocene age. It is followed upward by the Mikheimen Formation, which is formed of grey to yellowish grey conglomerates and conglomeratic sandstones of Miocene-Pliocene age. This section is overlain by the Gar El Muluk Formation of lower Pliocene age, a grayish to dark grey claystone with grey to greenish grey sandstones and few beds of yellowish white fossiliferous limestone.

The Gar El Muluk Formation is overlain by the Solymanya Formation that is of lower Pliocene age and consisting of greenish grey sandstones intercalated with fossiliferous limestone at the top. Upward in the sequence, the Kalakh Formation, which is a pink cross-bedded calcarenite with the karstified columnar structure at the top, is documented and depicts the Pliocene- Pleistocene age. The succession is capped by the Hamzi Formation, which represents the Wadi El Natrun facies with white porcelaneous and pink limestones that are underlain by conglomerates.

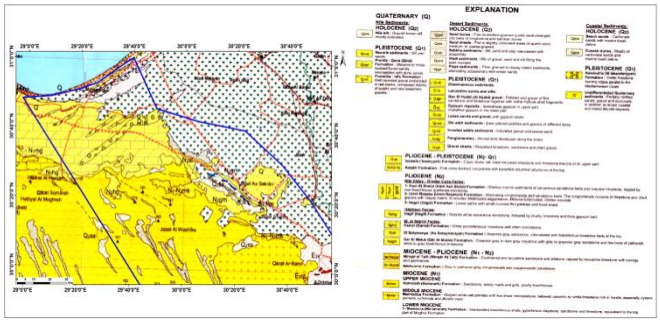

Figure 3. Geologic map of the study area,[13] the blue border shows the area of study.

The morphotectonic surface structure indicates repeated down-faulting towards the SW on the WNW- oriented normal faults. These are further transected by; (1) ENE- to NE-oriented folds of Late Cretaceous to Eocene age (The Syrian Arc Folds), (2) Oligocene to Early Miocene NW-SE trending faults, which were associated with a major uplifting movement to the south, (3) Late Miocene to Pliocene subsidence in the Nile Delta, which are localized along axis of the Nile Valley and controlled by N, NNW and NE oriented faults.[14]

METHODOLOGY

In the present study, the adopted methods to locate the saline lakes and analysis of their mineral potentiality are the remote sensing data (satellite and hyperspectral) and the chemical analyses of the salt minerals and deposits.

Remote sensing data

Satellite data

In the present study, the Landsat 8 (OLI) and Thermal Infrared Sensor (TIRS) images are processed and interpreted. The scene LC81770392016263LGN00, Path177, Row39, Acquisition date 19/9/2015 was used during this study. The data consists of nine spectral bands, with a spatial resolution of 30 m for bands 1 to 7 and 9. The approximate coverage area of such scene is 170 km N-S by 183 km E-W (106 miles by 114 miles). It contains seven spectral data in the visible, near infrared (VNIR) and shortwave infrared (SWIR) bands of the electromagnetic spectrum.

Hyperspectral data

Several field trips were conducted to visit the study area in different seasons. Intensive field work for ground truth using remotely-sensed data and aided by the geological map of the north Western Desert of Egypt[13] (UNESCO, 2006) was achieved. During these trips, representative samples from the various lithologies, lake's bottom sediments, salt deposits, as well as water samples from the Wadi El Natrun lakes have been collected for applying the analytical techniques. The ASD Field Spectroradiometer has been used for detecting different spectral measurements in the study area. The ASD device (Field Spec3) of Full-range detection capacity (350 nm– 2500 nm) has been used for this purpose. It provides uniform Vis/NIR/SWIR data collection across the entire solar irradiance spectrum.

Pre-processing of the remotely-sensed data

The Satellite data of Landsat 8 has been pre-processed for correcting the data from the atmosphere noises influence for valid and enhanced image processing. The pre-processing steps as radiometric calibration and atmospheric correction have been processed using the FLAASH method, Resolution merge and constructing mosaic pictures for the study area.

Moreover, the hyperspectral measurements were pre-processed by Quick Atmospheric Correction (QUAC) to define the atmospheric correction parameters directly from the observed pixel spectra in a scene without ancillary information. The QUAC is the best confident method producing reflectance spectra within a range of approximately 10 % of the ground truth.[15] These measurements were re-sampled to match the Landsat 8 bands after removing the bad and noise bands. The spectral measurements have been interpreted by using the Spectral Angle Mapper (SAM) and Maximum Likelihood Techniques (MLT). The SAM classification is an automated method that compares the spectral similarity between the used image spectra and the ASD measured spectra. It permits a rapid supervised classification as well as an accurate mapping.[16]

Chemical analyses

Selected 10 water samples and 10 salt samples from Wadi El Natrun lakes have been chemically analyzed for the major and trace elements, which are dissolved in saline water and constitute relatively the total salts in these lakes and their nearby Sabkhas. The analyses were conducted using XRF analysis in the Central Laboratory of the Egyptian Mineral Resource Authority (EMRA). The samples were diluted and prepared for measuring of the major elements and ions (e.g. Na, Ca, Mg, K, Cl, SO_4, NO_3, CO_3, HCO_3), and the trace elements such as Mn, Fe, Ni, Cu, Zn, Cd and Pb, total alkalinity of the saline water Lakes was also detected(Tables 1, 2, 3, 4).

RESULTS

Interpretation of the field work and lakes description

The saline lakes along Wadi El Natrun are distributed in a fluvial environment consisting of Hill slopes, Mud plains, and Perennial or Ephemeral Lakes. The Hill slopes form locations of active erosion and transportation of finer sediments to the close Mud plains.[17,18] The width of the Mud plains reaches up to 15 m and consists of fine siliciclastic sands and clays, commonly covered by vegetations. Ephemeral thin crusts of Natron and Halite salts occur interstitially within the Mud at the surface, between May and August.

During the field work, three distinct types of sedimentary deposits within the lakes are recognized; (1) clay-rich siliciclastic sediments deposited in a freshwater marsh environment, intercalated with organic materials, (2) compact Halite and Burkeite crusts, and (3) salt marshes composed of Aeolian quartz sands cemented by salts. The evaporates of the Miocene rocks exposed in the western end of the Wadi ELNatrun (Figure 4) and disappearing to the east in the depression. Several Quaternary structural elements such as fault scarps of NW-SE trend, normal faults of both NW-SE and NE-SW trends and NE–SW trending left-lateral strike-slip faults are also observed (Figure 5).

Figure 4. The evaporites of the Miocene rocks in the western end of Wadi ELNatrun.

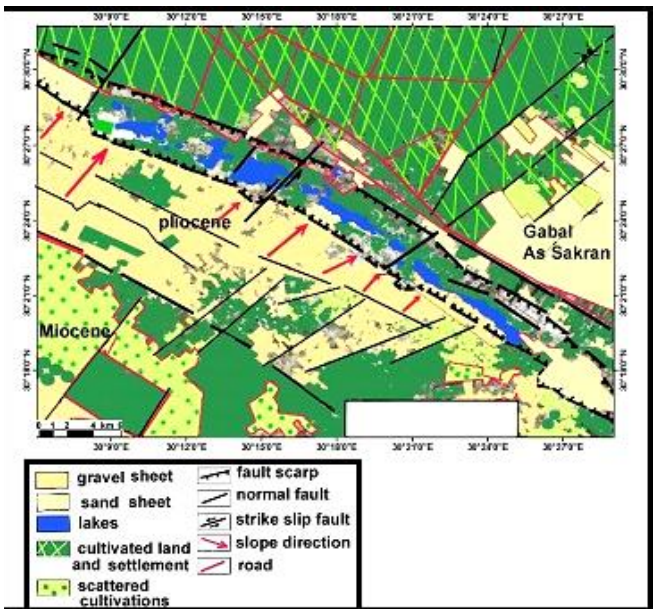

Figure 5. Morpho-structural map of the Wadi El Natrun area prepared from Landsat 8 image 2016.

Moreover, during the field work, a composite sketch diagram (Figure 6) for the Wadi El Natrun lakes has drawn. Field photographs for each lake, its lithology, and related geological features have been described as follows:

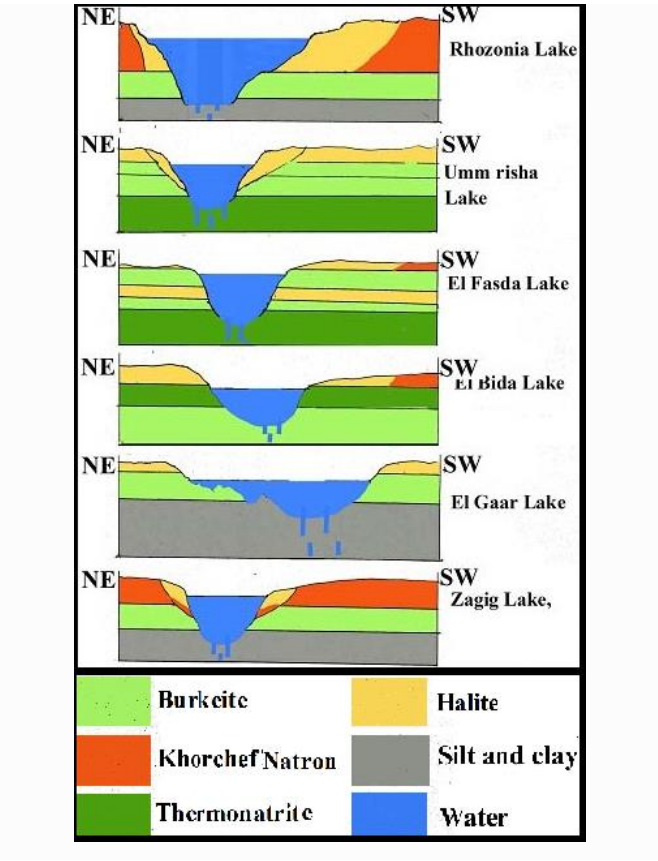

Figure 6. A composite sketch diagram illustrating the different lakes of the Wadi El Natrun and their related geological features, from N to S.

El Gaar Lake

It forms one of the biggest lakes in Wadi El Natrun area. It is never dry and contains permanently a water typical composition surrounded by Sabkhas, all over the year. Halite is an abundant salt component in the water of the lake along with Sabkha's precipitates. Other accessory salts of mixed carbonates and sulfates (Trona and Burkeite) are also recorded.

El Beida Lake

El Beida Lake area characterizes by white color, where it is almost dry with only limited water showings at the left of its center and edges due to variation in depths. The Sabkhas and salt precipitates consist of varicolored salt types occupying vast areas from the lake, which is exploited for Halite and Thenardite production.

Zug-Hamra Lakes

Zug and Hamra lakes are connected together by a small canal in the northwestern end of Zug Lake. They form together a longitudinal single lake. The water of the lake stands above a bottom surface of the evaporate deposits of Halite and Torona to a depth of a few centimeters. The Sabkha deposits and the salt precipitates extend across the entire width of the lake to a depth of 10 cm, consisting of thick deposits of Halite and sodium sulfates (Thenardite) surrounded by Kerchief deposits (Natron).

Lake Ruzounia (Razunia)

Ruzounia Lake has been worked for Halite salt production as the sulfate and carbonate salt minerals are found in the lower bedding altitudes, while the Halite salt is relatively dominant in the upper layers.

Figure 7. A hard Halite crust of Umm Risha Lake

Umm Risha Lake

Umm Risha is a shallow lake has pinkish brown water and has been explored for halite salt production. A hard crust of Halite is formed over a fluid mass of crystalline phases and brine within the lake. The Sabkhas of the lake show white, off-white, brown and pink colors of salts and Sabkhas (Fig.7). Pools are frequent where the water existed beneath the surface crust.

El-Fazda Lake

It is a fairly dry lake formed of a thin dark brown silty layer, followed upward by Halite and Burkeite precipitates, which is in turn covered by a massive pinkish white layer mostly composed of sodium carbonates (Natron) with traces of Halite and Trona.

Interpretation of the spectral measurements

The Spectral Angle Mapper (SAM) tool has been used for detecting and locating the sabkha and salt minerals in all of the investigated Lakes. These sabkhas and related salt minerals appear on the Landsat 8 image in pale blue color. The waters are represented by different shades of blue color ranging from navy and azure to indigo blue. Except for Ruzounia and Umm Risha Lakes, the waters therein are shallower and appear in teal blue color (Figures8a, 9a, 10a, 11a, 12a, 13a). Applying the Maximum Likelihood Technique, each lake has been classified into three environmental zones; saline water, salts and Marshlands (Figures8b, 9b, 10b, 11b, 12b, 13b).

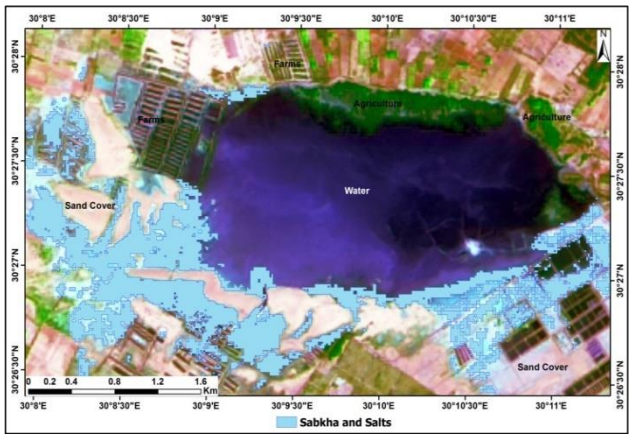

Figure 8a. SAM image of El Gaar Lake showing sabkhas and salts in pale blue color.

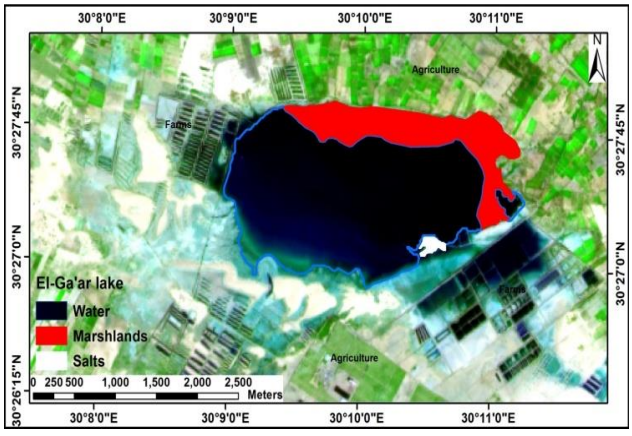

Figure 8b. Maximum Likelihood classification map of El Gaar Lake showing the different environmental zones.

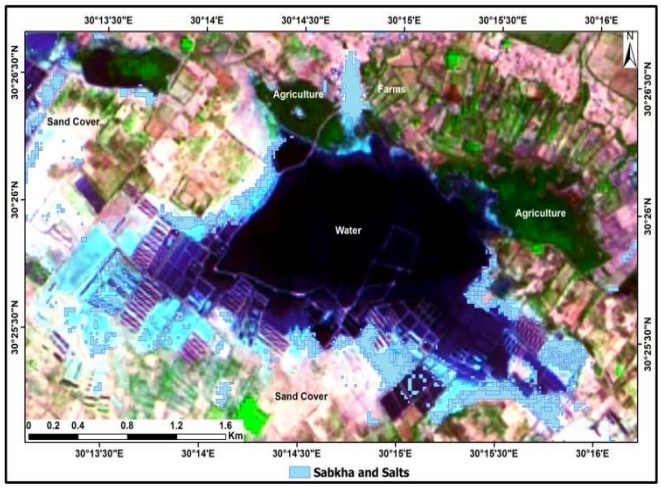

Figure 9a. SAM image of El Beida Lake showing sabkhas and salts in pale blue color.

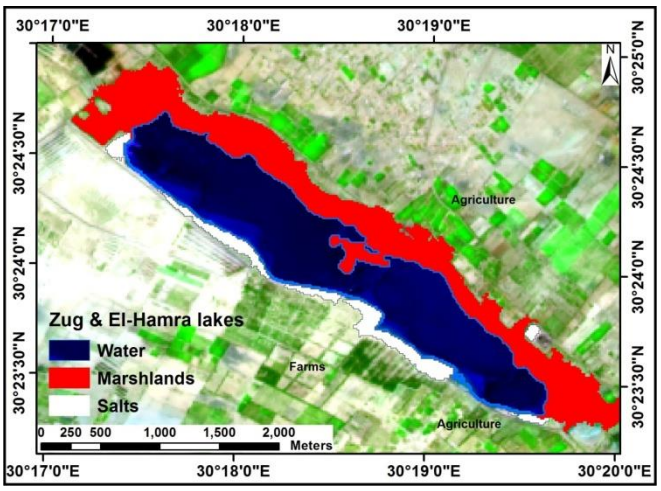

Figure 10b. Maximum Likelihood classification map of Zug-ElHamra Lakes illustrating the various environmental zones.

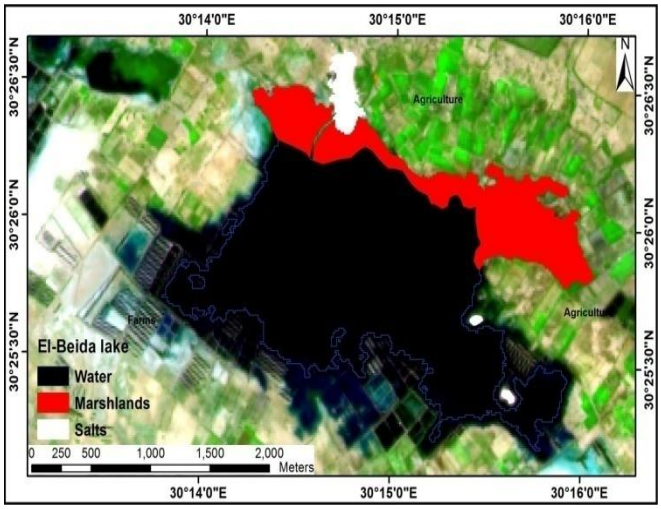

Figure 9b. Maximum Likelihood classification map of El Beida Lake.

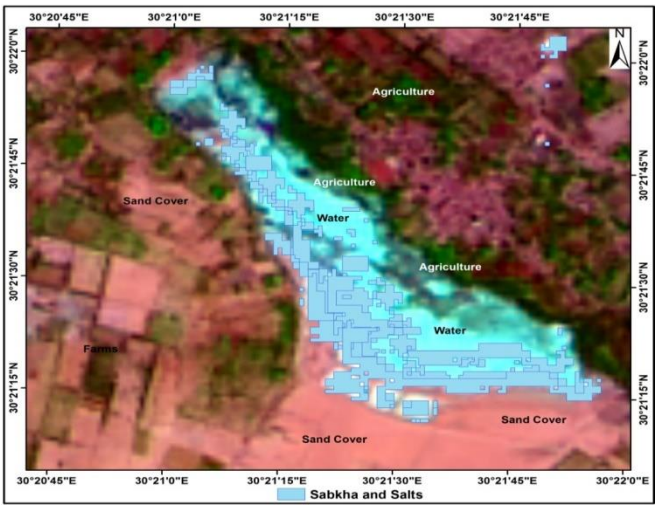

Figure 11a. SAM image of Ruzounia Lake showing sabkhas and salts in pale blue

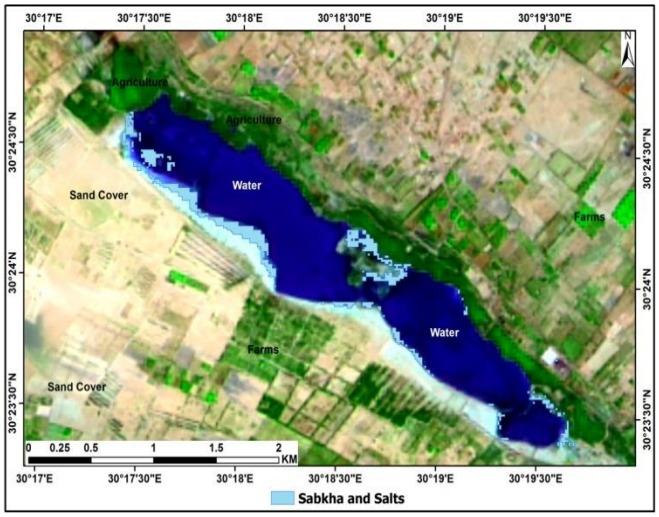

Figure 10a. SAM image of Zug-El-Hamra Lake showing sabkhas and salts in pale blue color.

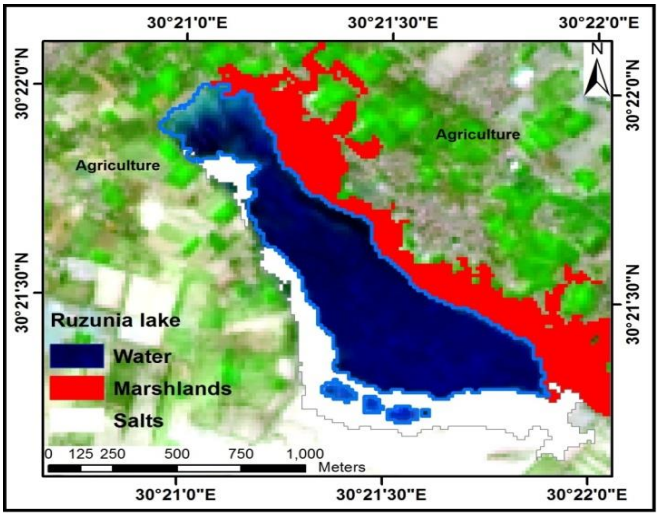

Figure 11b. Maximum Likelihood classification map of Ruzounia Lake.

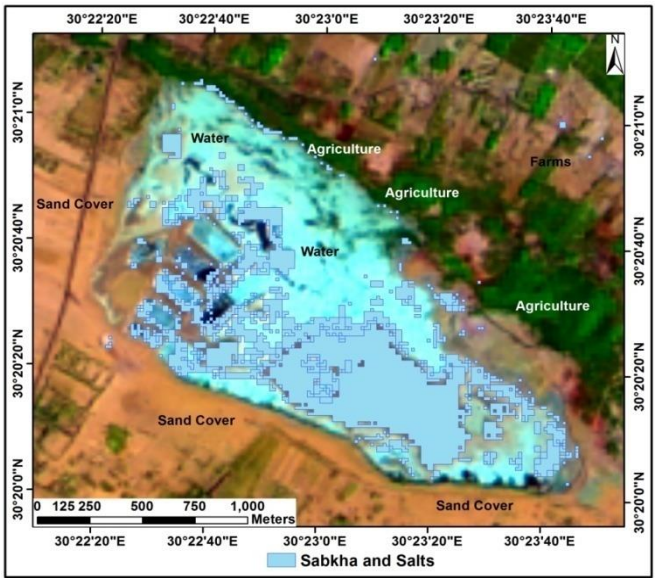

Figure 12a. SAM image of Lake Umm Risha showing sabkhas and salts in pale blue color.

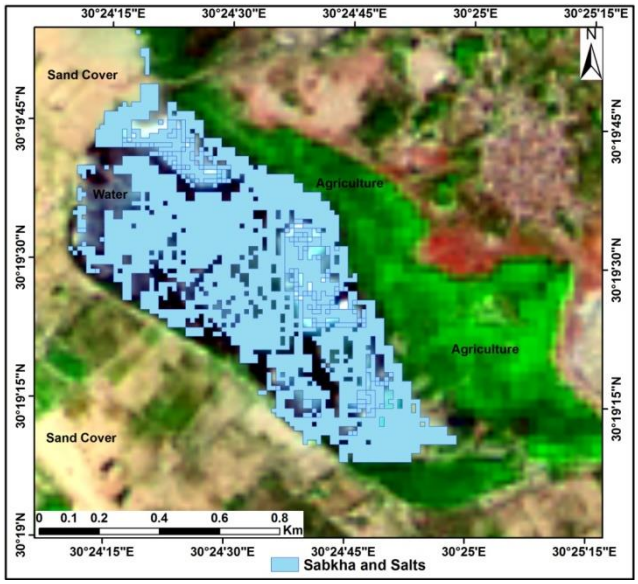

Figure 13a. SAM image of Lake El Fazda showing sabkhas and salts in pale blue color.

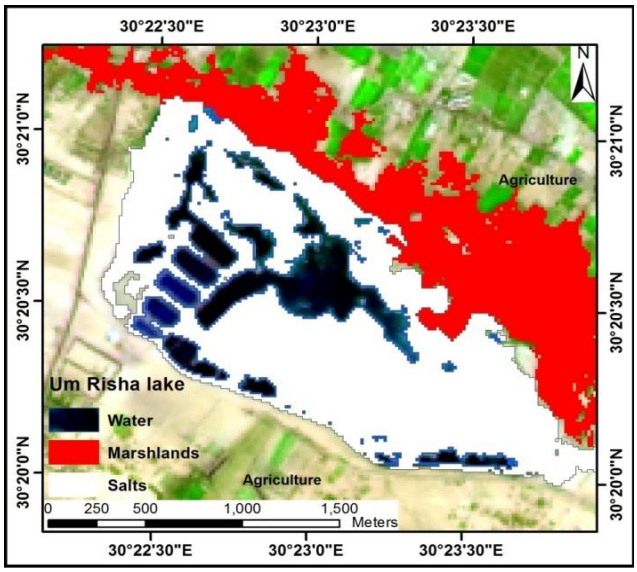

Figure 12b. Maximum likelihood classification map of Umm Risha Lake.

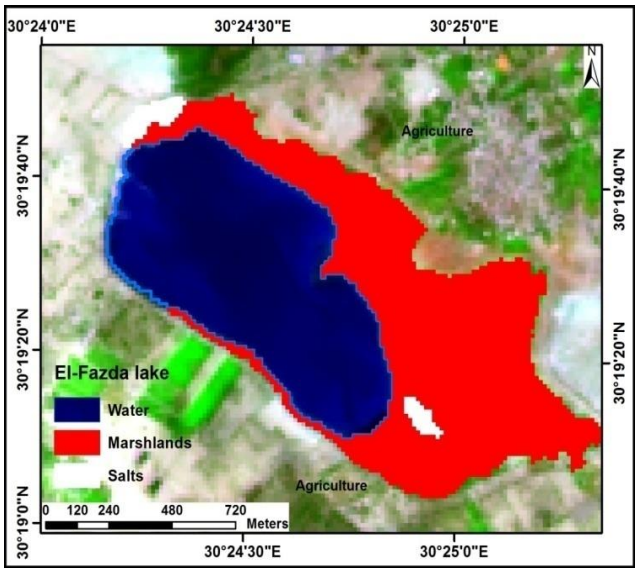

Figure 13b. Maximum Likelihood classification map of El Fazda Lake.

Chemical Analyses and Mineral Potentiality

The results of XRF analysis of the water and salt samples for major and minor elements were given in Tables 1, 2, 3, 4. The water analyses show an increase in Cl^- with the increasing of Na^+ and SO_4^{2-} coinciding with a decrease in Ca^{2+}, Mg^{2+}, and HCO_3^- in all lakes (Table 1), reflecting a predominance of Halite. In Wadi El Natrun brines, the minor elements (Table 2) shows that the concentration of Zn is much lower than that of Pb, indicating a significant loss of Zn from the surface water. The high concentration of Pb is due to the solution of Pb from the clastic material derived from surrounding weathered sediments. The metal concentrations decrease in the order Pb > Cu > Cd > Ni >Zn > Fe > Mn. This order is similar to the relative strength of the stability constants of the chloro-complexes of these metals except that of Cu which is higher than that of Zn (Table 3).

The salt analyses revealed abundance in Cl, Na, and K in all lakes, except Zug-El Hamra Lake, which shows low values of these elements. Rhozonia, Umm Risha, and El Beida lakes show a relative increase in sulfate-ion when compared to other lakes, which show normal values for these salts, suggesting a valid environment for the occurrence of sodium sulfate in the three lakes.

The content of carbonate-ion content is high in all lakes except in the Zug Lake, where it is low. The Ca-ion and Mg-ion are present in low amounts approximately in all lakes. This drop may be due to the precipitation of these elements as alkaline earth carbonates with an excess of hydrogen carbonate free of calcium and magnesium (Table 3). The increasing of Pb, Zn, Ni and Cd and in turn the decreasing of Fe and Mn in the salt samples is typical the behavior of these traces in salt samples have been originated from the saline water (Table 4).

Table 1. Chemical analyses of major elements (in ppm) in waters of Wadi El Natrun lakes.

Lake name	Na^+	Cl^-	Ca^{2+}	Mg^{2+}	SO_4^{2-}	NO_3^-	CO_3^{2-}	HCO_3^-	Total alkalinity
Rhozonia	279.6	86.4	n.d.	--	43.4	46.4	33.2	5.3	38.5
Rhozonia	279.6	86.4	n.d.	-	44.9	46.4	43.4	279.6	n.d
Umm Risha	291.5	92.3	n.d.		40.1	66.8	36.6	2.0	38.6
Umm Risha	281.4	81.0	0.02		37.8	13.9	36.7	1.9	38.7
Fazda	274.0	85.8	0.02	n.d.	48.1	88.6	37.9	0.7	38.7
Fazda	270.3	91.2	n.d.	n.d.	41.7	87.2	36.4	2.0	38.5
El Bida	154.4	74.5	n.d.	n.d.	27.0	41.1	17.9	n.d.	22.9
Gaar	155.3	56.6	n.d.	n.d.	24.8	43.1	20.6	n.d.	22.9
Gaar	155.3	59.2	n.d.	0.02	27.5	72.1	20.4	n.d.	22.7
Zug-El Hamra	30.2	12.7	0.03	0.004	9.0	40.2	0.2	0.0	0.29

Table 2. Chemical analyses of minor metal ions (in ppm) in waters of Wadi El Natrun lakes.

Lake name	Fe	Ni	Mn	Cu	Pb	Zn	Cd
Rhozonia	62	120	34	126	276	113	118
Rhozonia	70	115	31	130	199	110	118
UmmRisha	44	118	24	132	126	110	117
UmmRisha	12	119	2	127	176	110	119
Fasda	64	120	21	126	156	100	118
Fasda	60	118	2	128	114	100	119
Bida	63	116	35	130	242	116	119
Gaar	2	12	115	128	104	121	141
Gaar	11	117	2	128	161	106	119
Zug	5	—	3	128	277	103	120

Table 3. Chemical analyses of major elements in salts of Wadi El Natrun lakes.

Lake Name	Na^+	Cl^-	K^+	Mg^{2+}	SO_4^{2-}	CO_3^{2-}	Ca^{2+}
Rhozonia	279.2	89.40	86.4	6.40	100.0	79.6	1.6
Rhozonia	295.1	41.4	93.0	7.10	40.9	95.2	12
UmmRisha	221.5	96.8	92.3	6.80	210.1	91.5	1.5
UmmRisha	281.4	13.9	81.0	13.9	37.8	81.4	12
ElFasda	244.0	88.6	85.8	8.6	48.1	274.0	13
ElFasda	250.3	87.2	91.2	7.2	41.7	270.3	11
El Bida	154.4	41.1	74.5	1.1	27.0	154.4	11.
El Gaar	135.3	43.1	56.6	3.1	24.8	155.3	0.7
El Gaar	125.3	72.1	59.2	2.1	27.5	155.3	0.02
Zug	30.2	40.2	12.7	70.2	9.0	30.2	0.04

Table 4. Trace metal ion concentrations (ppm) in salts of Wadi El Natrun lakes.

Lake name	Fe	Ni	Mn	Cu	Pb	Zn	Cd
Rhozonia	53	110	46	110	280	120	93
Rhozonia	60	120	40	120	210	120	93
Umm Risha	33	98	22	120	115	140	80
Umm Risha	16	99	7	88	190	100	100
Fasda	70	90	20	110	160	100	90
Fasda	63	100	2	128	120	110	90
Bida	63	116	35	130	242	116	119
Gaar	2	12	115	128	104	121	141
Gaar	11	117	2	128	161	106	119
Zug	5	—	3	128	277	103	120

Discussion

Interpretation of the integrated hyperspectral measurements (applied by TIR and SWIR bands of Landsat 8) together with the field verifications and chemical analyses, were used to map the saline lakes of Wadi El Natrun and to differentiate between salt types and surrounding areas in each Lake as well as to define the different environmental zones (waters, marshland and sabkhas) within these lakes.

Ref[13] have described the geology of Wadi EL-Natrun depression as filled by Neogene clastic sediments in the Miocene-Pliocene age. These sediments were deposited in a river with fewer meanders and a greater slope gradient than the other branches of the Nile; and, thus got a larger part of the water passing through it. The distribution and origin of the saline water and salt minerals in Wadi El Natrun have been discussed by many authors. The origin of the lakes waters is suggested to be from the Nile water infiltrating through the sands and gravels forming the main strata separating Wadi El Natrun from the Nile River.[19] These percolating waters wash the salts from the rocks through which they travel and turn into weak brines. Hence waters that flow primarily through limestones usually produce brines rich in lime and carbonates, dolomite gives waters rich in magnesium and shales and sulfide-rich rocks yield sulfates.[20] The distinct spatial-temporal distribution of the salt minerals at Wadi ELNatrun area suggests emplacement by re-sedimentation rather than an authigenic or artifact origin.[21] Microbial mats grow periodically under a 1 mm thick layer of sand on the lake floors as well as along their margins 3. Due to the microbial propagations, the Perennial saline lakes appear in different colors. A model for salt differentiation have been proposed by Ref[22], as the water evaporates at 85 % of the starting volume; the first mineral Halite begins to precipitate. This continues and is joined by Burkeite and Nahcolite when the water is down to about 45 % and 30 % respectively. Since salinity of the lake's water is fluctuate between concentration and dilution due to the evaporation rates, the salt precipitation from the saline waters is seasonally controlled, depending on the salt types, grade of concentrations and the associated minor and trace elements in the saline waters. The salt minerals that precipitate during the evaporation sink to the bottom of the lakes forming solid crusts of mixed salts, which are often extensively extended outside the lakes.

Conclusion

The result of remote sensing, fieldwork, and analytical techniques enabled to an accurate mapping of the significant areas of the saline lakes, as well as characterizing the environmental zones of these Lakes and associated salt type of each Lake. The chemical analyses showed that the salts of sodium chlorides, sodium sulfates and sodium carbonates and bicarbonates are the most minerals accumulated and deposited in these lakes and surrounding areas with a dominance of Halite in all of the lakes. The chemical characterization and lithology of the saline lakes illustrated that El Rhozonia is the most economic Lake, as it includes the Halite salt in the upper layers and the sulfate and carbonate minerals in the lower bedding altitudes. Umm Risha Lake shows pink to reddish pink colors due to the presence of high sulfate and carbonate minerals in lower bedding altitudes, and high Halite content in the upper layers. El Fazda Lake contains a large thickness of sodium carbonates and Halite in the upper layers. El Bida Lake is also an economic salt lake as it comprises 72 % of Halite, 15 % Na_2SO_4, 6 % K_2CO_3 and 7 % Natron. El Gaar Lake is mainly dominated by Halite (~70 %), Na_2SO_4 is 8 %, K_2CO_3 10 %, and Natron 5 %. Zug-Hamra Lake comprises thick deposits of Na_2SO_4 and is surrounded by Kerchief deposits and overlain by Halite. The high concentrations of sulfate in El-Beida and Gaar Lakes are possibly due to the weathering of Miocene evaporates.

This study demonstrates the dominance of chloride ions in the saline water of Wadi El Natrun lakes suggesting that the source of these waters came from the Mediterranean Sea water that passed as seepage water through the NW-SE trending fractures to the lakes (Sea water intrusion). The saline waters of these lakes are composed of varied solute minerals and ions leached from the lithologies into which these waters pass to such lakes. These dissolved minerals have precipitated under certain conditions and limitations leaving deposits from the corresponding soluble salts in the floors of the lakes and their environs. The continuous evaporation of the waters under the climatic changes from the past (Pliocene) to the Present in temperatures, pH of the water and morphology of the lakes, which became more shallower, led to the deposition of salt types under the present conditions are different from those Natron salts that were deposited and dominated in the past and gave the name Natrun to the Wadi El Natrun itself. Now, there is abundance and dominance of Halite, mixed carbonates and sulfates (Burkeite and Thenardite) with some sodium sulfates at the expense of the Natron salts which are found as relics in low quantities in some lakes.

The results of this study appreciate the role of remote sensing detection of the salt minerals as a cost-effective alternative method in salt minerals exploration in Egypt, and in similar settings worldwide.

Acknowledgments

Great thanks to the National Authority for Remote Sensing and Space Sciences (NARSS) for providing the hyperspectral data and chemical analyses used during this study.

References

[1]Abdallah, A.Y., Petrology of some Pliocene-Recent Rocks in Wadi El Natrun, Beni Suef Area, Egypt. M.Sc. Thesis, Faculty of Science, *Ain Shams University, Cairo, Egypt* **1970.**

[2]Said, R. Geomorphology chapter 2 in: The Geology of Egypt, Edited by R. Said. *Balkema, Rotterdam.***, 1990,** 9-26.

[3]Taher, A., Inland saline lakes of Wadi El Natrun Depression, Egypt. Intern. *J. Salt Lake Res.***1999,** *8*, 149-169. doi: 10.1007/ BF02442128.

[4]Shortland, A.J., Degryse, P., Walton, M., Salou, L., The evaporitic deposits of Lake Fazda (Wadi Natrun, Egypt) and their use In Roman glass production. *J. Archaeometry*, **2011,** *53*, 916-929. doi: 10.1111/j.1475-4754.2010.00573.x

[5]Bolis, S.N., Comparative Mineralogic study of the "Korchef" Saline Deposits of Wadi El-Natrun, Egypt, U.A.R. M.Sc. Thesis, *Faculty of Science, Ain Shams University, Cairo* **1969.**

[6]Imhoff, J.E, Sahl, H.G., Soliman, G.S.H., TriJper, H.G., The Wadi Natrun: Chemical composition and Microbial Mass Developments in Alkaline Brines of Eutrophic Desert Lakes. *Geomicrobiology,* **1979,** *1*(5), 219-234. http://dx.doi.org/10.1080/01490457909377733

[7]Goetz, A.F., Srivastava, V., Mineralogical mapping in the Cuprite mining district, Nevada. *Third Annual JPL Airborne Geoscience Workshop*. Vol1: AVIRIS Workshop; **1985,** p 147–149.

[8]Kruse F. A. Use of airborne imaging spectrometer data to map minerals associated with hydrothermally altered rocks in the northern grapevine mountains, Nevada, and California. *Remote Sens Environ.*, **1988,** *24(1):* 31–51. https://doi.org/10.1016/0034-4257(88)90004-1

[9]*Zhang, X.*, Li, P., Lithological mapping from hyperspectral data by improved use of spectral angle mapper. *Int. J. Appl. Earth Obs. Geoinf.*, **2014**, *31*, 95-109. doi.org/10.1016/j.jag.2014.03.007

[10]Salem, S.M., ASD field hyperspectral measurements for discrimination of the ferruginous rocks and the iron ore types at El Gedida-Ghorabi area, Bahariya Oasis, Western Desert, Egypt. *Arab. J. Geosci,.* 2016,10:166. DOI 10.1007/s12517-017-2944-x.

[11] Zazi, L. Boutaleb, A., Guettouche, M. S., Identification and mapping of clay minerals in the region of Djebel Meni (Northwestern Algeria) using hyperspectral imaging, EO-1 Hyperion sensor. *AJS,* **2017**, *10:* 252. DOI 10.1007/s12517-017-3015-z

[12]Cherif, O., Gabr, S. El Bastawesy, M., and El Saadawi, O., Evaluation of subsidence in the Nile Delta by using Radar Interferometry. *STDF project cooperation between NARSS with Michigen University (US), final report***, 2016.**

[13]UNESCO**,** The geological map of Egypt. *Project Capacity Building for the Egyptian Geological Survey and National Authority for Remote Sensing and Space Sciences, Egypt***, 2006.**

[14]EGPC**.** Nile Delta & North Sinai: Fields, Discoveries and Hydrocarbon Potentialities (*A Comparative Overview). EGPC, Cairo, Egypt***, 1994.**

[15]Bernstein, L.S., Adler-Golden, S.M., Jin, X., Gregor, B., Sundberg, R.L., Quick atmospheric correction (QUAC) code for VNIR-SWIR spectral imagery: Algorithm details. In Hyperspectral Image and Signal Processing *(WHISPERS), 4th Workshop* **2012**, 1-4. https://doi.org/10.1109/WHISPERS.2012.6874311

[16]Hunter, E.L., Power, C.H., An assessment of two classification methods for mapping Thames Estuary intertidal habitats using CASI data. *Int. J. Remote Sens.***, 2002,** *23*, 2989-3008. doi/pdf/10.1080/01431160110075596

[17]Eugster, H.P., Hardy, L.A., Saline lakes, in Lakes; chemistry, geology, physics. *(ed. A. Lerman), Springer-Verlag, New York*, **1978.**

[18]Renaut, R.W., Long, P.R., Sedimentology of the saline lakes of the Cariboo Plateau, Interior British Columbia, Canada. *Sedim. Geol*. **1989,** *64*,239–364. https://doi.org/10.1016/00370738(89)90051-1

[19]Atia, A. K. M., Hilmy, M. E., Bolous, S. N., Mineralogy of the encrustation deposits of Wadi E1 Natrun. *Desert Institute Bulletin*. **1970,** *2*, 301-325.

[20]Warren, J., Evaporites; their evolution and economics, *Blackwell Science, Oxford*, **1999.**

[21]Stanley, D. J., Sheng, H., Trona in Nile Cone Late Quaternary sediments: Probable redepositional origin. *Marine Geology*, **1979**, *31(1-2):* M21-M28. https://doi.org/10.1016/00253227(79)90049-5

[22]Shortland, A.J., Evaporites of the wadi natrun: seasonal and annual variation and its implication for ancient exploitation. *J. Archaeometry*, **2004,** *46*,497–516. DOI: 10.1111/j.14754754.2004.00170.x

Received: 20.11.2017.
Accepted: 08.04.2018.

A CONVENIENT COST-EFFECTIVE METHOD FOR RECYCLIZATION OF THE AQUEOUS WASTE EFFLUENTS OF CAR-PAINTING INDUSTRY

László Kótai,*[a,b] Tünde Kocsis,[a] Anna Jánosity,[a] Imre Kovács,[c] Kalyan K. Banerji[d] and Anna Mária Keszler[a]

Keywords: car-painting rinsing water; recycling; purification; coagulation;

Non-sedimentation nanoparticles containing alkaline wastewater as effluent from the cleaning process of car-painting lines can be purified by sedimentation after adding of mineral acids to adjust the pH below 5. Using 10 % aq. sulfuric acid to coagulate and filtrate the colloid particles, and adjusting the effluent pH with 10 wt. % aq. NaOH to the original value (~9), the wastewater can be recycled with ca. 0.3 % salt content into the cleaning process of the painting line (rinsing) technology.

* Corresponding Authors
E-Mail: kotai.laszlo@ttk.mta.hu
[a] Research Centre for Natural Sciences, Hungarian Academy of Sciences, Magyar Tudósok krt. 2., Budapest, H-1117, Hungary.
[b] Deuton-X Ltd., H-2030, Érd, Selmeci u. 89.
[c] Nógrád Chemical Works, Tolmács, Arany J. u. 2.
[d] J.N.V. University, Jodhpur 342005, Rajasthan, India.

Introduction

During the paint processes in car plants, the paint to be applied to the car bodies are changed frequently. To avoid intermixing of different colors the application systems has to be cleaned before every change by means of a rinsing liquid.[1] These rinsing waters are recycled based on an evaporation or a fractionated condensation process with the treatment of the condensates.[2] The energy demand of evaporation, however, initiated finding new possibilities, like the oxidation processes, for example with ozone, ozone combined with hydrogen peroxide, photo-Fenton treatment, and coagulation-flocculation methods as well.[3] The aqueous rinsing liquids, however, contains not only the pigment particles but some organic components like butyl glycol or tensides as well, thus oxidation processes destroy these components. The bacterial treatment of these type of wastewaters is time consuming and further treatments are needed to recycle the purified water into the technological processes.[4]

The aim of the present study was the development of a simple and cost-effective method to remove the suspended solids and recycling the cleaning liquid into the car-painting plant with coagulation technique without using oxidants, bacteria, and high-cost evaporation processes.

Experimental

The wastewaters (two samples were taken at the same time in every day for 6 days (6x2 black sample (1a,b-6a,b) and 4x1 purple samples (7-10)) were taken from an operational car-painting line washing liquor. The samples were stored for 2 weeks without the appearance of any sedimentation. The neutralization was done with 1 M HCl or H_2SO_4 and 1.5 M HNO_3 solutions. In the experiments performed with H_2SO_4 (1M, ~10 %), a sample was selected which had the highest acid consumption and the amount of sulfuric acid (1.50 % toward the wastewater sample) required to reach the pH 4 was determined. This amount of 10 % aq. sulfuric acid was used to acidify the all other further samples. The acidified samples were filtered with filter paper, the filter cake was dried and weighted, then the filtrate was treated with 10 % aq. NaOH to control the pH to near the starting value. The adjustment of pH was done with using standard pH meter.

All the chemicals used were supplied by Deuton-X Ltd, Hungary. X-ray powder diffractograms were recorded using a Philips PW-1050 Bragg-Brentano parafocusing goniometer. It was equipped with a Cu tube (40 kV and 35 mA), a secondary beam graphite monochromator and a proportional counter. Scans were recorded in step mode. The diffraction patterns were evaluated by full profile fitting techniques.

Results and Discussions

The starting pH values of the samples were varied between 8.86 and 9.37 and there was no observed sedimentation in a week. The stable colloid state is supposed to be due to hydroxide ion adsorption and repulsion of negatively charged nanoparticles. According to this, compensation of negative charges was expected to initiate aggregation and sedimentation by adding different mineral acids. The results can be seen in Table 1.

As it can be seen from Table 1, the nitric acid cannot decrease the pH to the level available with HCl or H_2SO_4 due to its oxidative nature and consumption of the acid for oxidation of some organic contaminant. therefore, using nitric acid is not suggested. Since the HCl and H_2SO_4 solutions gave almost the same results, and because the sulfuric acid is much cheaper than aq. HCl, only the sulfuric acid was used in the further experiments.

Table 1. Effects of mineral acids on car painting wastewater sedimentation ability

Wastewater (200 mL) , initial pH=8.65	**1 M HCl**	**1.5 M HNO**	**1.5 M HNO_3**	**1 M H_2SO_4**	**1 M H_2SO_4**
	Sample 1	**Sample 1**	**Sample 2**	**Sample 1**	**Sample 2**
Added acid amount	4.6 mL	3.0 mL	2.9 mL	2.8 mL	2.9 mL
pH after acid addition	4.6	4.6	5.25	4.6	4.2
Amount of dry precipitate, g	2.56	2.55	2.52	2.56	2.53
Filtrate, pH	5.0	6.0	5.5	6.0	5.2
NaOH added, 10% (wt.), in mL to reach pH =8.63	1.2	1.1	1.2	1.0	1.0

Table 2. Results of sulfuric acid precipitation and re-alkalization of the car-painting plant aqueous effluents.

Sample	**Initial pH**			**Dry material. % (wt.)**	**V_{NaOH}/V_{H2SO4}**
	Initial value	**After acid addition**	**After NaOH addition**		
1a	8.86	3.88	8.89	0.85	1.00
1b	9.08	3.81	9.17	0.85	1.07
2a	9.01	4.01	8.98	0.86	1.00
2b	9.04	3.91	8.92	0.85	1.00
3a	9.37	2.23	9.25	0.33	1.13
3b	9.37	2.24	9.20	0.33	1.07
4a	9.36	2.23	9.36	0.33	1.13
4b	9.33	2.30	9.38	0.33	0.97
5a	9.36	2.29	9.44	0.33	1.13
5b	9.35	2.26	9.22	0.33	1.10
6a	9.07	4.13	9.07	0.84	0.97
6b	9.09	4.02	9.11	0.83	1.00
7	8.90	2.76	9.09	0.78	1.13
8	9.04	3.70	9.07	0.86	1.00
9	9.26	3.55	9.06	0.98	1.00
10	9.26	3.90	9.21	0.98	1.00

Use of 10 % aq. sulfuric acid to neutralize the surface-bound hydroxide ions with the hydroxonium ions, resulted in a fast aggregation, and sedimentation of the particles was observed below pH 5. Depending on the composition of the wastewaters, the same amount of sulfuric acid resulted in different pH values, therefore 1.5 % amount of a 10 % (wt.) sulfuric acid was used in every case, and the pH values found after acid addition can be seen in Table 2.

The aggregated solids could easily be filtered in every case. The amount of the wet filter cake and the dry solid residue are also given in Table 2.

The reaction mixtures were filtered and the filter cake was dried in air at room temperature, then the filtrate was treated with 10 % aq. NaOH to adjust the pH near the initial pH value of the wastewater. Comparing the ratio of 10 % aq. NaOH volume toward the previously used 10 % aq. H_2SO_4 volume clearly shows that this value was varied between 0.97 and 1.13, thus the salt amount forms in the system is below 0.3 %. This low salt content permits to recycle the treated and alkalinized cleaning liquid into the original technology.

Two cubic meters of wastewater was treated with 1.5 % amount of 10 % aq. sulfuric acid, then after filtering and alkalinizing with 1.5 % aq. NaOH, the operating painting line could use that in a usual way without appearance of any adverse effect.

The solid residues removed by filtration were proved to be X-ray amorphous, but their heat treatment at 500 and 1000 °C led to the crystalline calcite ($CaCO_3$) and wollastonite ($CaSiO_3$), respectively. (Heat treatment was used to compact the volume/amount of solid residue). Some amount of amorphous materials was also detected in both heat-treated samples (Supplementary Figures 1 and 2). The reason for the difference in the phases observed at 500 and 1000 °C is that the amorphous SiO_2 particles can react above 500 °C with $CaCO_3$ and results in the formation of $CaSiO_3$. A small amount of TiO_2 was also found, but TiO_2 can react in an analogous way with $CaCO_3$ as the SiO_2 but with the formation of $CaTiO_3$.

In order to eliminate/diminish salt-formation and accumulation of these salts in the purified cleaning liquid, a solid tertiary-amine based ion-exchange (solid base) technology has just been studied and tested to neutralize the sulfuric acid content of the cleaning liquid.

Conclusion

Nanoparticles containing alkaline wastewater from the car-painting factories can be purified with an addition of 10 % aq. sulfuric acid to coagulate the colloid particles, and the effluent can also be recycled with ca. 0.3 % salt content into the cleaning process after filtration of the solid sediments and adjusting the pH with the same amount of 10 % aq, NaOH as the amount of sulfuric acid solution was used.

References

[1]Wilhelm, F., Recycling of water-based paint, *Metal Finishing*, **1993**, *91(10)*, 23-29

[2]Baumann, W., Dinglreiter, U., Method for reprocessing and recycling of aqueous rinsing liquids from car painting with water-based paints in automobile industry, *Heat and Mass Transfer/Waerme- und Stoffuebertragung*, **2011**, *47(8)*, 1043-1049; DOI: 10.1007/s00231-011-0861-1

[3]Consejo, C., Ormad, M. P. Sarasa, J., Ovelleiro, J. L., Treatment of wastewater coming from painting processes: Application of conventional and advanced oxidation technologies, *Ozone: Sci. Eng.*, **2005**, *27(4)*, 279-286. DOI: 10.1080/01919510591006274

[4]Stoffels, M., Amann, R., Ludwig, W., Hekmat, D., Schleifer, K.-H., Bacterial community dynamics during start-up of a trickle-bed bioreactor degrading aromatic compounds, *Appl. Environ. Microbiol*., **1998**, *64(3)*, 930-939.

Received: 10.04.2018
Accepted: 23.04.2018.

PROTECTION OF FEMALE C3H MICE AGAINST WHOLE-BODY γ-IRRADIATION WITH 2,3-DIMETHYL-6-((2-DIMETHYLAMINO)ETHYL)-6*H*-INDOLO[2,3-*b*]QUINOXALINE (B220)

Tim Hofer[a, b]* and Lennart Möller[a]

Keywords: development, lethal dose 50 % (LD_{50}), 3,3'-diindolylmethane (DIM), reactive oxygen species (ROS), radical, radioprotector

Radioprotection by 2,3-dimethyl-6-(2-(dimethylamino)ethyl)-6*H*-indolo[2,3-*b*]quinoxaline (B220) on survival and growth of female C3H mice exposed to acute whole-body gamma-radiation was evaluated for 7.5-8 months following irradiation in two separate experiments. For adult (12 weeks old) mice, B220 administration increased median survival after 8 Gy by a factor of 1.27 when given within 24 h pre-irradiation, administration up to 24 h post-irradiation had a similar effect (1.20) but in addition resulted in 1 of 9 (11 %) mice alive after 32 weeks. For adult mice irradiated with 10-14 Gy, B220 had no significant effect on survival. For very young mice (4 weeks old), however, B220 administration within 24 h pre-irradiation protected from growth retardation at both 1 and 6 Gy, and from gray-hairing at 6 Gy. In conclusion, the well tolerated drug B220 offered radioprotection in both studies and its administration could be further optimized.

* Corresponding Authors
E-Mail: Tim.Hofer@fhi.no
[a] Analytical toxicology and clinical applications, Department of Biosciences and Nutrition, Karolinska Institutet, 141 83 Huddinge, Stockholm, Sweden.
[b] Present address: Norwegian Institute of Public Health, Department of Toxicology and Risk Assessment, Oslo, Norway.

INTRODUCTION

Ionising gamma (γ)-irradiation causes radiation damage in biological organisms. Reactive species are produced through radiolysis of water (e.g. $HO^{\bullet}$, $H^{\bullet}$, e_{aq}^{-}) and ionization of biomolecules such as proteins, DNA and lipids make them prone to reactions with molecular oxygen (O_2).[1,2] The damage (disintegration and oxidation of organic molecules) initiates an inflammatory response with attacking neutrophils (granulocytes, monocytes and macrophages) releasing various reactive oxygen species (ROS).[1,2]

Drugs initially found to protect from γ-irradiation, such as sulfhydryls[3] and WR-2721 (amifostine)[4] give side effects at high doses or offer limited protection in certain organs (e.g. the central nervous system).[1,5] More recently, however, some interesting examples have been reported including flavonoids,[6] caffeine,[7] α-TMG (vitamin E analog),[8] *Mentha arvensis* (mint),[9] 5-androstenediol,[10] Tempol,[11] molecular hydrogen (H_2) containing water,[5] Ex-Rad™,[12] JNJ7777120 (indole),[13] and particularly the recently studied indole 3,3'-diindolylmethane (DIM; derived from ingestion of indole-3-carbinol found in cruciferous vegetables such as cabbage, Brussels sprouts and broccoli) that offered astonishing radioprotection also at very high doses (up to 13 Gy) both *in vivo* and in cell culture.[14]

The synthetic indole-drug 2,3-dimethyl-6-((2-(dimethylamino)ethyl)-6*H*-indolo[2,3-*b*]quinoxaline (B220, structure shown in figure 1) has been found to be well tolerated, having preventative effects on growth of 12-*O*-tetradecanoylphorbol-13-acetate (TPA) promoted skin tumours *in vivo* possibly by interfering with enzymes involved in the generation of ROS in the inflammatory response to TPA,[15] and was found to downregulate phagocyte NADPH-oxidase activity *in vitro*, inhibiting release of ROS, by affecting signalling downstream of protein kinase C (PKC).[16]

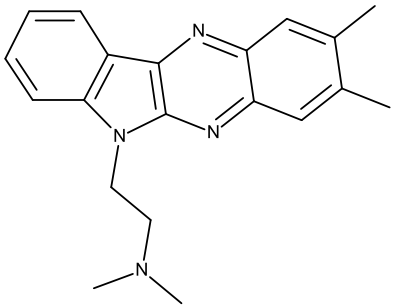

Figure 1. 2,3-Dimethyl-6-((2-dimethylamino)ethyl)-6*H*-indolo-[2,3-*b*]quinoxaline (B220).

Based on these protective roles of B220 on reducing ROS production, the aim of this study was to test if B220 would have any protective effect on γ-irradiation *in vivo*. Mortality, weight gain (growth) and other possible complications was investigated after whole-body γ-irradiation of C3H female mice given B220 intraperitoneally (*i.p.*) at a dose similar to those used in some previous radioprotector studies.[7,9]

RESULTS

Study I: adult (12 weeks old) mice exposed to 0-14 Gy

As shown in Table 1 and Figure 2, at high doses γ-radiation (10, 12, 14 Gy) all the 12 weeks old mice had died after 13 days and no effect of B220 was seen. A sharp threshold for survival was noticed between 6 and 8 Gy: nearly all mice exposed to 6 Gy survived (one animal in the

6 Gy control group died 31 weeks after irradiation) during the investigated period over 32 weeks (7.5 months) following irradiation, but most mice exposed to 8 Gy died within 25 days. At 8 Gy, pre-administration of B220 increased the median survival time by 27 % (from 15 to 19 days). B220 given post-irradiation increased the median survival time by 20 % (from 15 to 18 days) and in addition resulted in 11.1 % long-term survival as one mouse was still alive at the end of study (this mouse became gray-haired 10 weeks after irradiation, at age 23 weeks).

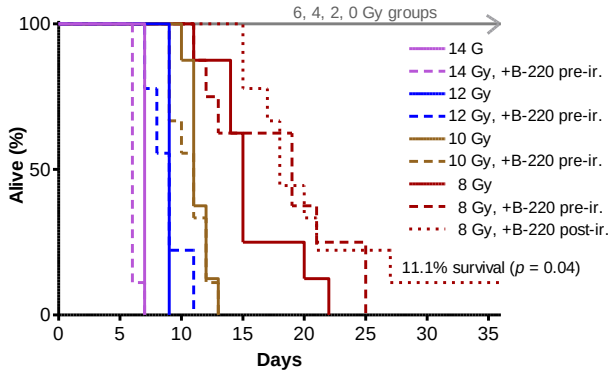

Figure 2. Survival curves as % alive for adult (12 weeks old) female C3H mice exposed to 0-14 Gy whole-body γ-radiation.

The Gehan-Breslow-Wilcoxon survival curve analysis test showed that administration of B220 post-irradiation significantly increased the survival compared to no B220 administration at 8 Gy (p=0.04). The 6 Gy mice developed gray-haired skin 11 weeks after irradiation, at age 24 weeks.

Table 1. Lethality and effect of B220 upon whole-body γ-irradiation of adult (12 weeks old) female C3H mice followed for 32 weeks.

	Median survival in days			Effect of B220
Gy	Control	+B220 pre-ir.	+B220 post-ir.	
14	7 (N=8)	6 (N=9)	-	none
12	9 (N=8)	9 (N=9)	-	none
10	11(N=8)	11(N=9)	-	none
8	15 (N=8)	19 (N=8)	18 (N=9)	pre-ir: 27 % increase post-ir.: 20 % increase and 11 % long time survival
6	one death after 31 weeks (N=8)	no death (N=9)	-	none
4	no death (N=8)	no death (N=9)	-	none
2	no death (N=8)	no death (N=9)	-	none
0	no death (N=8)	no death (N=8)	-	none

Mice in the 4, 2 and 0 Gy groups all survived and had not become gray-haired at end of the study. Mean body weights for the 17 groups at the beginning of the study (12 weeks old) lay in the range 23.3-26.5 g. At the end of study, mean body weights in surviving groups (6, 4, 2 and 0 Gy) lay in the range 34.7-41.8 g and no significant effect due to irradiation could be seen among groups not administrated B220. Also, B220 had no effect on weight gain in these groups.

Study II: 4 weeks old mice exposed to 0, 1 and 6 Gy

As shown in figure 3, both 1 and 6 Gy retarded growth for the very young mice compared to non-irradiated mice. On the day of irradiation, the six groups' mean weights were 12.6-14.6 g. After rapidly gaining weight, average weights were 29.0-38.9 g at week 36 (8 months after irradiation, at 9 months of age), reflecting a 209-285 weight % increase versus the day of irradiation depending on group (Figure 3A). The weight % data for both individual mice and as group means could be well fitted to two-phase association curves (Figure 3A).

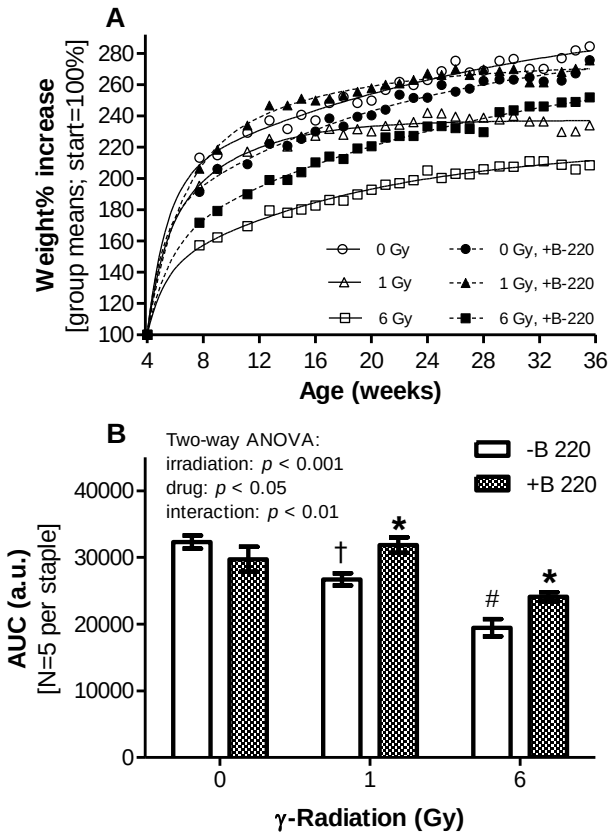

Figure 3. Effect of whole body γ-irradiation (0, 1 and 6 Gy) and B220 pre-administration on growth of 4-week-old female mice. Data shown as averages in A and means ± SEM in B.

Calculation of area under curve (AUC) values for the individual mice (N=5 per group) allowed statistical comparisons among groups. Analysis using two-way ANOVA (Figure 3B) determined that growth was overall retarded due to radiation ($p < 0.001$), that B220 exerted a protective effect ($p < 0.05$) and that there was an interaction between radiation and B220 ($p < 0.01$), thus that B220 counteracted growth retardation due to irradiation. The Bonferroni post test (*) identified protection by B220 at both 1 ($p < 0.05$) and 6 Gy ($p < 0.05$). At 0 Gy, however, B220 administration had no effect on weight gain. One-way

ANOVA analysis of groups not administered B220 showed that growth was retarded at 1 Gy ($p < 0.05$ (†)) and that 6 Gy affected growth even more ($p < 0.05$ (#)). At 6 Gy, the mice developed gray-haired skin about 18 weeks after irradiation (at age 22 weeks) and B220 reduced the degree of gray-hairing (visual observation). One mouse in each of the 6 Gy groups died 25 weeks after irradiation (for AUC calculations their weights were assumed constant until the end of study).

Toxicity of B220

No signs of clinical toxicity were seen after two i.p. administrations of B220 at 25 mg kg^{-1} body weight doses (in total 50 mg kg^{-1} body weight) with a gap of 22 h in between. Topical administration of 1 mg B220 alone twice a week for 20 weeks had previously not shown any apparent toxicity.[15]

DISCUSSION

This study provides detailed information regarding mortality and growth of female C3H mice after acute γ-irradiation. For adult mice (Study I), B220 showed protective effects at 8 Gy (Figure 2) when administrated 24 and 2 h before, or, 2 and 24 h after, irradiation. For 4 weeks old mice (Study II), B220 counteracted growth retardation at 1 and 6 Gy (Fig 3) and decreased gray hairing of skin at 6 Gy. For 4 weeks old mice, 1 Gy caused adverse developmental effects on growth, whereas further weight gain in adult mice was not affected by as much as 6 Gy. At 6 Gy, both the 12 and 4 week old mice became gray-haired at about the same age (at 24 and 22 weeks of age, respectively), thus the adult mice became gray-haired considerably sooner after irradiation.

Regarding drug administration pre- or post-irradiation for optimal protection from γ-radiation damage, studies by others have found that both ways can work. Dosing with DIM either before or up to 24 h after irradiation protected rats from lethal irradiation doses up to as high as 13 Gy.[14] The time-point of drug administration may indeed play a role. In a study on 7-8 week old C57BL/6 mice exposed to 8 Gy whole-body γ-irradiation, switching to a diet high in antioxidant supplements 24 h after the irradiation event significantly increased the survival and was considerably more efficient than when beginning the antioxidant administration 12 or 48 h after irradiation.[17] The reason for this is unclear. Also the dose and frequency of administration can play a role. For the two flavonoids orientin and vicenin, both worked better as radioprotectors at 50 than at 75 or 100 μg kg^{-1} body weight.[6] Maximum protection was achieved by administration 30 min before irradiation, injection at other time points (2 or 1 h before, or 30 min after) offered less protection.[6] DIM, however, offered better protection at 75 mg kg^{-1} body weight than at lower doses when administered on 14 consecutive days after irradiation to 13 Gy.[14]

Mechanistically, the various radioprotectors have been suggested to act very differently. Dephosphorylation of WR-2721 produces the active cell-permeant thiol metabolite WR-1065, which has been reported to suppress the reactivity of intralysosomal iron.[18] Flavonoids, α-TMG, H_2, and Tempol presumably react with or modify free radicals and ROS.[5,6,8,11] Ex-Rad™ was reported to manifest its protective effects through up-regulation of PI3-Kinase/AKT pathways in cells exposed to radiation.[19] A suggested protective mechanism for DIM proceeds through activation of the nuclear kinase at axiateleangiectasia mutated (ATM) regulating responses to DNA damage and oxidative stress, and NF-κB activation.[14] The indole JNJ7777120 acts as a potent and selective antagonist of the histamine H4 receptor,[13] a member of the G protein-coupled receptor super family. The mechanism for the observed protection of B220 is unclear but is possibly due to its observed ability to down-regulate the secondary release of ROS by neutrophils,[16] preventing further oxidative stress after irradiation, and is not likely due to $OH^{\bullet}$-scavenging as B220 has been reported to poorly scavenge $OH^{\bullet}$.[16] B220 is also a DNA intercalator.[20]

In conclusion, B220 was found to be well tolerated at the dose tested and somewhat radioprotective in whole-body γ-irradiated mice. As no toxicity from B220 was observed this raises the chance for optimisation of B220 administration in terms of quantity and number of doses over time, something that likely will enhance the protective effects of B220 further.

MATERIALS AND METHODS

Animals and experimental design

Dark female C3H mice were ordered from M&B A/S (Denmark) and were allowed to acclimatize at the animal facility for a minimum of 5 days. Two separate whole body γ-irradiation studies were performed: (I) evaluation of B220's effect on survival of adult (12 weeks old) mice exposed to 0–14 Gy (0, 2, 4, 6, 8, 10, 12, 14 Gy; n = 8–9 mice per group) ± pre-administration of B220 at all irradiation doses (for 8 Gy, a separate group given B220 post-irradiation was also included), and, (II) evaluation of B220's effect on growth of very young mice (4 weeks old) irradiated with 0, 1 and 6 Gy (n = 5 mice per group). Animals were randomly allocated to groups. In both studies, surviving mice were carefully examined (physical appearance, body weight, etc.) weekly for at least 7.5 months after irradiation when they were humanely euthanized. The groups were kept in separate cages at the animal facility at Huddinge Hospital under controlled conditions with food and water available before and after irradiation. Cage size was adjusted to group size. The ethical permit for the study was S141/96, approved by Stockholm South Ethical Committee on Animal Research, and all experiments were performed in accordance with relevant guidelines and regulations.

Preparation of B220

B220 base was synthesised according to an earlier published method.[21] B220 was dissolved in acetone, then fresh corn oil was added and the solution stirred until all acetone had evaporated giving a final concentration of 1.7-3.2 mg B220 mL^{-1}, depending on the study. The solutions were stored protected from light at room temperature.

Administration of B220

After recording body weights, B220 was administrated. Animals received two 200 µl doses (*i.p.*) of corn oil containing B220 at a concentration giving 25 mg kg^{-1} of body weight each (in total 50 mg kg^{-1} of body weight), administered either before or after irradiation. Controls received corn oil. For pre-administration, the first dose was given 24 h before and the other dose 2 h before irradiation. For post-administration, one dose was given 2 h and the other 24 h after irradiation.

Irradiation of mice

On the day of γ-irradiation the mice were transported to the Department of Radiation Biology, Stockholm University. Irradiation was carried out using ^{137}Cs at 0.65 Gy min^{-1} inside a routinely dosimetry checked apparatus from Instrument AB Scanditronix (Uppsala, Sweden). Animals were whole-body exposed in round well-ventilated compartmentalised plastic boxes (taking up to 10 mice simultaneously).

Observation

The mice were carefully monitored daily the first month after γ-irradiation and then once a week for at least 32 weeks (7.5 months), checking signs of clinical toxicity (survival, weight, physical appearance, etc.). Survival curves were plotted using the Kaplan-Meier method.

Statistical analyses

Statistical significance was set to $p<0.05$ and analyses conducted using GraphPad Prism 5 (San Diego, California). Survival curves were compared using Log-rank (Mantel-Cox) and Gehan-Breslow-Wilcoxon tests. After normalizing body weights to the time-point of irradiation (set to 100 %), the areas under the growth curves were integrated (gives AUC values) for statistical comparison using one- and two-way ANOVA analyses.

ACKNOWLEDGEMENTS

The authors thank research engineer Mary-Ann Zetterqvist for animal care assistance and Prof. Jan Bergman for donating the B220 drug (both at Karolinska Institute in Huddinge).

REFERENCES

[1]Nias, A. H. W. *An Introduction to Radiobiology*. Second ed. John Wiley & Sons, **1998**.

[2]Von Sonntag, C. *The chemical basis of radiation biology,* Taylor & Francis, **1987**.

[3]Patt, H. M., Tyree, E. B., Straube, R. L. and Smith, D. E. Cysteine protection against X irradiation. *Science*, **1949**, *110*, 213-214. https://doi.org/10.1126/science.110.2852.213

[4]Cairnie, A. B. Adverse effects of radioprotector WR2721. *Radiat. Res*., **1983**, *94*, 221-226. https://doi.org/10.2307/3575878

[5]Chuai, Y., Qian, L., Sun, X. and Cai, J. Molecular hydrogen and radiation protection. *Free Radical Res*., **2012**, *46*, 1061-1067. https://doi.org/10.3109/10715762.2012.689429

[6]Uma Devi, P., Ganasoundari, A., Rao, B. S. S. and Srinivasan, K. K. In vivo radioprotection by ocimum flavonoids: survival of mice. *Radiat. Res.*, **1999**, *151*, 74-78. https://doi.org/10.2307/3579750

[7]George, K. C., Hebbar, S. A., Kale, S. P. and Kesavan, P. C. Caffeine protects mice against whole-body lethal dose of gamma-irradiation. *J. Radiol. Prot.*, **1999**, *19*, 171-176. https://doi.org/10.1088/0952-4746/19/2/306

[8]Satyamitra, M., Devi, P. U., Murase, H. and Kagiya, V. T. In vivo postirradiation protection by a vitamin E analog, alpha-TMG. *Radiat. Res.*, **2003**, *160*, 655-661, https://doi.org/10.1667/RR3077

[9]Jagetia, G. C. and Baliga, M. S. Influence of the leaf extract of Mentha arvensis Linn. (mint) on the survival of mice exposed to different doses of gamma radiation. *Strahlenther. Onkol*. **2002**, *178*, 91-98. https://doi.org/10.1007/s00066-002-0841-y

[10]Whitnall, M. H., Elliott, T. B., Landauer, M. R., Wilhelmsen, C. L., McKinney, L., Kumar, K. S., Srinivasan, V., Ledney, G. D. and Seed, T. M., Protection against gamma-irradiation with 5-androstenediol. *Mil. Med*., **2002**, *167*, 64-65. https://doi.org/10.1093/milmed/167.suppl_1.64

[11]Mitchell, J. B., Anver, M. R., Sowers, A. L., Rosenberg, P. S., Figueroa, M., Thetford, A., Krishna, M. C., Albert, P. S. and Cook, J. A., The Antioxidant Tempol Reduces Carcinogenesis and Enhances Survival in Mice When Administered after Nonlethal Total Body Radiation. *Cancer Res.*, **2012**, *72*, 4846-4855, https://doi.org/10.1158/0008-5472.CAN-12-1879

[12]Ghosh, S. P., Perkins, M. W., Hieber, K., Kulkarni, S., Kao, T.-C., Reddy, E. P., Reddy, M. V. R., Maniar, M., Seed, T. and Kumar, K. S., Radiation Protection by a New Chemical Entity, Ex-Rad(TM): Efficacy and Mechanisms. *Radiat. Res.*, **2009**, *171*, 173-179, https://doi.org/10.1667/RR1367.1

[13]Lamas, D. J. M., Carabajal, E., Prestifilippo, J. P., Rossi, L., Elverdin, J. C., Merani, S., Bergoc, R. M., Rivera, E. S. and Medina V. A., Protection of Radiation-Induced Damage to the Hematopoietic System, Small Intestine and Salivary Glands in Rats by JNJ7777120 Compound, a Histamine H4 Ligand. *Plos One*, **2013**, 8, ARTN e69106, https://doi.org/10.1371/journal.pone.0069106

[14]Fan, S., Meng, Q., Xu, J., Jiao, Y., Zhao, L., Zhang, X., Sarkar, F. H., Brown, M. L., Dritschilo, A. and Rosen, E. M. DIM (3,3'-diindolylmethane) confers protection against ionizing radiation by a unique mechanism. *Proc. Natl. Acad. Sci. USA*, **2013**, *110*, 18650-18655. https://doi.org/10.1073/pnas.1308206110

[15]Skarin, T., Rozell, B. L., Bergman, J., Toftgård, R. and Möller, L. Protection against 12-O-tetradecanoylphorbol-13-acetate induced skin-hyperplasia and tumor promotion, in a two-stage carcinogenesis mouse model, by the 2,3-dimethyl-6-(2-(dimethylamino)ethyl)-6H-indolo-[2,3-*b*]quinoxaline analogue of ellipticine. *Chem. Biol. Interact*., **1999**, *122*, 89-106. https://doi.org/10.1016/S0009-2797(99)00117-9

[16]Harbecke, O., Dahlgren, C., Bergman, J. and Möller, L. The synthetic non-toxic drug 2,3-dimethyl-6-((2-dimethylamino)ethyl)-6H-indolo[2,3-b]quinoxaline inhibits neutrophil production of reactive oxygen species. *J. Leukoc. Biol*., **1999**, *65*, 771-777. https://doi.org/10.1002/jlb.65.6.771

[17]Brown, S. L. Kolozsvary, A., Liu, J., Jenrow, K. A., Ryu, S. and Kim, J. H. Antioxidant Diet Supplementation Starting 24 Hours after Exposure Reduces Radiation Lethality. Radiat. Res., 2010, 173, 462-468, https://doi.org/10.1667/RR1716.1

[18]Yu, Z. Q., Eaton, J. W. and Persson, H. L. The radioprotective agent, amifostine, suppresses the reactivity of intralysosomal

iron. Redox Rep., **2003**, *8*, 347-355, https://doi.org/10.1179/135100003225003384

[19]Kang, A. D., Cosenza, S.C., Bonagura, M., Manair, M., Reddy, M. V. and Reddy, E.P. ON01210.Na (Ex-RAD$^{(R)}$) Mitigates Radiation Damage through Activation of the AKT Pathway. *Plos One*, **2013**, *8*, ARTN e58355. https://doi.org/10.1371/journal.pone.0058355

[20]Moorthy, N. S. H. N., Manivannan, E., Karthikeyan, C. and Trivedi, P. 6H-Indolo[2,3-*b*]quinoxalines: DNA and Protein Interacting Scaffold for Pharmacological Activities. *Mini-Rev. Med. Chem.*, **2013**, *13*, 1415-1420. https://doi.org/10.2174/13895575113139990005

[21]Zegar, I., Gräslund, A., Bergman, J., Eriksson, M. and Norden, B. Interaction of ellipticine and an indolo[2,3-*b*]quinoxaline derivative with DNA and synthetic polynucleotides. *Chem. Biol. Interact.* **1989,** *72*, 277-293. https://doi.org/10.1016/0009-2797(89)90004-5

Received: 09.04.2018.
Accepted: 28.04.2018.

MODIFIED DOUBLE-DISC SYNERGY TEST (MDDST) FOR DETECTION OF EXTENDED-SPECTRUM β-LACTAMASES IN AmpC β-LACTAMASE-PRODUCING *KLEBSIELLA* CLINICAL ISOLATES

Atef M. Diab,[a] M. H. Abul-Aziz,[a] Iman M. A. El-Kholy[b] and Mona A. Rezk[b]*

Keywords: AmpC β-lactamase, extended-spectrum β-lactamases (ESBLs), *Klebsiella spp*., modified double-disc synergy test (MDDST), double-disc synergy test (DDST), phenotypic confirmatory test (E-test), modified three-dimensional test (MTDT)

The detection of extended spectrum β-lactamases ($ESBL_{(S)}$) in Gram-negative bacteria that produce AmpC β-lactamases is problematic. In the present study, the performance of modified double-disc synergy test (MDDST) that employs a combination of cefepime and piperacillin-tazobactam for the detection of $ESBL_{(S)}$ *Klebsiella* producing AmpC β-lactamases was evaluated and compared with double-disc synergy test (DDST). E-test phenotypic confirmatory and modified three-dimensional tests (MTDT) were adopted for more data confidence. A total of 100 clinical isolates of *Klebsiella*, which met the CLSI (2012) screening criteria as having broth microdilution (BMD) MIC > or =2 mg mL^{-1} for at least one extended-spectrum cephalosporin [ceftazidime (CAZ), cefotaxime (CTX) and cefpodoxime], were accurately-selected for the study. MDDST detected ESBLs in 62 out of the100 studied isolates with 100 % sensitivity and specificity, whereas DDST detected ESBLs in only 52 isolates with 92.9 % sensitivity and 100 % specificity. E-test could detect ESBLs in 62 isolates, while as many as 34/62 ESBL positive isolates were confirmed to be AmpC beta-lactamase positive by the MTDT. MDDST and E-Test could detect ESBLs in all the 34 AmpC positive isolates, whereas DDST detects ESBLs in only 26 isolates. The study recommended MDDST as superior to DDST for the detection of ESBLs in AmpC β-lactamase-producing *Klebsiella spp*. and this was confirmed by MTDT and E-Tests.

* Corresponding Author
E-Mail: monarezq24@yahoo.com
[a] Suez Canal University, Faculty of Science, Egypt
[b] Ain Shams University Hospital, Egypt.

Introduction

Extended-spectrum β-lactamases (ESBLs) are mutant, plasmid-mediated β-lactamases derived from older, broad-spectrum β-lactamases and confer resistance to all extended-spectrum cephalosporins (ESCs) and aztreonam, except cephamycin and carbapenem derivatives.[1,2] Although ESBLs have been detected in Gram-negative bacteria such *Enterobacter*, *Salmonella*, *Citrobacter*, *Serratia marcescens*, *Proteus* spp. and *Pseudomonas aeruginosa*,[2,3] it is most commonly encountered in K*lebsiella spp.* AmpC β-lactamases are cephalosporinases that are poorly inhibited by clavulanic acid (CLA) and can be differentiated from ESBLs by their ability to hydrolyze cephamycins.[4] A wide variety of Gram-negative bacteria, *Klebsiella pneumonia*, in particular, have been shown to harbor AmpC β-lactamases.[5,6]

The detection of ESBLs in AmpC-producing species of gram-negative bacteria is problematic. The increased prevalence of bacterial pathogens producing both ESBLs and AmpC β-lactamases creates a requirement for laboratory testing methods that can accurately detect the presence of these enzymes in clinical isolates.[7] The inhibitor-based confirmatory test approach is most promising for isolates that do not co-produce an inhibitor-resistant β-lactamase like AmpC. However, a high-level production of AmpC may prevent the detection of an ESBL. This problem is frequently observed in tests with species or strains that produce a chromosomally encoded inducible AmpC β-lactamase (e.g., *Klebsiella* spp., *Enterobacter* spp., *Citrobacter* spp., *Serratia* spp., *Proteus* spp. and *Pseudomonas aeruginosa*). Moreover, in these organisms, CLA may act as an inducer of high-level AmpC production resulting in an increase in the resistance of the isolate to other screening drugs, producing a false-negative result in the ESBL detection test. Tazobactam and Sulbactam are much less likely to induce AmpC β-lactamases and are, therefore, preferable inhibitors for ESBL detection tests with these organisms.[8]

Another approach is to include cefepime (FEP) as an indicator drug.[1] High-level AmpC production has a minimal effect on the activity of FEP, making this drug a more reliable detection agent for ESBLs in the presence of an AmpC β-lactamase.[1] A test incorporating FEP and piperacillin-tazobactam (TZP) for the detection of Enterobacteriaceae that produce an extended spectrum and AmpC β-lactamases have been described.[7]

We describe here a modified double-disc synergy test (MDDST), which differs from the original double-disc synergy test[9] in two respects; first, the addition of discs of FEP and TZP; second, adjustment of the distances between various discs for accurately detecting the synergy between Augmentin/TZP and extended-spectrum cephalosporin. The test was evaluated for detecting ESBL in AmpC β-lactamase-producing *Klebsiella* and compared with original double-disc synergy test (DDST) and phenotypic confirmatory test (E-test). The production of AmpC β-lactamases in ESBL positive isolates was confirmed by the modified three-dimensional test (MTDT).

Material and Methods

A total of 100 consecutive, non-repetitive clinical isolates of *Klebsiella* isolates was collected from a variety of clinical specimens, viz., urine, pus, wound swab and high vaginal swab, referred to the Central Microbiology Laboratory of Ain Shams University Hospitals for routine culture and sensitivity from September to December 2015.

Screening for ESBLs -Disc diffusion method (DDM)

The test inoculum (0.5 McFarland turbidity) was spread onto Mueller-Hinton agar plate, an interpretation of zone diameter of (CPD ≤17mm, CAZ ≤ 22 and CTX ≤27), this may indicate ESBL production (i.e.) positive screening for ESBL. However, FEP disc not included by CLSI (Clinical and Laboratory Standards Institute) for ESBL screening but FEP zone diameter FEP≤14mm indicate resistance which we considered as presumptive ESBL.[10]

Detection of ESBLs-Double-disc synergy test

The test inoculum (0.5 McFarland turbidity) was spread onto Mueller-Hinton agar (MHA; HiMedia) using a sterile cotton swab. A disc of augmentin (20 µg Amoxycillin + 10 µg CLA) was placed on the surface of MHA; then discs of cefpodoxime (30 µg), CAZ (30 µg) and CTX (30 µg) were kept around it in such a way that each disc was at distance ranging between 16 and 20 mm from the augmentin disc (centre to centre). The plate was incubated at 37 °C overnight. Distances between the discs were required to be suitably adjusted for each strain in order to accurately detect the synergy. The organisms were considered to be producing ESBL when the zone of inhibition around any of the expanded-spectrum cephalosporin discs showed a clear-cut increase towards the Augmentin disc.[9]

Modified double-disc synergy test

The original DDST was modified for detecting ESBLs in AmpC-producing clinical isolates of *P. mirabilis* by placing a disc of TZP (100/10 µg) at a distance ranging between 22 and 25 mm from FEP (30 µg) disc. Briefly, a disc of augmentin (20 µg amoxycillin + 10 µg CLA) was placed on the surface of MHA; then discs of cefpodoxime (30 µg), CAZ (30 µg), CTX (30 µg) and FEP (30 µg) were kept around it in such a way that each disc was at distance ranging between 16 and 20 mm from the augmentin disc (centre to centre), and a disc of TZP (100/10 µg) was placed at a distance ranging between 22 and 25 mm from the FEP disc. Distances between the discs were required to be suitably adjusted depending on the zone of inhibition obtained with extended-spectrum cephalosporin disc in a particular isolate in order to accurately detect the synergy.

The organisms were considered to be producing ESBL when the zone of inhibition around FEP or any of the extended-spectrum cephalosporin discs showed a clear-cut increase towards the TZP disc. The discs of ciprofloxacin (5 µg), amikacin (30 µg), gentamicin (10 µg) and cefoxitin (30 µg) were also included so as to find out the susceptibility of the isolates to commonly used antibiotics Figure 1.

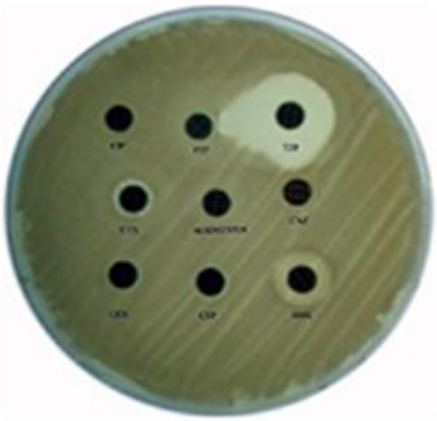

Figure 1. Modified double-disc synergy test (MDDST) showing synergy between cefepime (FEP)/ceftazidime (CAZ) and piperacillin-tazobactam (TZP)

Phenotypic disc confirmatory test - E-test

This test was recommended by CLSI (E-test ESBL strip).[10] The MIC value was read from the scale in terms of ug/ml where the ellipse edge intersects the strip. ESBL production is inferred if the MIC ratio for cephalosporin alone/cephalosporin plus clavulanate MIC is ≥8. ESBL production was also identified by the presence of a phantom zone or a deformation of the CAZ inhibition zone independent of the MIC ratios. If the MIC ratio is <8 it is indicative of non-ESBL production. When MIC values were above the test device range, the interpretation was 'non-determinable'.

Detection of AmpC β-lactamases -Modified three-dimensional test

The presence of AmpC β-lactamases in ESBL positive isolates with reduced susceptibility to cefoxitin was detected by MTDT.[4] Briefly, fresh overnight growth from MHA was transferred to a reweighed sterile microcentrifuge tube. The tube was weighed again to determine the weight of bacterial mass to obtain 10-15 mg of bacterial wet weight. The bacterial mass was suspended in peptone water and pelleted by centrifugation at 3000 rpm for 15 minutes. Crude enzyme extract was prepared by freezing and thawing the bacterial pellet (five cycles). Lawn culture of *E. coli* ATCC 25922 was prepared on MHA plates, and a cefoxitin (30 µg) disc was placed on the surface of the medium. Linear slits (3 cm long) were cut using sterile surgical blade up to a point 3 mm away from the edge of the cefoxitin disc. Wells of 8 mm diameter were made on the slits at a distance 5 mm inside from the outer end of the slit using a sterile Pasteur pipette. The wells were loaded with enzyme extract in 10 µL increments until the well was full. Approximately 30-40 µL of extract was loaded in a well. The plates were incubated at 37 °C overnight. Three different kinds of results were recorded. Isolates that showed clear distortion of the zone of inhibition of cefoxitin were taken as AmpC producers. Isolates with no distortion were taken as AmpC non-producers, and isolates with minimal distortion were taken as intermediate strains.

A known AmpC-positive isolate of *Klebsiella pneumoniae* was used as control reference strain (Figure 2).

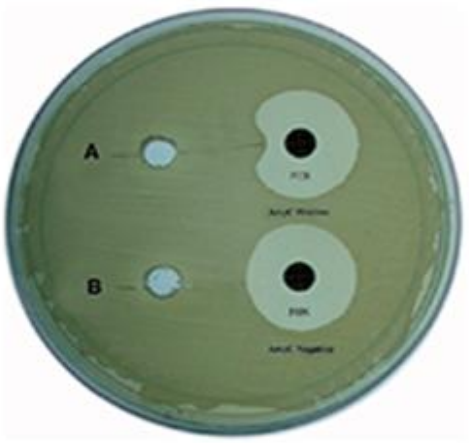

Figure 2. Modified three-dimensional test showing AmpC positive (A) and negative (B) results

Results

Sixty two/100 isolates were ESBL positive by E-test (golden standard test). Fifty-two out of 62 were positive by DDST, while MDDST detected all the 62 ESBL positive isolates. Sixty-seven out of 100 isolates were AmpC producers by M3D (golden standard test). Sixty-four out of 67 isolates that were positive by M3D test were resistant to FOX with a sensitivity of 95.5 % and specificity of 63.6 % for detection of AmpC production with positive predictive value and negative predictive value of (84.2% and 87.5 %) respectively. Sixty-seven out of 100 isolates were positive AmpC by M3D test. Thirty-four out of 67 isolates were positive ESBL by MDDST. On the other hand, 26/67 were positive by DDST. The sensitivity of DDST was 76.5 % and specificity of 100 % for detection of ESBL in presence of AmpC. Thirty-three out of 100 isolates were negative AmpC by M3D test. Twenty-eight out of 33 isolates were positive ESBL by MDDST. Twenty-six out of 33 were positive by double disc synergy test. The sensitivity of DDST was 92.9 % and specificity of 100% for detection of ESBL in absence of AmpC in the isolates.

This means that the sensitivity of the DDST when M3D was negative is better from its sensitivity when the latter was positive, where MDDST is positive in eight isolates more than double disc test in positive M3D isolates and two in negative M3D isolates.

Discussion

In our study, 62/100 isolates were positive by E-test. The DDST at a distance of 20mm center to center detected 52/62 (83.9 %) ESBL positive isolates by E-test with a sensitivity of 83.9% and specificity of 100 %. CAZ and CTX were found to be the best substrates, as they revealed synergism with AMC in 37/62 (59.7 %) and 35/62 (56.5 %) isolates respectively, followed by FEP which detected 21/62 (33.9 %). while the least detection was with CPD as it detected 11/62 (17.7 %). isolates. Also, Bamidele et al.[16] demonstrated that DDST using CTX, CAZ, CRO and ATM discs around AMC disc at a distance 15-20 mm center to center, on 54 isolates of *P. aeruginosa* collected from five different tertiary hospitals in Southwest Nigeria. Twenty-nine out of 54 were resistant to two or more expanded-spectrum cephalosporins. CRO and CTX were found to be the best substrate, as they revealed synergism with AMC in 29/54 (53.7 %) and 28/54 (51.8 %) respectively. On the other hand, ATM and FEP showed synergism in 24/54 (44.4 %) and 10/54 (18.6 %) isolates respectively, while CAZ showed the least synergy only in 9/54 (16.7 %).

In our study 67/100 isolates were AmpC producers by the M3D test. Thirty-four out of 67 AmpC producers were ESBL positive by E- test, and MDDST while by DDST 26/67 were ESBL positive showing 76.5 % sensitivity and 100 % specificity for detection of ESBL in the presence of AmpC. On the other hand, 26/33 (78.8 %) non-AmpC producers were positive by DDST Showing 92.9 % sensitivity and 100 % specificity of detection of ESBL in absence of AmpC. While, MDDST showed 100 % sensitivity and specificity in detection of ESBL in the presence and absence of AmpC as it identified the 10 isolates, which were not detected by DDST where MDDST was positive in eight AmpC producer isolates and the two AmpC negative isolates (i.e. all 62 ESBL positive isolates).

Similarly, Dhara et al.[15] demonstrated that 44/54 K*lebsiella* isolates collected from a blood culture from neonatal intensive care unit (NICU) patients referred to microbiology lab of B.J. Medical College, at Ahmedabad in India, were ESBL positive isolates by PCDDT and coproduce AmpC enzyme which was confirmed by the M3D test. MDDST detected the all 44 (100 %) ESBL positive isolates. Thus MDDST showed 100 % sensitivity and specificity for detection of ESBL in the presence of AmpC compared to the standard test DDST which detected 36/44 ESBL positive isolates.

In our study, 64/67 M3D-positive isolates were resistant to FOX with a sensitivity of (95.5 %) and a specificity of (63.6 %) in the detection of AmpC production. While 12/33 (36.4 %) M3D test negative was FOX resistant. While FOX susceptibility in three out of 67 (4.5 %) M3D-positive isolates may be explained by Peter-Getzlaff et al.[14] who stated that strains carrying ACC gene may appear FOX susceptible.

Conclusion

Double disc synergy test may be used for detection of ESBL in the isolates which produce only ESBL and not for detection of ESBL in isolates coproducing AmpC enzyme like *Enterobacter, Serratia, Citrobacter* and also with *Klebsiella spp.*

Modified double disc synergy test using TZP and FEP at a distance 20mm center to center may serve as a reliable confirmatory test for detection of ESBLs in AmpC positive isolates instead of DDST.

References

[1]Thomson, K. S., Controversies about extended-spectrum and AmpC β-lactamases. *Emerg. Infect. Dis.*, **2001,** *7*, 333-6. DOI: 10.3201/eid0702.700333

[2]Bush, K., Jacoby, G. A., Medeiros, A. A. A functional classification scheme for β-lactamases and its correlation with molecular structure. *Antimicrob. Agents Chemother.*, **1995,** *39*, 1211-33.

[3]Ho, P. L., Ho, A. Y., Chow, K. H., Wong, R. C., Duan, R. S., Ho, W. L., , Mak, G. C., Tsang K. W., Yam, W. C., Yuen, K. C., Occurrence and molecular analysis of extended spectrum β-lactamase-producing *Proteus mirabilis* in Hong Kong, 1999-2002. *J. Antimicrob. Chemother.*, **2005,** *55*, 840-5. doi.org/10.4236/ojcd.2014.41011

[4]Manchanda, V., Singh, N. P., Occurrence and detection of AmpC β-lactamases among gram negative clinical isolates using a modified three-dimensional test at Guru Tegh Bahadur Hospital, Delhi, India. *J. Antimicrob. Chemother.*, **2003,** *51*, 415-8.

[5]Singhal, S., Mathur, T., Khan, S., Upadhyay, D. J., Chugh, S., Gaind, R., Rattan, A., Evaluation of methods for AmpC β-lactamase in Gram-negative clinical isolates from tertiary care hospitals. *Indian J. Med. Microbiol.;* **2005,** *23*, 120-4.

[6]Naas, T., Benaoudia, F., Massuard, S., Nordmann, P., Integron located VEB-1 extended spectrum β-lactamase gene in a *Proteus mirabilis* clinical isolate from Vietnam. *J. Antimicrob. Chemother.*, **2000,** *46*, 703-11.

[7]Pitout, J. D., Reisbig, M. D., Venter, E. C., Church, D. L., Hanson, N. D., Modification of the double-disc test for detection of Enterobacteriaceae producing extended-spectrum and AmpC β-lactamases. *J. Clin. Microbiol.*, **2003,** *41*, 3933-5. DOI: 10.4103/0255-0857.38860

[8]Thomson, K. S., Sanders, C. C., Moland, E. S., Use of microdilution panels with and without β-lactamase inhibitors as a phenotypic test for β-lactamase production among *Escherichia coli*, *Klebsiella* spp, *Enterobacter* spp, *Citrobacter freundiim* and *Serratia marcescens*. *Antimicrob. Agents Chemother.*, **1999,** *43*, 1393-400. PMCID: PMC89285

[9]Jarlier, V., Nicolas, M., Fournier, G., Philippon, A., Extended-spectrum β-lactamases conferring transferable resistance to newer β-lactam agents in Enterobacteriaceae: Hospital prevalence and susceptibility patterns. *Rev. Infect. Dis.*, **1988,** *10*, 867-78. PMID: 3263690

[10]Clinical and Laboratory Standards Institute guidelines by CLSI/NCCLS - CLSI informational supplement. Approved standard M100-S15 Wayne, PA, 2000. **2005.**

[11]Shukla, I., Tiwari, R., Agrawal, M., Prevalence of extended spectrum β-lactamase producing *Klebsiella pneumonia* in a Tertiary Care Hospital. *Indian J. Med. Microbiol.*, **2004,** *22*, 87-91. PMID: 17642702

[12]De Gheldre, Y., Avesani, V., Berhin, C., Delmıe, M., Glupczynski, Y., Evaluation of the oxoid combination discs for detection of extended spectrum β-lactamases. *J. Antimicrob. Chemother.*, **2003,** *52*, 591-7. DOI: 10.1093/jac/dkg415

[13]Luzzaro, F., Perilli, M., Amicosante, G., Lombardi, G., Belloni, R., Zollo, A., Bianchi, C., Toniolo, A., Properties of multidrug-resistant, ESBL producing Proteus mirabilis isolates and possible role of β-lactam/β-lactamase inhibitor combinations. *Int. J. Antimicrob. Agents;* **2001,** *17*, 131-5. PMID: 11165117

[14]Peter-Getzlaff, S., Polsfuss, S., Poledica, M., Hombach, M., Giger, J., Bottger, E. C., Zbinden, R. and Bloemberg, G. V., Detection of AmpC β-Lactamase in *Escherichia coli*: Comparison of Three Phenotypic Confirmation Assays and Genetic Analysis. *J. Clin. Microbiol.*, **2011,** *49(8)*, 2924-2932. doi: 10.1128/JCM.00091-11

[15]Dhara, M., Disha, P., Sachin, P., Manisha, J., Seema, B. and Vegad M., Comparison of various methods for the detection of extended spectrum β-lactamase in *Klebsiella* pneumoniae isolated from neonatal intensive care unit, Ahmedabad. *N. J. Medical Res.*, **2012,** *2*, 348-349. eISSN: 2277 8810

[16]Bamidele, O., Bola, A., Olusegun, S. and Hannah, D. A., Phenotypic detection of extended-spectrum ß-lactamases producing *Pseudomonas aeruginosa* from hospitals in South west Nigeria. *Global J. Pharm. Res.*, **2012,** *1*, 708-714.

Received: 31.12.2017.
Accepted: 04.05.2018.